TÉCNICO LISBOA

Study of four point bending specimen geometry

João Subtil Lobo

Thesis to obtain the Master of Science Degree in

Mechanical Engineering

Supervisors: Prof. António Manuel Relógio Ribeiro
Prof. Luís Filipe Galrão dos Reis

Examination Committee

Chairperson: Prof. João Orlando Marques Gameiro Folgado
Supervisor: Prof. Luís Filipe Galrão dos Reis
Member of the Committee: Prof. Rosa Maria Marquito Marat Mendes

October 2020

Agradecimentos

Em primeiro lugar quero agradecer à minha família todo o suporte que me deram, seja ele emocional ou financeiro estiveram sempre dispostos a ajudar de todas as maneiras possíveis. Portanto, Pai, Mãe e Miguel não sei se um obrigado chega para agradecer a oportunidade de fazer este curso, mas mesmo assim, obrigado.

Obrigado também aos amigos que vi passar ao longo destes anos, foram vocês que para mim tornaram este curso numa experiência da qual não me arrependo, nunca me esquecerei de vocês, estejam onde estiverem.

Quero claro, agradecer aos meus orientadores, António Relógio e Luís Reis por me encaminharem nesta última etapa mesmo que eu não tenha sido a pessoa mais comunicativa e colaboradora deste processo.

Agradeço imenso pela ajuda voluntaria da Professora Virgínia Infante, Pedro Teixeira e o aluno João Marques “bacano de Tires” por me ajudarem com a parte experimental da tese.

Os últimos agradecimentos vão para a as inúmeras pessoas do Laboratório de Desenvolvimento do Produto por disponibilizarem os seus conhecimentos e familiaridades com o processo de impressão 3D.

Resumo

Nos testes em flexão a quatro pontos, algumas amostras revelam zonas de falha nas proximidades dos rolos de carregamento, onde a tensão de von Mises não é rigorosamente calculável por meio analiticos. Este carregamento não afeta apenas os materiais suscetíveis a falha por indentação nos roletes, a concentração de tensão próxima aos rolos de carregamento pode enviesar qualquer estudo que tente avaliar as propriedades do material ao usar flexão em quatro pontos.

Para contribuir para uma melhoria no método, o trabalho que se segue introduz uma geometria bem conhecida, o design ”dog bone”, geralmente utilizado noutros tipos de testes mecânicos no ensaio de flexão a quatro pontos. O objetivo é determinar como esta geometria altera o campo de tensões imposto em relação às amostras construídas de acordo com os padrões ASTM e os benefícios que isso pode trazer ao teste de flexão.

Como ponto de partida, forem realizadas simulações numéricas para observar a evolução do campo de tensões ao alterar os novos parâmetros inerentes à nova geometria e determinar a melhor combinação dos parâmetros referidos. Depois de se estabelecerem as geometrias finais das amostras, estas foram fabricadas com a tecnologia FDM e sujeitas a testes de flexão em quatro pontos para validar os resultados numéricos do trabalho. Com os resultados dos testes mecânicos validou-se parcialmente o modelo númerico e a utilização da expressão para o cálculo de tensões para estas novas geometrias. Verificou-se também um aumento de tensão na zona central do provete significando menores influências por parte dos roletes.

Palavras-chave: Coeficiente de tensões, zona de transição, zona de contacto, parâmetros de impressão, flexão a quatro pontos.

Abstract

As the four point bending tests continue being used to determine flexural properties of materials, s ome specimens reveal failure zones in the vicinity of the loading rollers where the von Mises stress is not easily calculable through expressions. As of now this loading does not only affect the materials susceptible to this type of failure, the stress concentration near the loading rollers can misguide any study trying to evaluate the material properties through this test.

In order to combat this, the following work introduces a well known geometry, the ”dog bone” design, usually used in other types of mechanical testing into the realm of four point bending. The objective is to determine how this geometry alters the stress field over the specimens built according to ASTM standards and the benefits this might bring to the bending test.

As a starting point, numerical simulations were used to observe the stress evolution when changing the new parameters inherent to the new geometry, and determine the best combination of said parameters. After establishing the final specimen geometries, they were manufactured using FDM technology and imposed to four point bending tests to validate the numerical results of the work. With the results gathered from the mechanical testing the numerical work was partially validated as well as the use of the equation for calculating stress at the mid-span. An increase in stress at the mid-span was also verified meaning a reduction on the influence of the rollers on the test.

Keywords: Stress coefficients, transition zone, contact zone, printing parameters, four point bending.

Contents

List of Tables

List of Figures

Nomenculature

- 3D Three-Dimensional
- A Distance between supporting and loading rollers
- ABS Acrylonitrile Butadiene Styrene
- AISI American Iron and Steel Institute
- ASTM American Society for Testing and Materials
- CAD Computer Aided Design
- E Young Modulus
- ESO Evolutionary Structural Optimization
- d Distance between the contact zone to the beginning of the transition
- ϵ Strain
- ϵ_{max} Maximum strain
- FDM Fused Deposition Modeling
- FEA Finite Element Analysis
- FEM Finite Element Model
- F_0 Total force applied by both loading rollers
- F_u Ultimate force for failure at mid-span
- I Inertia moment
- ISO International Organization for Standardization
- K_f Stress concentration factor
- K_t Stress concentration factor in the transition zone
- L Support span
- l Loading span
- M Momentum
- n_i number of entries for group i
- η_A Horizontal distance from the centre of the supporting cylinder to its contact zone
- η_C Horizontal distance from the centre of the loading cylinder to its contact zone

- PLA Polylactic Acid
- R Cross-head rate of the loading rollers
- R_x Radius of the elliptical transition along the x direction
- R_y Radius of the elliptical transition along the y direction
- r Radius of the rollers
- r_1 Radius 1 of double-arced transitions
- r_2 Radius 2 of double-arced transitions
- r_{V_A} Equivalent radius of the ellipse at point A
- S_i^2 Variance of group i
- SC_r Stress coefficient beneath the loading rollers
- SC_t Stress coefficient at the root of the transition
- σ Stress
- σ_{max} Maximum stress
- σ_n Nominal stress
- σ_r Maximum stress beneath the loading rollers
- σ_t Maximum stress at the transition zone
- t Thickness of the specimen
- tr Distance between the start from the opposite
- tz Test zone
- τ_{max} Maximum shear stress
- V Transverse effort
- w Width at the mid-span of the specimen
- W Width taking into account the R_y parameter
- $\bar{y_i}$ Mean of group i

Chapter 1

Introduction

Every day we rely on machines and structures to accomplish our goals and progress towards the future, but that path may be riddled with dangerous inconveniences. Such may be failure of their components due to fatigue, excessive deformation and over loading of the material just to name a few. Knowledge over the material properties is essential in avoiding these risks. By also taking into account the geometry and boundary condition the behaviour of materials becomes predictable.

Material testing is used as a measurement tool for the characteristics and behaviour of materials, usually metals, ceramics or plastics. The data output provides a wealth of information about the tested materials and can be used to judge whether or not the material in question is appropriate for the application needed. This proves to be extremely important when products are involved in critical applications where an unpredicted failure by the component may result serious injuries and casualties.

The results of material testing can vary depending on the procedure behind the experiments. Variables such as the geometry of the test specimen and its constraints and loading apparatus can impact on our knowledge of the material. In order to obtain consistent and comparable results there was a need to establish standard test methods, This was accomplished through the International Organization for Standardization (ISO) ,which has published 22656 International Standards and counts with 164 national standard bodies [1]. And in a similar fashion the American Society for Testing and Materials (ASTM) that started in the U.S. and has been expanding to Europe, Latin America, China and Canada, the former organization was founded in 1947 and the latter in 1898 [2].

1.1 Motivation

The four-point bending test is a material test that focuses on determining mechanical properties of its test subject. There are several standards such as ASTM D6272-10 [3] and many others that provide guide lines for the experiment and analysis of data. This is in order to have minimal differences between test conditions all around the globe. The values of the material properties reported from these measurements are considered adequate with enough confidence for use in applications of the material.

One problem that rises from simple observation of the test procedure is the clear influence of the

loading fixtures on the experiment. In a test where its main purpose is to analyse the response from the material to the stress distribution in the mid-section of the test subject the specimens will, more often than not, fail near the loading points. This is due to the enforcement of loads to the material through a very finite area and leads to an increased stress in its vicinity making this region the most probable failure zone [4]. Since the higher stresses are located near the loading rollers the mid-section is not stressed to its limit. Coupled this with the expressions not being able to calculate stress near the contact area, the value of the material properties that will be determined should be lower than real mechanical properties of the material. This thesis is an effort to approximate the test results to the real characteristics of the materials by diminishing the complex stress near the loading fixtures to provide more accurate knowledge on materials tested in four-point bending.

1.2 Objectives

The main objective of this master's thesis is to propose and research an alternative specimen shape and analyse the influence of different parameters of its geometry for four-point bending tests. Not only will individual parameters be tested in order to understand how they will affect the end result of the experiment but also, the combination of various factors and their levels to study the reaction between different parameters.

The purpose behind this work is to reduce the effect of the concentrated loading stresses along the area of contact of the loading apparatus with the specimen. This would result in a more accurate representation of the materials that are tested using four-point bending and provide new guide lines that are alternatives to today's standards for the geometry of the test specimen.

To achieve the objectives stated a quick research to discover previous findings about four-point bending tests will be performed, going over the principles and importance of this particular experiment, failure modes, stress simulations and results of similar investigations to enlighten the subject and the development of this work.

1.3 Thesis Outline

To follow a logical path towards the end goal, research on existing works was required to inform about the current state of four point bending. After which starts the experimental planning phase where geometries are proposed and methods are established to study said geometries. To save resources such as material and time, numerical studies were used to determine their impact on four-point bending tests and obtain the optimized geometries for the next chapter. Moving on, it is time to test the specimens created, and so they have to be built and the mechanical test prepared. With the tests done there is only the results to be presented, analysed and discussed in order to reach the conclusions taken from this work.

This thesis is arranged in the following chapters chapters:

- Chapter 2: It contains a revision of related works in the past with a brief introduction to bending tests, their stress concentrations and a look to solutions found for the problem in similar mechanical tests.
- Chapter 3: It hypothesises on how to solve the problem at hand, defines methods for all stages of the work.
- Chapter 4: It describes every detail of how the numerical simulations were built and reasoning behind each choice.
- Chapter 5: It presents the final specimen geometries, their manufacturing process and the preparation for their mechanical testing.
- Chapter 6: Results from both parts of the work, numerical and mechanical, are displayed.
- Chapter 7: Results from Chapter 6 are discussed.
- Chapter 8: Conclusions are drawn from the previous chapters, achievements and future works.

Chapter 2

Background

2.1 Bending Tests

One problem encountered in early material testing was the influence of gripping the test specimen, this was much more observable while tensile testing unidirectional composites. The use of conventional specimens for tensile test could result in a premature failure near the grips by shear stress. Through careful design of the test specimen or eliminating the necessity of gripping all together this problem could be avoided [5]. So the improved design for the tensile test specimen and an alternative bending test method were adopted.

Bending tests are performed on beams and often used to determine the mechanical properties of materials and there are two types that are the most commonly used, three and four point bending.

Three point bending uses a central cylinder to apply loads perpendicular to the specimen while the two outer supports, usually placed at the same distance from the central load, remain stationary. Since these bending tests are static there is an equilibrium of forces and so the outer support also apply force to the specimen. This loading geometry will produce a bending moment with a value of zero at the outer supports and grows linearly until it reaches a maximum at the central loading roller. The perpendicular forces cause shear stress in the material and the bending moment is responsible for both tension and compression stresses.

Four point bending is widely used to determine the flexural strength and flexural modulus. The already established standards are simpler to use then tensile tests. Since there is no need for special gripping of the specimen it makes it convenient for plastic and brittle material testing [6]. This test works in a similar fashion to the previous three point bending, the main difference being the arrangement of the test fixture. It consist on a set of four cylindrical rollers. These are divided into a pair of inner rollers and a pair of outer supports which are normally symmetrically positioned in relation to the test specimen, with equal loads being applied by the two central supports [7]. This type of arrangement will lead to three distinct areas of the specimen. The sections between the outer and inner rollers will have a constant transverse loading applied and a bending moment that starts at zero at the outer support and reaches its maximum at the inner support. The other is the section between the two inner rollers that will only

have a uniform bending moment resulting in pure tension and compression stresses. All can be seen in Figure 2.1. Because of the arrangement of this method a large volume of the test specimen undergoes pure tension and compression. This is due to the uniform stress at the mid-section and thus the results are more representative of the properties of the material [5].

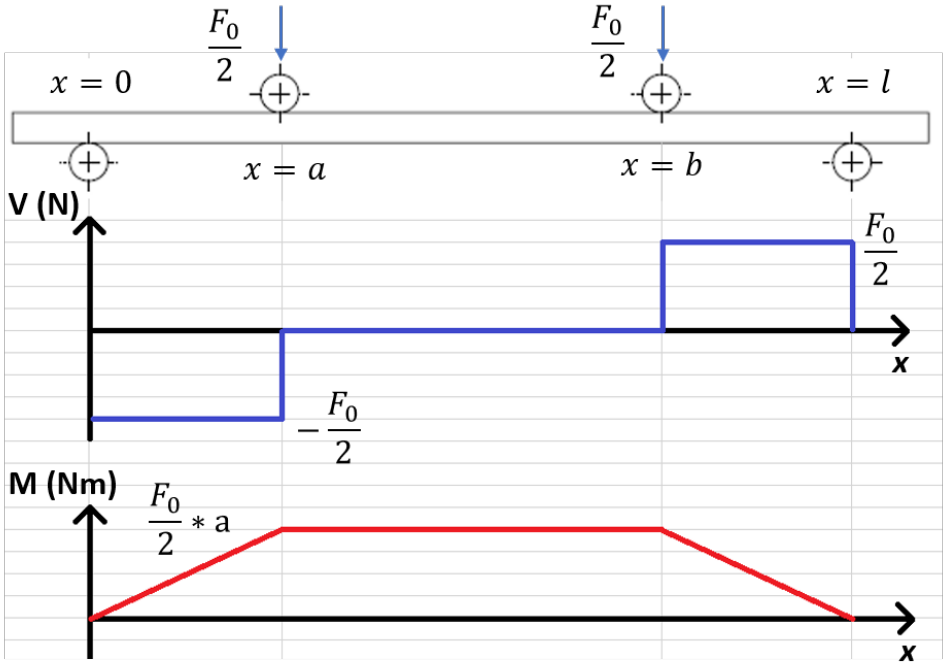

Figure 2.1: Free body diagram of a four point bending test.

The Theory of Four Point Dynamic Bending Test by Pronk [8] demonstrates and summarizes how the formulas used for the calculation of stresses in four point bending came to be. Dividing the specimen in the three regions mentioned previously, being the main test area, the span between the inner rollers and the two other regions representing the part of the specimen which has theoretical transverse effort.

The bending moment is the main feature of the four point bending as it is responsible for the stresses found on region 1. Throughout its development in region 2 it grows directly proportional with the increase of the lever arm and so assumes the formula:

$$M(x) = \frac{F_0}{2} \times x \tag{2.1}$$

Where F_0 is the total downward force applied by both loading noses and x is the distance to the left support cylinder. Once it gets to the inner loading nose, M reaches its maximum value and remains constant along the entirety of the central region. This stems from an equal force entering the momentum balance, the loading roller force will produce a momentum in the contrary direction to the one generated by the supporting roller. As equal forces the only difference between them is their positioning, and so the following happens:

$$M(x) = \frac{F_0}{2} \times x - \frac{F_0}{2} \times (x - a) \tag{2.2}$$

The peak momentum generated throughout the whole central region is when $x > a$ and $x < b$, so the

bending force applied across the total test area will be:

$$M(x) = \frac{F_0}{2} \times a \tag{2.3}$$

And it can be seen that the bending stress that the test section is subjected to depends only on the force exerted by the rollers and the distance between the support and loading noses. Next Pronk presents a general formula for calculating the strain for both regions and further develops it to find the maximum strain. To find maximum strain in the specimen one must look to where the maximum momentum and maximum distance to the neutral centreline of the specimen represented by the variable y exist:

$$\epsilon(x,y) = \frac{M(x) \times y}{E \times I} \rightarrow \epsilon_{max} = \frac{\frac{F_0}{2} \times a \times \frac{t}{2}}{E \times I} \tag{2.4}$$

Where t is the thickness of the test sample and $\frac{t}{2}$ is the distance between the centreline and the surface of the specimen. Now relating the strain to stress through the Young Modulus maximum stress formula can be deducted:

$$\sigma(x,y) = E \times \epsilon = \frac{M(x) \times y}{I} \tag{2.5}$$

With momentum of inertia for a rectangular cross-section,

$$I = \frac{w \times t^3}{12} \rightarrow \sigma = \frac{12M(x) \times y}{w \times t^3} \tag{2.6}$$

Looking at the earlier Equation (2.5) one can say that the maximum stress occurs when the strain is also maximum since the Young's Modulus is constant, so:

$$\sigma_{max} = E \times \epsilon_{max} = \frac{12 \times F_0 \times a}{4 \times w \times t^2} \tag{2.7}$$

Where w is the width of the test specimen. This leads us to the usual formulas found on the four point bending standards such as ASTM 6272-10 [3] where the length of the lever arm A is set to one of two possibilities $L/3$ or $L/4$. Placing the proper values the formula reaches its final state:

$$a = \frac{L}{3} \rightarrow \sigma_{max} = \frac{F_0 \times L}{w \times t^2} \qquad a = \frac{L}{4} \rightarrow \sigma_{max} = \frac{3 \times F_0 \times L}{4 \times w \times t^2} \tag{2.8}$$

With this equation in conjunction with displacement of the loading rollers we can obtain the yield stress and maximum stress of the material. As for the Young Modulus it's given by the following expression:

$$E = \frac{\sigma_{max}}{\epsilon_{max}} \tag{2.9}$$

Which further develops into the the form encountered in the ASTM standard:

$$A = \frac{L}{3} \rightarrow E = \frac{0.21 \times L^3 \times m}{w \times t^3} \qquad A = \frac{L}{4} \rightarrow E = \frac{0.17 \times L^3 \times m}{w \times t^3} \tag{2.10}$$

Where m is the slope of the steepest initial straight line of the load-deflection curve attained during the mechanical test. The equation that relates the boundary conditions to give the shear stress as the output for rectangular cross-sections is the following:

$$\tau_{max} = \frac{3 \times F_0}{4 \times w \times t} \tag{2.11}$$

Despite it being widely used, four point bending has some error associated with it that are mostly unaccounted for by testing standards. While the loading noses apply the force and the specimen suffers increasing bending the contact points between the material and the cylindrical supports will change due to the rotation of the cross section during the deformation process [9], this happens in both inner and outer supports. Timoshenko [10] mentioned this fact applied to three point bending where the outer supporting surfaces move inwards and the span diminishes as the central load increases as a problem to demonstrate the limitations of the method of superposition.

Figure 2.2: Movement of contact zones in four point bending tests [9]

Different span ratios between inner and outer supports can lead to systematic errors in determining the flexural strength. Furthermore it has been recognised that there is a lack of detailed knowledge of four point bending measurements [11] [12]. As an example ASTM D6272-10 [3] recommends two geometries for the loading noses just because of its easy set up and being less sensitive to positioning errors [6]. Theobald et al. [13] carried out an experimental research in order to analyse the influence of load and geometric configuration on four point bending tests. The distance between loading supports was changed throughout the bending tests to study the influence it had on flexural strength and flexural modulus. They discovered that bending strength decreased as the span between the two inner noses increased and that the flexural modulus was independent to the changes made to the geometry.

On top of slight errors in the measurement of flexural strength the calculation of the shear strength of the specimen through classical beam theory can also lead to arguable results. Studies via Finite Element Analysis show shear stress distributions at multiple cross-sections between the supporting and loading roller and compare it to classical beam theory. Rather than peaking at the middle of the thickness the shear stress displays marginally higher values near the surface in cross-sections located in the vicinity of the rollers. While the rest of the cross sections of the span in Region 2 follows more closely the parabolic approximation of the classical beam theory [14] [15].

2.2 Saint Venant's Principle

Bending, tension and torsion are often used in practical material testing to determine their elastic constants. These methods to obtain the properties of materials induce stress concentrations at the loading zone of the test subject. In the case of four point bending this is true under the loading rollers that transfer the force through a narrow strip of contact, another example is the clamping required for tensile testing. Though stress concentrations can cause various problems while testing including premature failure they can be neglected in the calculation of the elastic constants in certain conditions. This ability comes from the validity of the Principle of St. Venant proposed in 1855. It states that "the strains that are produced in a body by the application to a small part of its surface of a system of forces statically equivalent to zero force and zero couple, are of negligible magnitude at distances which are large compared with the linear dimensions of the part" [16]. This means that at a certain distance the distribution of forces at the loading zone, may it be uniform or irregular, will become evenly distributed and the manner that the force is transferred to the material will not impact the results at a distance. In practice we only need to consider the resultant force for the calculations of elastic constants [17].

In isotropic materials the St. Venant's Principle is observable after a very short span of a test specimen. Effects of stress distribution (end effects) become insignificant at about a specimen's width away from the loading point, and end effects can be neglected compared with included errors in the measurement of material properties. In practice, a ratio between length and width of 10 is sufficient to eliminate the stress concentrations effect on the calculations of elastic constants [17].

In anisotropic materials, end effects are not mitigated at the same rate as in the previously mentioned isotropic materials. This behaviour of slow stress decay was observed experimentally by Folkes and Arridge while conducting torsional pendulum tests designed to determine the longitudinal shear modulus of a polymeric microcomposite [18] [19]. This highly anisotropic material showed the end effects persisting over a longer length of the test specimen when compared to isotropic materials. The effect caused difficulties when trying to obtain values for this material's modulus. The Modulus depended on the sample's length to width ratio until this ratio reached the value of about 100, by then the shear modulus would become consistent [18].

Saint Venant stated that the principle was valid for perfect cylinders only. Experiments by Toupin [20] on a beam with a dumbbell cross-section loaded at one end by a resulting force of zero persisted further through the specimen, this showed that St. Venant's Principle is not always applicable for arbitrary cross-sections. Because of this there was a need for a more general principle. Using a criterion that involved energy-decay inequalities developed by Knowles [21], Toupin obtained the upper bounds for "characteristic decay lengths" [22]. While discussing St. Venant's Principle in plane linear elasticity, Horgan [23] found an exponential decay with distance from the applied load for the stress irregularities at interior points given by:

$$\sigma = Ke^{-kz} \tag{2.12}$$

Where z is the distance to the loading point and K and k are constants. The inverse of k is the length

known as the characteristic decay length. He also showed that this length took the form of:

$$\lambda = b\sqrt{E/G} \tag{2.13}$$

Where b is the maximum lateral dimension, E and G are the Young's Modulus in the fibres direction and longitudinal shear modulus respectively. In more anisotropic materials the ratio E/G will have a higher value resulting in a larger decay length and slower decay of stress [18].

2.3 Stress concentrations in bending tests

While performing a four point bending test the force imposed on the specimen is transmitted through the loading rollers which are cylindrical and made from a much stiffer material so that it will not flex significantly or deform during the experiment and influence the results. The loading noses have a finely ground surface free of indentation and no sharp edges as specified in some of the ASTM norms to enable uniform contact between the specimen and noses across all its width. With this said the contact between a cylinder and a flat specimen is (theoretically) but a single line, and so this generates the first problem with applying force through cylinders. The high contact stresses directly beneath the loading roller may cause cracking in this area [24].

On top of causing premature failure, the stress concentration may affect the stress distribution along the full length of the specimen. During a study Berg et al. [25] analysed short beam three point bending composite specimens using finite elements he found that the distribution of shear stress never reached a state comparable with classical beam theory. Another study [26] on beams with low span-to-width ration showed that the yield stress concentration effects were never mitigated by the St. Venant's Principle affecting the stress distribution throughout the whole specimen. Both of the previous studies assumed a uniformly applied concentrated load with a small area rather then with simulated contact.

Later investigations [14] done in ABAQUS using contact theory on their numerical simulations on unidirectional composites found that contact stress distributions under both loading and supporting cylinders is close to an ellipse. It also showed that high stress concentrations occur in a very small vicinity to the loading area and that shear stress is slightly greater near the loading nose than the supporting one. The shear stress along a section near the rollers does not follow the classical parabolic assumption of the beam theory, as the maximum shear is not found in the centre of the section but rather near the top surface close to the loading nose. This value is also higher than classical beam theory by a factor of 1.14. He concluded that using four point bending instead of three point reduces shear stress concentrations by 20%. The reduction in the maximum compressive bending and transverse stresses can prove important in avoiding local damage under the loading cylinders was also among the conclusions.

Although it seems that the only area to have concentrated stress on the test specimen would be directly under the loading roller due to the nature of the contact between the flat sample and cylinder that is not the case. Most of the times there is a zone in the vicinity of the loading cylinder on the tension side of the specimen that undergoes a phenomenon designated by wedging. This is the second problem

that arises from the application of force in four point bending. By applying the load through cylinders only the surface of the specimen is being loaded rather than its entire cross-section, this gives birth to wedging stresses [11]. Wedging stresses affect the distribution of tensile stress on the side opposite to the loading rollers and the tensile stress originated from the pure bending moment and the compressive stress given by the descending roller are overlapped at the bottom side of the specimen.

The wedging stress, depicted in Figure 2.3, was later that year summarized and explained with a study form Carus Wilson [27] displayed at Timoshenko's Theory of Elasticity. The experiment from Carus was a three point bending test and using a polarized light he showed that the stress distribution beneath the central loading roller is normal taking into account the contact stresses. However when analysing that cross-section the stress distribution did not take the linear form. The stress at the tension side of the specimen was smaller than the expected results given by beam theory as the radial compressive force from the roller counteracted the tension produced by the moment but only in the cross-section directly under the loading area. The wedging stress then takes the value of 0 just to either side of the contact zone and later becomes tensile usually presenting higher stress than beam theory predicted as described in the graph below, this phenomenon is what leads test specimens to premature failures near the loading noses [24].

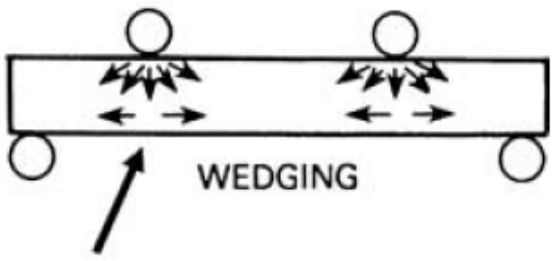

Figure 2.3: Forces involved in wedging process [24]

The geometry of the test sample has a great impact on how the wedging stresses take part in the stress distribution. Wedging stresses are affected by parameters such as span to depth ratios and the relation between inner and outer spans. Studies from T. Zhai et al. [6] and Xiaolong Dong et al. [7] using finite element analysis reveal how the stress distribution varies with different parameters. Starting with the first mentioned, it begins by studying the stress distribution over the entire inner span of the test sample and observing the changes while varying the inner span (l) to depth (t) ratio and maintaining the stress at the load-span at 600MPa according to Eq. (2.8). When inspecting the graph produced by the results they noticed that for a ratio of 1.33 the wedging stress seemed to disappear and thus there might be another reason for the existence of said stress or else the phenomena would show itself in every test run. Another conclusion drawn from the graph is that the stress distribution in the pure bending section of the specimen is not exactly uniform even after the wedging stresses have dissipated. By changing the l/t ratio the maximum tension might occur in different parts of the sample, for example for low ratios the peak stresses can be found at the middle of the span while the high ratios have a much more uniform stress distribution but, at the ends of the span, stress is primarily controlled by wedging

and this is where the maximum stress is encountered. The results from this study fell right in line with previous experiments done by Yates an Miller [28]; and Güngör and Edwards [29] according to T. Zhai et al., where mechanical tests done to specimens with a inner span to thickness ratio l/t of 1 failed at the mid span whilst specimens with ratios of 2,5 broke near the loading noses.

Further along the study by T. Zhai et al. [6] they went on to analyse the stress distribution across the whole mid-span though this time the parameter being varied was the ratio between support span (L) and loading span (l) L/l using finite elements. After plotting the graph from the results seen in Fig. 2.4 below, it's much easier to observe the evolution of the stress distribution. There is a noticeable fluctuation in the stress at the pure bending, especially for ratios lower than 3. Their conclusion was that testing geometries had to be taken into account when calculating mechanical properties with four point bending.

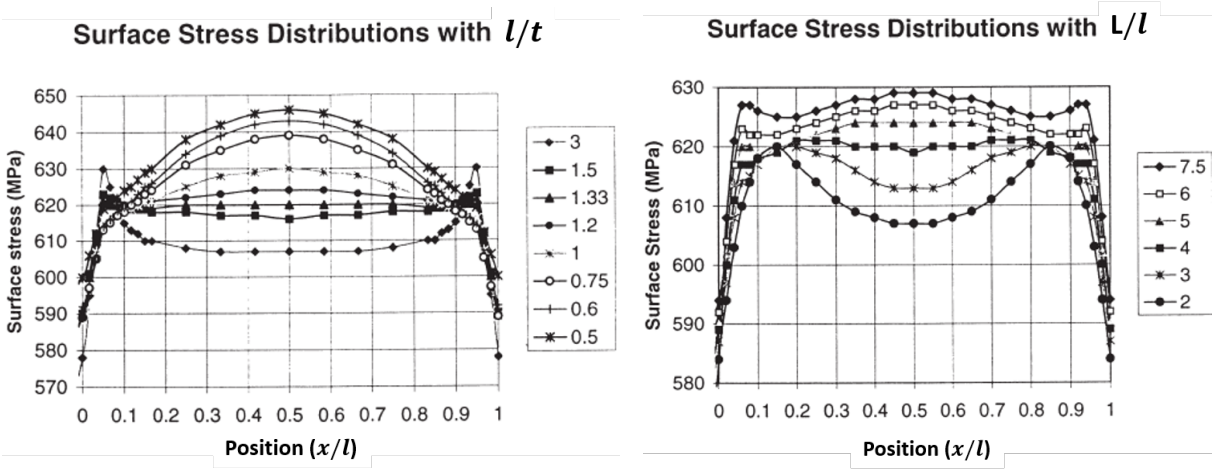

(a) Stress distribution along the span between the two inner rollers with varying inner span to thickness ratios [6]

(b) Stress distribution along the span between the two inner rollers with varying outer span to inner span ratios [6]

Figure 2.4: Stress distribution of four point bending specimens between the inner loading cylinders

The other study mentioned earlier, the one done by Xialong et al., showed once again that the stress distribution in the pure bending section was not uniform. They start by presenting two figures which show the response of the material with each change of the inner span/outer span ratio l/L, the first figure is from a specimen with 1mm of thickness and the second one is 2mm thick. Previous discoveries are present in the figures, increasing the inner span while the outer span remains constant will give rise to a stronger influence of the wedging stresses and by analysing both of these graph it's easy to see the same effect represented in Fig. 2.5, where higher values of thickness present a more pronounced wedging stress near the loading roller section than thinner samples.

The first new conclusion taken from the author of the study was the observation that the stress distribution changes when the applied load increases. In the elastic region the wedging stresses were predominant in almost every test run with one test having its peak stress directly under the loading nose. When the load is increased to ensure the sample is in plastic regime the graph obtained is dramatically different. The maximum stress of the specimen can either be found at the ends of the inner span in case of low values of l/L ratio or in the mid span of the pure bending section for higher values of l/L.

They recommend using an inner span always less than $\frac{1}{2}$ of the outer span suggested by four point bending standards. This is true for a sample thickness of 1mm as the figure changes once again when the thickness is raised to 2mm, with a thicker geometry the wedging stresses reinstate their dominance over the end sections of the inner span much like the elastic stage. Though the non uniformity of stress at the mid-span is becoming more apparent, the points at which the stress begins to rise due to wedging are all placed much closer to the middle section then before. Low l/L ratios have almost no length of the specimen without the influence of wedging. At higher l/L ratios the stress near the loading noses is higher and there is still a tendency for the stress values to rise in the mid-span but it is in a much lesser magnitude than the previous sample geometry.

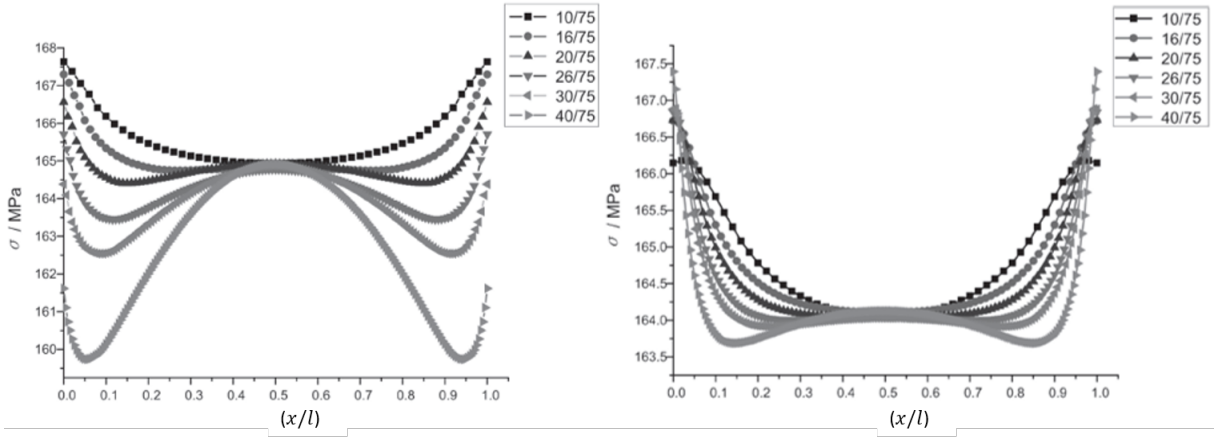

Figure 2.5: Stress distribution along the inner span taken from the study done by Xialong [7] with a thickness of 1 mm (left) and 2 mm (right) in plastic regime.

2.4 Optimization of specimen geometry (similar studies)

Many mechanical tests suffer from the same problems, since stress concentrations are often found where the specimen meets the fixture either through grips or contact. These can lead to early failures and unreliable results due to an unknown amount of stress. The ideal scenario for the researchers is far different, they want a breaking point located in a cross section that every single variable is known to better evaluate the properties of the material tested. To ensure the test sample will fail in a predetermined area researchers have to guarantee that that area is the most loaded across the entire specimen, this can be achieved with a few improvements in geometry. Many specimens for various test types had their geometry improved by researchers over the years, though four point bending specimens stayed relatively unchanged. To withdraw inspiration for improvements to apply to the four point bending specimen geometry we will look towards other types of tests and the work done towards reaching a test zone as the most loaded of the specimen.

Today tensile of standardized test specimens counteract the stress concentrations caused by the direct application of loads by having a larger volume of material to distribute the increased stress while the uniform test section remains at a smaller cross-section (dog bone specimen). The heads of the specimen end up with an overall lower stress value than the prearranged failure zone. The heads of the

test samples and the uniform test section are usually connected by a traditional quarter circular notch to provide a smooth cross-section transition [30].

With the increase in contact are that leads to lower stress values at the connecting point between specimen and testing machine the new stress concentrator is the notch introduced for the transition of cross-sections. Despite being necessary to connect both parts of the test sample this detail has a serious influence on the stress distribution in its immediate presence by concentrating nominal stress,

$$K_f = \sigma/\sigma_n \tag{2.14}$$

Is the usual way of quantifying the stress concentration factor where σ is the maximum stress located around the root of the notch and σ_n is the nominal stress in the uniform test section. As shown in the previous expression high values of K_f mean high values of maximum stress and generally lead to brittle fracture or crack initiation in case of fatigue testing [31]. However some materials are not influenced to such a degree, stress concentrations are not as big of a problem for ductile materials as they can plastically deform and redistribute the stress [32]. Many studies have been made and many graphs charted regarding the evolution of K_f in relation to the type of loading and notch inserted. Its easy to observe that abrupt transition with small radii bring forth higher values of K_t and so should be avoided and to mitigate stress concentration a smooth notch is the best option especially near the end of the transition [30].

Despite knowing that smooth transitions result in lower stress concentration factor values researchers still wanted to find the ideal transition geometry. One of them observed Nature to see how She dealt with stress concentrations. Inspired by the shape of trees and how they split their branches and roots Mattheck and Burkhardt went on to apply the concept in the field of engineering design copying a tree's growth mechanism in a chain link as an example [33]. The discovery of a tree's improved notch shapes later lead to the development of graphical way of generating varying radius fillets by Mattheck based on the tree's preference for triangular transitions called the method of tensile triangles [34] and describes a way of creating safer notches rather than one extremely dangerous and abrupt notch.

Another researcher, Baud [35], compared shoulder fillets to a jet of water under laminar steady state flow as if a large tank of water had an opening at the bottom. The constant velocity of the flow of water could be transported to a mechanical component as a constant tangential stress along the transition fillet. That results in a minimum stress concentration factor and since the solution to the hydrodynamic problem was known the shape of the fillet was easily created with a few adjustments.

Other ingenious methods of optimizing in stress concentration factor were attempted, Sonmez [36] much like Baud, relied on a thermodynamic analogy in order to find the lowest energy state, that also meant the lowest tangential stress for a fillet boundary shape. This study concluded that it was possible for a fillet with common circular arc to have a 20% higher stress concentration factor than the resulting optimized fillet. Again, in trying to optimize the stress concentration factor in a fillet Das et al. [37] employed an ESO algorithm (evolutionary structural optimization). This removes material that did not have influence on the overall structure of the component building an optimum shape, both of these

studies had roughly the same results as the one from Baud.

While conducting tensile tests on a particle-reinforced plastic composite, Garrel et al. [32] using the ASTM D638 Type IV flat test specimens noticed that the fracture of the sample with reduced ductility always started where the uniform test section ends and the curved transition begins. This effect did not show on the tests with unreinforced plastic as it deformed extensively without fracture. After reaching the conclusion that this must be the result of a stress concentration and it could prompt an underestimation of the materials true characteristics it led to an investigation on the sample's stress concentration factors. One of the objectives was keeping the overall size of the specimen the same since longer and bigger tension specimens require more material and a more costly injection mould die. With this in mind Garrel used finite element analysis to compare the recommended geometries from the ASTM standard and the ones they had created. The type IV geometry from the original test where the stress concentration effects were observed has a double-arc transition so, alternatives with single-arc and double-arc geometries were analysed. For single-arced notches the conclusions were obvious, the larger the arc's radii the lower is the resultant K_f and for the same length of specimen this value was reduced from 1.112 to 1.040. As for the double-arc transitions the radii nearest to the gripping head (r_2) does not affect the stress concentration factor. So by reducing r_2 the curve that begins at the test section (r_1) can be increased achieving a K_f of 1,051 also lower than the ASTM's recommended geometry and again revealing that larger arcs near the end of the transition are ideal to reduce tress concentrations.

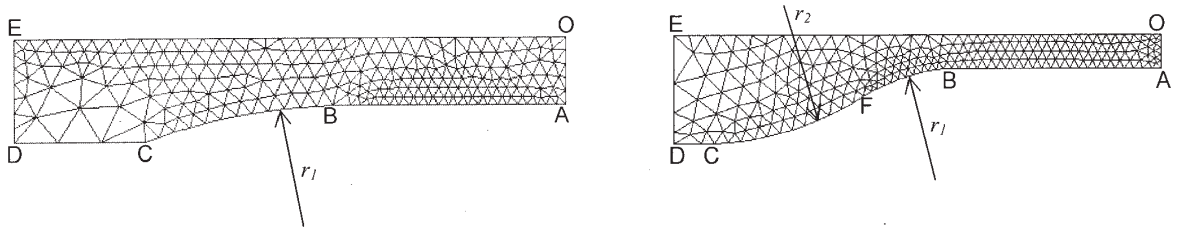

Figure 2.6: Single arc transition (right) and double arc transition (left) [32].

Another study, this one from Simões et al. [30], takes aim at current mechanical fatigue test standards, analysing the possibility of using variable radius curves to construct a better transition between the larger heads and slimmer test section of test samples, using a gradientless optimization algorithm which relied on a simple premise, remove material where the stresses are low and add where they show higher values. The objective was to reach a uniform von Mises stress along the notch to meet Baud and Neuber's criteria [38]. They applied the algorithm and compared the results to typical push-pull, rotary bending and alternate bending fatigue tests to the redesign specimens. As seen in their results the optimized test samples can achieve the same stress concentration factor with a much shorter specimen length that requires less material and is more buckle resistant. The optimization is especially effective in the lower ranges of radius to width ratios (r/w) whereas at high values of r/w the difference becomes less apparent.

More recently a mechanical test was brought to the light of day as it gained the interest of researchers. The biaxial fatigue was demonstrated to be very important to the main application of materials such as aluminium alloys and composite materials. This includes most notably their common use

on aircraft components that are subjected to a biaxial stress state originating from external loads where tension, bending, shear and torsion stresses can be biaxially combined along with the local peak stress [39]. Of course, not only aircraft suffer from the aforementioned stress combinations as most practical problems involving metal fatigue in machinery and structures are associated with multi-axial loading [40]. This being a new test the scientific community started experimenting different loading apparatus and specimen geometries to acquire the material properties. So, when Baptista et al. [41] enrolled in their study many geometries had been used by different authors with no consensus on a geometry accepted by all. Variations of the cruciform test specimen were proposed in trying to optimize its geometry with the main objective being a uniform strain and stress along the test area of the sample that is subjected to the biaxial loads while assuring that it presents the highest levels of stress across the whole specimen. One way found by Hanabusa and Takizawa [42] to guarantee the uniformity of the stress fields in the centre of the sample was to laser cut small parallel slits along the arms so stress measurement errors would be kept at a minimum. Other attempts lead to the use of wider arms and non-circular notches to elevate the stress values in the centre of the test specimen and reduce the stress concentrations on the transition from arm to test area [43].

Lastly to further alleviate stresses from the arms of the specimen and concentrate them on the test area, specimens with reduced central thickness were experimented with. This iteration still allowed for the stress and strain fields to be uniform all across the intended failure zone. The transition could be made with either straight or curve profiles or even have a two staged thickness reduction connecting the central area to the arms with an intermediate step [44] but displayed the better results when it took on the form of a spline profile [45]. In order to further build knowledge on the specimen's geometry Baptista et al. [41] studied a sample that included most of the previous advancements like elliptical notches and thickness reduction. They then related the variables with the arm thickness so that the geometry could be applied to a variety of specimen sizes rather than being specific to one particular dimension. The end result showed how the optimal variables evolved when the arm thickness was changed. Taking a look at the elliptic fillet related variables the ratios between both radii and arm thickness were very dependent of the arm's dimension at lower values and seemed to converge as the arms gained thickness. As for the central thickness reduction ratio it reveal itself to be the most important variable that was studied having a dominant effect over all other variables. According to Baptista et al. the centre to arm thickness ratio and the variables linked to this reduction, the centre spline radius and the spline exit angle have the same effect. If they were to be increased the peak tension would rise while the uniformity of the stress field becomes less uniform [41] in similar fashion to four point bending and the wedging stresses in thinner specimens as seen before.

2.5 Failure Mechanisms

In order to better understand the disadvantages and shortcomings of the four point bending test knowledge of the failure mechanisms of specimens subjected to its constraints is required. These failure mechanisms can be divided in wanted and unwanted, depending on if they affect or not the final calcula-

tion of the material properties. In this subchapter several of these mechanisms will be reviewed across different material samples and specimen types so that the work done in this thesis might be applied to multiple material and specimens.

Starting with the failure modes that allow for a more correct measurement of properties we have quasi-static failure through compression and tension. Both occur when the material's strength is surpassed by the stress imposed by the test. While investigating flexural failure in unidirectional glass fibre reinforced thermoplastic, Chen et al. [46] came across a cooperative fibre buckling mode in low Modulus matrixes. Where the fibre located on the compression surface suddenly and simultaneously buckled upwards with none of the fibres actually breaking, through about two thirds of the thickness of the test sample, Figure 2.7(a). When testing a similar material with higher value of Young's Modulus, the failure mechanism remained compressive although it revealed to be significantly different, surface delamination started to appear in small blocks of fibres which then buckled shortly after. These microbucklings did not show any considerable drop in stress, yet at higher loads more and more bundles of fibres began to buckle and the stress drop was no longer negligible, Figure 2.7(b). The buckling only occurred on the outermost fibres, this failure mode was also experienced by Shih and Ebert [47]. It seems that the first of the failure mechanisms is governed by the matrix Young Modulus as its failure stress is equal to the composite's shear modulus. The second failure mechanism is controlled by the matrix strength and adhesion between the matrix and the fibres [48, 49].

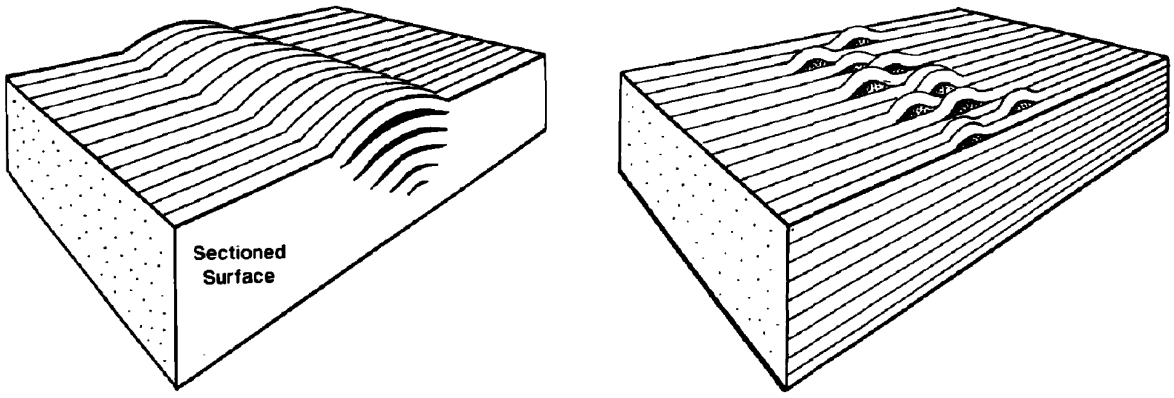

(a) Cooperative microbuckling [46].

(b) Surface delamination splitting microbuckling [46].

Figure 2.7: Failure modes observed by Cheng et al. [46]

Sandwich specimens have been on the rise and its facings are also prone to compressive failure as it is the highest uniaxial loaded part of the sample. In the case of a sandwich specimen with composite facings, the compressive side is usually the most favourable to fail as its compressive resistance is weaker in comparison to its tensile strength. Compressive facing failure was observed by Daniel et al. [50] in a carbon/epoxy facing with aluminium honeycomb core and a reinforced outer section so it would resist failure mechanisms such as indentation and shear. The failure was dominated by the carbon/epoxy's compressive strength and presented a higher value than under direct compression test due to the support from the core preventing a tendency of buckling. A similar failure mode is the compressive facing wrinkling or localized short wavelength buckling tough it's more commonly observed in sandwich

structures where the core has a lower modulus through-the-thickness as in typical foam cores [50].

As for failure on the tensile side of the specimen Shih and Ebert [47] noticed when testing a glass-fibre reinforced sample the formation of small ridges by fibres along the surface followed by matrix cracking perpendicular to the direction of tensile stress. The number of these cracks and bulges increases as more load is applied, matrix cracks tend to elongate and join together increasing their overall size. These cracks were only a couple of fibres deep but break every fibre they come across leading to a higher load on the remaining fibres and eventually failure of the test specimen.

Next one up to be discussed is shear failure. In bending, for lower span-to-thickness the shear stresses overcome the compressive tension leaving short beam four point bending test vulnerable to shear failure. Of course, the four point bending test has other uses besides calculating properties from the uniform uniaxial tension produced between the inner rollers. Because it has less stress concentration directly underneath the loading noses some researchers prefer it to three point bending for calculating shear strength of materials. So, shear failure can be another desired failure mode, and such was the case of Cui et al. [15] they were using three and four point bending to find the interlaminar shear strength of a unidirectional fibre-reinforced composite. However they found the four point variation more suitable for the measurement with a short beam configuration in order to trigger the respective failure mode. The tested specimens displayed horizontal cracks in either one or both vertical sides of the sample in between the outer support cylinder and the inner loading nose. The cracks appeared not only in the mid-plane of the specimen, despite classical beam theory predicting that it is the most loaded area by shear of the cross-section and were spread randomly within 30% and 70% of the specimens thickness due to the true stress distribution in Figure 2.8. This very same failure mode was also observed by Marshall [51] when testing smaller ratios of distance between supporting and loading roller to specimen thickness although only reporting cracks materializing along the neutral mid-plane of the specimen. It was witnessed again by Parry and Wronski [52] when testing span-to depth ratios of 5, however the interlaminar shear failure could be suppressed with the assistance of external pressure.

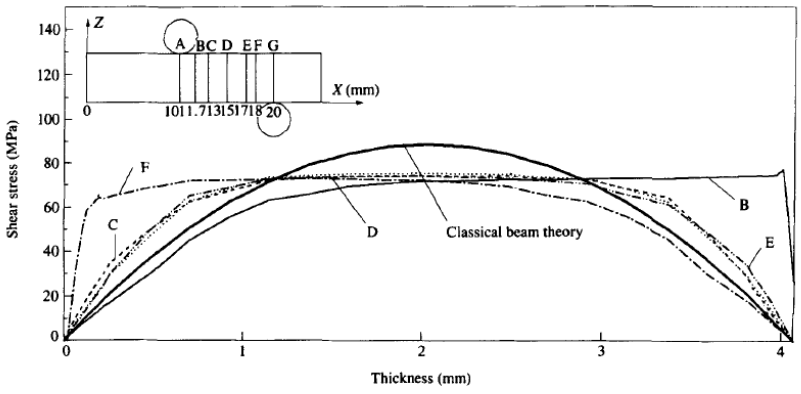

Figure 2.8: Shear stress distribution in four point bending [15].

Sandwich specimens can also suffer from shear failure, these structures are built so the facings can handle the axial stresses while the inner core is responsible for bearing the transverse efforts resembling a multi-material I-beam. During a four point fatigue test of two configurations of sandwich beams

Belouettar et al. [53] visually observed shear failure of the aramid fibre core for two orientations showing cracks propagating through said core with later signs of shear buckling along the vertical cells in the region where the transverse effort is dominant. This kind of failure is much more commonly reported in three point bending tests [50] as the main purpose behind that test arrangement is to test samples in shear.

The best and most prominent example of an unwanted failure mode is kinking or indentation as it is caused by the way the loads are imposed on the test specimen rather than stresses predicted by classical beam theory. Indentation failure is the dominant mode in highly localized external loads, for example, forces transmitted through spots or lines. The material under the loading roller, in the case of four point bending, reaches its yield strength and deforms under triaxial stress state of compression due to the bending momentum, compression applied from the loading cylinder and shear stress derived also from the downwards force of the cylinder. The damage from the triaxial compression leads to kinking also described as compressive buckling and compression creasing by other researchers [52]. Kinks are often just a catalyser for other failure modes, specimens don't break directly because of the compression of the roller, however they promote failure of a more visible failure mechanism. In the instance of the research of Parry and partner, they witnessed microscopic damage under the roller in Figure 2.9, they even had to polish the surface through a few layers of the carbon-fibre reinforced plastic that were unloaded in various stages of the test to obtain clear evidence of kinking The kink's propagation eventually lead to interlaminar cracks and failure at the span-to-thickness ratio of 5, for the other ratios tested, the highest one valued at 40, showed signs of kinking . The specimens with ratio of 15 appeared to evolve in the same manner displaying compressive and tensile failure zones meeting at the neutral mid-plane succeeding the kinking's growth.

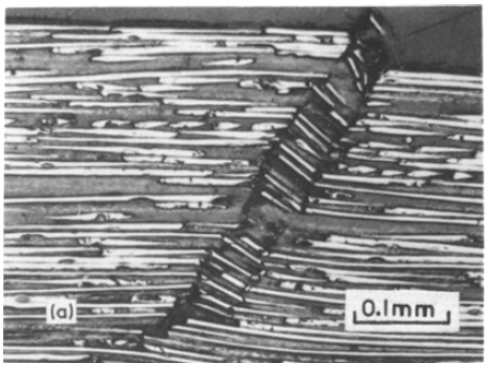

Figure 2.9: Microscopic kinking under the loading rollers [52].

Indentation failure mechanism is a predominant failure mode of sandwich construction and again results from localized loads under the loading roller. The compressive downwards force from the cylinder yields the core deforming both the core and the facing. Several studies have reported the mechanism in three point bending [50, 54, 55] while Sha et al. [56] observed indentation failure in four point bending along with shear core failure and facing failure. Their experiment resulted in a load-deflection curve with two peak loads. Before the first peak the behaviour of the specimen was almost linear and at the peak the two inner rollers begin to penetrate the sample and crushing the core followed by a decrease in load.

The depth of the penetration increases as the displacement advances and stops its development at the second peak maintaining its depth for the rest of the test, Figure 2.10. Due to the accumulated strain of the core under the rollers, shear fractures formed and spread throughout the thickness leading to core shear failure. The sandwich structures that are more sensitive to this accelerated failure are the ones which incorporate a low through-thickness stiffness core such as foam cores.

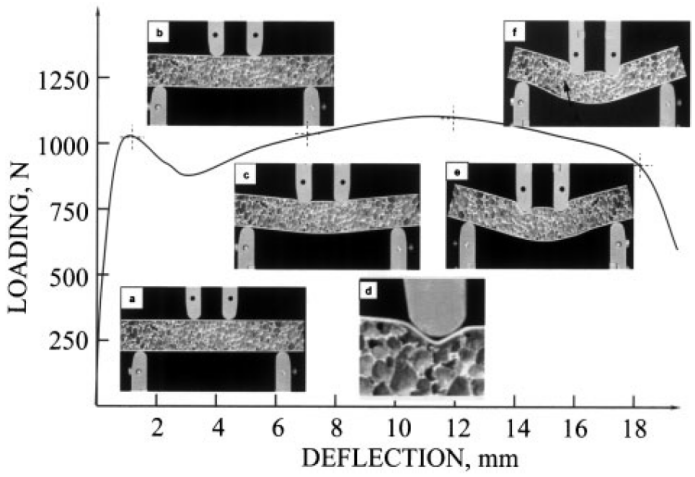

Figure 2.10: Load-deflection curve of indentation failure in four point bending [56].

2.6 Design Of the Experiment

In the everyday life people often play and experiment with certain processes, for example cooking, in order to learn the outcome or even discover a better way of dealing with that process, this may come out of need or perhaps curiosity. In engineering, experiments are an important tool to find new product designs, optimized parameters, maximized performance so on and so forth. These experiments are tests in which variables suspected of having influence in the process are changed in a controlled manner to observe the response of the system and rationalize the reason behind its changes. These experiments involve careful planning and several strategies may be used by the experimenter to find the influence of the input factors on the output response of the system or process [57].

When the investigators have a clear understanding of related and similar systems to the one that they are about to conduct the experiment on, it's often used a best guess approach where arbitrary combinations of factors are used and then adapted according to the output results. This strategy works moderately well due to the extensive technical and theoretical knowledge of the person in charge of the experiments [57].

A different strategy is to define the whole set of factors and the values they can take (levels), select a baseline and while varying one factor throughout its range keep the remaining factors constant and record the output, this is called the one-factor-at-a-time approach. The influence of a variable is determined by constructing a graph for each varying factor which are simple to interpret. One big flaw of this strategy is that it may fail to detect a possible interaction between several factors. If the baseline

levels for the factors that are kept constant were to be of a different value the resulting graph could be unrecognizable in relation to the one from the original experiment [57].

On the other hand, the factorial experiment strategy requires the factors to vary together and does not suffer from the serious disadvantage as the previous strategy. Since the factors are varied simultaneously, factorial experiments require less experimentation in order to study the same factors plus their interaction. Although this method is very efficient with the collection of data, by adding factors and levels the number of tests needed rapidly increases. If there are k factors with n levels the number of tests required would be n^k, that is all of the possible combinations. This presents a problem for the more in-depth studies with a greater number of factors and levels and becomes a serious obstacle that consumes too much time. It is at this point where the fractional factorial experiment strategy comes into play, which does not require all of the test combinations often cutting the number of runs necessary by half and still provide good information about the influence of the factors and their interaction [57].

2.6.1 Basic Principles

While these strategies can analyse the data very efficiently, the results might be inconclusive without the use of statistical design of experiments that submits the data to statistical methods. This helps to mitigate experimental errors during the data collection and so, bring out meaningful results from an experiment with some uncontrollable variables [57].

In order to analyse the data through statistical methods the experiments must follow the three basic principles of experimental design: Replication, randomization and blocking. While conducting an experiment, if the experimenter would just collect one set of data he could not say for sure if the factors that he was studying truly influenced the response or if was just the combination of experimental errors and uncontrollable variables. By comparison if the tests were replicated several times the experimenter could estimate the experimental error and not only determine a more precise estimate of the effect of the factors using the mean result of the tests, but also if the acquired data is statistically different [57].

External and uncontrollable factors may act randomly throughout the course of the experiment. If tests were done in batches one of them could be severely affected by these factors and that particular set of tests would be either favoured or put at a disadvantage in relation to the other experimental tests. This involuntary introduction of systematic bias into the results will hinder their validity. A way of “averaging out” the influence of the external factors is to randomize the order of the tests in the experiment. This way it randomly assigns external variables to each run therefore validating the statistical methods used to analyse the results [57].

In addition to the random uncontrollable factors there are also nuisance factors. These types of variables can be controllable or uncontrollable, but they are always measurable, so the experimenter knows when they will affect the test runs. For example, in the case that one batch of material is not enough for the whole experiment then multiple batches of material have to be used and can often contain some differences between them. Since this supplier variability is not a factor that we wish to study but nevertheless it still influences the results of the tests, experimenters will often use a blocking technique.

This separates the results of one batch of material from the other dividing the observations into blocks and then statistical methods are applied to each block. The blocking technique boosts the precision of the comparisons between the influences of the factors of interest by disposing of the variability between blocks which is often greater than the variability within the blocks [57].

2.7 FDM Printing Parameters

The last stint of this work, the experimental testing of the test specimens, will require a manufacturing process for said specimens. The chosen process was FDM or Fused Deposition Modeling so knowledge over the process is necessary build a well thought out specimen. This section will focus on the impact that the printing parameters have on the material properties.

It is a well known fact that the printing parameters of FDM manufactured components affects their mechanical properties and behaviour. To better tailor the specimen to the needs of this work research was done to help select the printing settings.

When investigating how the time between layers affected the mechanical properties of the tensile specimens Tomás Martins [58] had to print samples with different sizes. Using the same parameters for the infill % and Shell wall thickness and witnessed different overall bidimensional densities for the specimens. This resulted in him having to use a blocking method to account for the difference in the mechanical properties and the results from the smaller specimens could not be compared with the larger ones.

A parameter that usually defines the printing quality is the layer height. Chancón et al. [59] studied the effects of the process parameters on the mechanical properties of PLA specimens in tensile and three point bending tests with layer thickness being among them. For the intended printing orientation the specimens did not demonstrate much variance except for the lowest thickness where the tensile strength rose while the flexural strength declined. The maximum plastic strain in both tests decreased with greater values of layer height and the opposite trend was verified for the stiffness. A finite element done by Y. Zhang and K. Chou [60] with the properties of ABS in conjunction with experimental comparisons revealed that for larger layer thicknesses the specimens showed increased levels of distortion. This was not reported by Chancón et al. since their work was done using PLA that by having a much lower extrusion temperature it has lower levels of distortions. One other convenience of using taller layer thickness is the decreased printing time.

In their research Chancón et al. also studied build orientation of the specimens, in a vertical, on-edge and flat orientations, this reveal the anisotropy of the PLA test samples through the disparity in results from each orientation to another in Figure 2.11. More importantly, the vertically printed specimen fractured in a brittle nature while the on-edge reveal a more ductile behaviour with the flat wise specimen being in between the previous two with a slight ductile behaviour.

Additionally Chancón et al. studied the effect of the feed rate and noted that the variation of maximum tensile and flexural strengths for flat oriented specimens were significant with a few atypical results. More importantly is its effect on the material's plastic behaviour, the maximum strain at fracture of the spec-

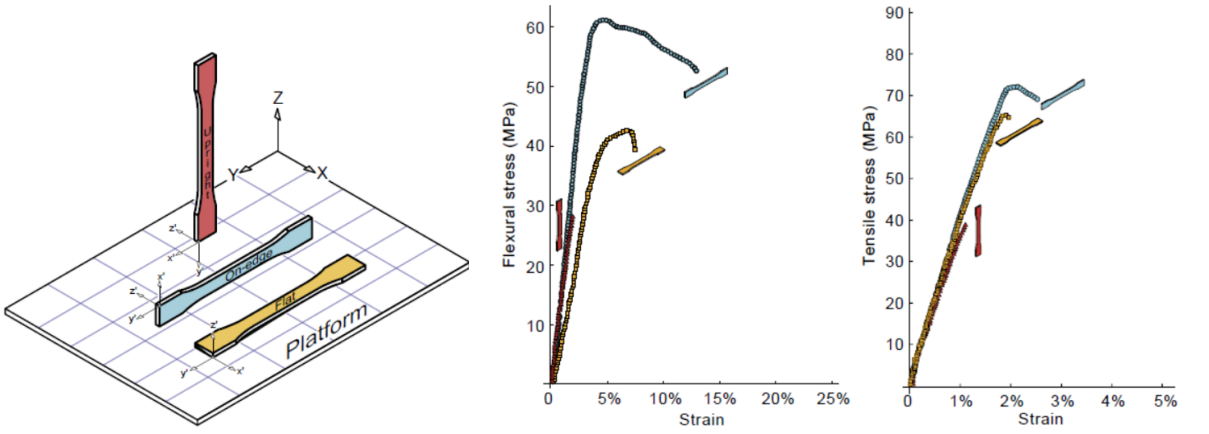

(a) Specimen orientations in Chancón's study [59]

(b) Average results of three point bending (right image) and tensile (left image) tests of Chancón's study with layer thickness at 0.24 mm and a feed rate of 80 mm/s [59]

Figure 2.11: Specimen orientation and mechanical test results while varying feed rate [59].

imens decreased in both types of test reducing their ductility though with lower impact than increasing layer thickness.

Sood et al. [61] in their work concluded that small raster angles lead to longer rasters, this results in higher temperature differences within the same raster which will increase the residual stresses along the direction of the raster culminating in higher distortion values using ABS.

One hidden parameter that also affects the properties of the final test samples is the time between the deposition of each layer. The study done by Tomás [58] for ABS prints reveals that for larger amounts of time between depositions the difference in time brings no significant statistical change in the material properties while for smaller differences in time such as reducing from 87 seconds to 38 seconds resulted in a 5% increase in maximum stress.

The parameters that are inputted on the slicing software are not the only ones affecting the material properties of the prints. A study by Tymrak et al. in 2014 revealed that for similar printing parameters the results from the mechanical tests presented a significant discrepancy while tensile testing specimens with different parameters using various printers and slicing softwares. This lead to a conclusion that the printers had different unstandardised settings that can have serious effects on the end results being even more influential than the controllable parameters [62].

Chapter 3

Methodology

The main objective of this work is to test a geometry that can lead the maximum stresses generated by four point bending to the intended zone of testing while keeping the advantages of the original bending test such as the close to uniform stress distribution [6] over a large volume of the specimen. The most trustworthy way to find and test this geometry would be by mechanical experiments. This way, the results of the tests would be real and could be assumed as correct.

Mechanical tests often provide us with the most realistic results possible when executed properly. Yet when factors like time and resources have to be taken into account physical testing is not always the best move to make. In order to reach the final objective a geometry for the test specimen that can achieve the main goal of the thesis has to be found. So throughout this work, picking parameters and adjusting them will be indispensable to attain the final geometry.

For the sake of trailing a logical path on the way to encounter and test the final geometry a decision had to be made. Despite being the most reliable method to obtain material properties being mechanical testing, as said before it takes up to many resources. Thus numerical studies will be taking place before the final mechanical tests. Since going in blind with the direct goal of finding the optimal geometry would be a bit of trial and error, first we must develop our understanding of what effect the chosen parameters have. The purpose of the preliminary numerical study (Study 1) is to understand the influence that the chosen parameters, also called target parameters, have on the stress field of the specimen while removing any influence from any other geometric parameter.

Equipped with the knowledge of the first study a second numerical study (Study 2) will be done this time with the intention of finding the final geometry. It will start with a given level of the parameters and will progress towards the desired geometry. The geometry for this second study will be closely related to ASTM D6272-10 in order to be more easily be compared to current works involving four point bending. Both of these studies will be done with a finite element analysis program considering that it saves resources, time and can provide information on stress fields at the full length of the specimen.

With the numerical studies, the optimal geometries are uncovered and the stress concentrations are known, or at least that would be if the simulation could be trusted. To validate the findings of the numerical studies, a batch of specimens were printed and tested via four point bending. Only after the

tests are done and their results analysed that definitive conclusions can be taken.

3.1 Specimen geometry

After research described in the Background on how other types of mechanical tests dealt with the problem of stress concentration in the areas where forces were applied, and looking more closely at the example of the tensile test specimens, a “dog bone” geometry was chosen. Illustrated in Figure 3.1 this geometry will be used because the reasons why it was suitable for tensile testing seemed to be applicable to the four point bending test from a theoretical point of view. Namely a larger contact area between the specimen and the test device to reduce stresses in areas where forces are imposed and a zone of curved transition to reduce stress concentration inherent in the specimen width reduction. This transition will have an elliptical configuration to provide a large apparent radii at the root of the notch where the problems that arise from stress concentrations are more prominent. This while trying to keep the total length of the test specimen on lower values so the flexural strength of the material won’t be severely affected.

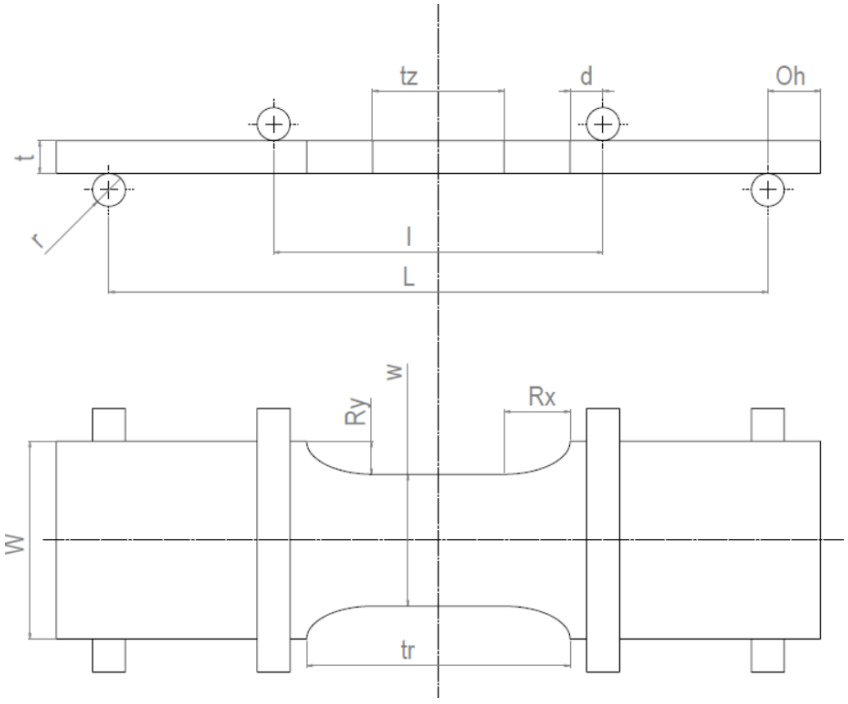

Figure 3.1: Specimen’s technical drawing with supporting and loading rollers.

The radius of the curvature of the ellipse at the root of the transition zone V_a can be calculated through the following expression [63] using the dimensions of Figure 3.2:

$$r_{V_a} = \frac{b^2}{a} \tag{3.1}$$

Since this thesis was developed at the Product Development Laboratory, there was a possibility of

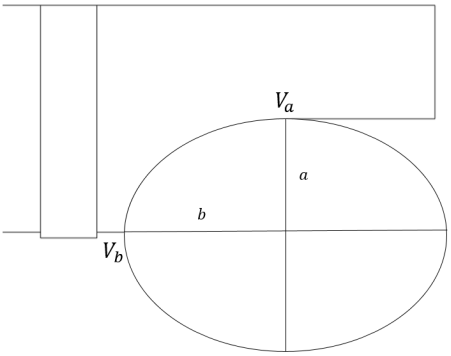

Figure 3.2: Specimen's elliptical transition.

creating any sort of specimen with any configuration of novel parameters due to access to 3D printing technology. Though the possibility is there, not every researcher has access to the technology plus the materials and samples that are being tested can be incompatible with unusually shaped geometries. This means that the specimen has to be easy to machine, for this reason no thickness changes were implemented along of the whole specimen, unlike the cruciform specimen, as it would require an extra dimension of machining compared to a simple dog bone specimen.

3.2 Selection of target parameters

To provide a larger contact area between the specimen and the test fixture the width in that region has to be increased. So the first parameter to be analysed will be the width difference between the test zone and the area where the loads are applied. This width difference is used in other types of mechanical testing to reduce stress concentrations caused by mounting brackets or clamps. Since the loads can be distributed through a larger contact area, for the same load the stresses on those regions will tend to have smaller values. In turn, this parameter deviates the higher stress values from under the loading rollers, thus lowering the effect that the loading rollers have on the four-point bending test. This difference in widths will be assigned to the parameter R_y seen in Figure 3.1 and it will also be the value of one of the radii of the curved elliptical transition. Due to the introduction width difference there needs to be a transition zone to connect both of the different width along the specimen. With transition zones there are new stress concentrations being introduced at the root of said transition. The more abrupt the transition the higher these stress concentrations are, with this transition being elliptical, by increasing the value of R_y the more abrupt the transition becomes as seen in subchapter 2.4. So, with the increase in width difference the stresses in the contact zone will diminish and will concentrate instead on the root of the transition created by the width difference.

Since there is a transition, a transition length has to be defined. So the second parameter to be studied will be this length and be associated to the variable R_x. The parameter will be coincident with the remaining radius of the elliptical transition in the same way of the fist parameter. The increase of this parameter results in a smoother, less abrupt transition and for the root of the transition has the opposite effect of R_y decreasing stress concentrations. In usual four point bending tests the length of

the specimen located between the loading rollers is defined as one half or one third of the supporting cylinder span. This leaves two ways to integrate the transition length into four point bending geometry. One can either maintain the distance between the loading rollers or the test zone length. In the first option the increase in R_x will lead to a decrease in test zone length partially removing the advantage of using four point bending as seen on the right of Figure 3.3. The alternative is keeping the test zone length constant while shifting the transition length and consequently, the loading span. This in turn results in an increase in the specimen's total length/thickness ratio represented in the left part of Figure 3.3. As mentioned earlier, this unwanted increase causes the material properties to change [13].

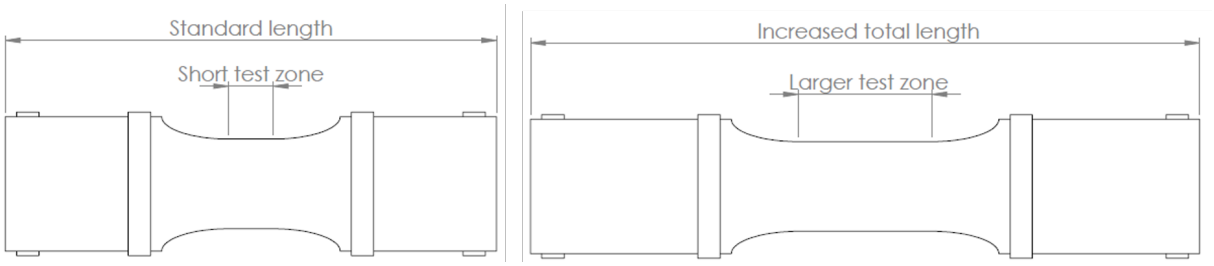

Figure 3.3: Exaggerated options for applying large transitions

In this next study the volume of material with constant section in the test zone will be kept constant and the effect of the second option will be reduced due to the fact that the distance between the load and support rollers has been fixed due to needs explained later. If there is an increase in the length of the central zone the added span of the specimen will be kept at a minimum since the increase of the central area will not add length to the remaining parts.

The third parameter to be analysed is the distance between the load rollers and the beginning of the transition zone. The principle behind the choice of this parameter is related to the Saint-Venant effect [17] and wedging stresses [7], this parameter aims to distribute the induced stress concentration in the vicinity of the load rollers As previously mentioned these concentrations may be neglected given sufficient distance to the area of uneven stresses. Note that this parameter also has the same side effects as the transition zone length mentioned in the previous paragraph.

The parameters R_y and R_x end up completely defining the transition by being both their radii. This of course means that the beginning of the transition, on the wider side, forms a 90° angle with the side wall and is tangent to the side of the specimen's test zone. The fact that the parameters for the length and width of the transition can completely define it help reduce the number of factors at play in the study and simulations. By summarizing the transition in this manner, a lot of options are being left unattended because in only encompasses a quarter elliptical transitions.

3.3 Study 1

As mentioned earlier, this first study aims to understand the influence that the target parameters have on the stress state along the specimen. As this is only a preliminary study a simple way to understand the effects of each parameter is to use the one-factor-at-a-time methodology. By varying one

of the target parameters while keeping the remaining target parameters unchanged, it becomes easy to understand the effect that each parameter has individually on the results. It is a test that can be summarized by modelling the specimens through computer aided design according to the range of target parameters chosen, loading these geometries with finite element software and drawing conclusions from the results. This being a simple test it fails to detect interactions between parameters with the sole focus on uncovering the varying parameter's influence for those specific fixed target parameters [57]. In the case of this work, the other function of the preliminary study was also to determine if a factorial experiment strategy was required in the chance that the interactions were very noticeable. This lead to the creation of more series with different base values to confront this possibility, increasing the number of simulations but also dispel the need for a more complex preliminary study.

Firstly, every geometric parameter besides the target parameters will be specified so to provide easier results to compare. All the variations of target parameters are defined and then the work moves on to finite element analysis. Specimens are built in SolidWorks and imported to Siemens NX. In this program the meshing is applied as well as the boundary condition on the specimen. Since this is only a preliminary study there is no need to refine the mesh to great extents, as long as the results form each simulation are comparable within this study conclusions on the trends of the stress values can be taken. Also another less planned objective of this first study is to find flaws in my finite element model and improve it for the second study in which is important to get close to the stress values produced in real four point bending tests. After the simulation finish running, the stress values are taken from the area underneath the loading rollers, the root of the transition zone and the supposedly uniform test zone. Gathering and organizing the results is the next step, with this graphs will be made for each varying target parameters and their influence on stress will be easily visible. There is no need to quantify this influence as it is not the thesis main objective and the FEM for this study will not be validated by mechanical test results. After conclusions are taken there is enough information to move on to the search of the optimal specimens, study 2.

3.4 Study 2

This study's main goal is to find the final geometry parameters that will be used to print a test specimen and apply the four point bending mechanical test. Since, as seen in the last study, the parameters can all be raised to lower stresses in specific places, one can use exaggerated parameter dimensions in order to reduce the stress concentrations. For example, if stress is to high under the roller either the parameter R_y or d could be increased this in turn would lead to a raise in stress at the transition and as a result would force a higher value of R_x ending up with an oversized test specimen, a huge waste of material and span-to-depth ratio. This would most likely produce misleading test results derived from the increased inner span between the loading noses [13]. This study will start by finding the best configuration of parameters for a specimen with limited span in order to avoid the previously mentioned errors. The objective for the final specimen geometry is for the von Mises stress in the contact zone to be equal or slightly lower than the uniform stress encountered at the test site and for the transition stress to be as

low as possible.

Since what we want to compare is the stress in the contact zone with the stress at the mid-span, stress concentration factor can not be used as a term to describe this comparison. While regular specimens built entirely according to the standard have constant section values throughout the whole of the middle section the same can not be said about the dog bone geometry that has a larger width near the loading rollers. The regular specimens can have the same nominal value of stress in the denominator for calculating a stress concentration factor and since the section in both regions are equal it would be a fair comparison. In the new geometry if a stress concentration factor were to be used under the loading rollers it would have in its denominator the stress calculated theoretically for that cross-section which is different to the section at the mid-span making it difficult to achieve the comparison we want. For the region under the loading rollers it will be used a stress coefficient (SC) between the stress in that area and at the mid-span. Although in the transition zone the term stress concentration factor can still be used correctly as the maximum stress occurs in the part of the transition that has the same section as at the mid-span, for the sake of consistency we will use a stress coefficient also with the stress at the mid-span in the denominator, this will allow for fair comparisons between the stress zones.

$$SC_r = \frac{\sigma_r}{\sigma_n} \tag{3.2}$$

$$SC_t = \frac{\sigma_t}{\sigma_n} \tag{3.3}$$

Where SC_r is the stress coefficient for the zone under the rollers and compares the stress in that zone, σ_r, and the nominal stress at the mid-span σ_n, and SC_t is the stress coefficient between the stress at the transition σ_t and the previously mentioned stress at the mid-span. So the objective for this study is a specimen with $SC_r = 1$.

This study's geometry will resemble the past study very closely altering only the fixed parameters. This geometry will be closely related to the regular four point bending specimen described in ASTM D6272=10. In order to keep the specimens all with the same overall length the overall transition zone can not be allowed change length or else either the specimen would be forced to increase in length or reduce the test zone. Analysing the problem from a mathematical point of view if the inner and outer spans and the test zone length are to remain constant throughout the tests the sum of the parameters R_x and d will be a constant value. If the same load is applied in all the tests the same nominal stress will theoretically be achieved, so for now the restrictions put on the simulations are:

$$\begin{cases} R_x + d = \frac{l - tz}{2} \\ \sigma_r = \text{const.} < \sigma_n \end{cases} \tag{3.4}$$

Where σ_r is the maximum von Mises stress found in the region beneath the loading roller, σ_n is the nominal stress at the test zone.

The study will be carried out in the following fashion, five different combinations of $R_x + d$ will be selected with a arbitrary value of R_y to start, then for each combination the value of σ_r will be brought to

within 5 to 10% of the σ_n by adjusting the R_y parameter on all the chosen combinations of $R_x + d$. After that's done the next step is figuring out what combination provides the best overall stress coefficients from the results. This will find if its more effective to increase the parameter R_y or d to achieve the desired stress beneath the loading cylinder while keeping the transition zone as unloaded as possible.

Since there is no way of lowering both of the most loaded zones of the specimen culminating in either high stress at the transition or under the rollers another case will be explored. Trying to equalize the stress under the loading roller with the nominal stress will require a high value of R_y resulting in a high stress coefficient at the root of the transition. Instead, by allowing the stresses at the transition and at the loading zone to be over the nominal stress but their values close to one another, the maximum stress coefficient, be it at either of the two locations, would be decreased. To achieve this goal the parameter R_y has to be adjusted much in the same way as explained above until an approximately equal stress is found in the loading and transitions zones. This can be translated into $SC_r = SC_t$.

The study starts by defining the the fixed parameters so that the specimens are as close as possible to the ASTM standard. The following step is choosing the combinations of $R_x + d$ that will be studied along with the starting arbitrary value of R_y.

The next task is constructing the finite element model which will be different due to problems found in study 1. The biggest change is in the contact zone, after noticing some discrepancies between maximum stresses under the loading rollers with the same geometries and simulation parameters, corrective measures had to be taken. A study was then conducted to analyse the effectiveness of the new contact zone in obtaining precise results. Since this study will produce the final geometries that will be tested, it is in our interest to refine the critical areas until the maximum stress values converge to decrease the influence of the element size on the results.

The flow of the study will then depend on the result of the first simulation as there are two milestones that need to be reached: maximum stress in the contact zone equal to the nominal stress in the test zone; and maximum stress in the contact zone equal to the maximum stress in the transition zone. If the maximum stress under the loading rollers is higher than in the transition zone then another simulation is needed with lower values of R_y. This is an iterative process that continues until both milestones are reached, and all there is to it is adjusting the parameter R_y to get closer to the milestones.

After the two milestones are reached for the five combinations of $R_x + d$ conclusions can be drawn and the optimal geometry for ten millimetre thick specimens with $SC_r = 1$ and $SC_r = SC_t$.

3.5 Experimental testing

In order to conduct a successful experiment that can be recognized by the scientific community there is a certain standardized procedure that must be followed. In this work the experiment is the analysis of the material behaviour and calculation of its material properties. The material in question will be 3D printed plastic created through an addictive manufacturing technology named Fused Deposition Modelling or FDM for short.

The printer that will be used for this work will be the Ultimaker S5 depicted in figure 3.4(a) that

belongs to the Laboratório de Desenvolvimento de Produto do Departamento de Engenharia Mecânica of Instituto Superior Técnico and the slicing software is Ultinaker Cura 4.4 [64] used to produce the G-code that will be inputted in the printer. To perform the mechanical testing in four point bending it was used the Universal Testing Machine Instron 5566, figure 3.4(b), present at the Laboratório de Ensaios Mecânicos e de Materias (LEM^2) equipped with a 10KN load cell.

(a) Ultimaker S5

(b) Universal Testing Machine Instron 5566

Figure 3.4: Equipment used for printing and testing

When attempting to print the test specimens, a conclusion was quickly reached, it would be needed more than one roll of plastic filament to complete the print of all specimens. To avoid using two different material batches and so avoid the need of a blocking technique, the specimen was scaled down in size. The fixed parameters would be all scaled proportionally to one another while the target parameters would undergo a small study following the methodology from study 2 to obtain the optimal parameters once again. A thickness was chosen so that every specimen could be printed with the same filament and leave some room for printing errors.

The printing parameters inserted into the Cura slicing software were selected according to the research in section 2.7 with the end goal of producing a fragile specimen. This type of specimen would show the location of the highest stress concentration upon failure [32]. Each print contained one specimen of each type and they were marked accordingly. For the first print every specimen would be marked with a 1 and adding to it, the regular specimen is marked with an A, the $SC_r = 1$ specimen with a B and the $SC_r = SC_t$ specimen with a C. So, for example, the regular specimen print on the fourth run would be called specimen 4A.

With all the specimens printed the work moves on to mechanical testing. The Universal Testing Machine records force, deflection of the loading rollers and time. Forces are not comparable between specimens as they are not part of the material properties, so it is usually used stress to compare two different geometries. Specimen A's stress values can be reached through equation (2.8) present in the

ASTM standard. Theoretically the same equation would lead to the stress at the mid span of specimens B and C but this is yet to be verified. So, if tested while only recording the outputs from the Universal Testing Machine the results from specimens B and C can not be compared to the ones obtained from the fully ASTM built specimen A. In order to get comparable results between specimen types equation (2.8) needs to be validated for use in the new specimen geometries for four point bending.

To put it simply this validation will need the use of equation (2.9), strain gauges and equal printing parameters in the test zone of the specimen. By knowing that the specimen types were purposely built to have equal printing parameters in the test zone it is a known fact that the Young Modulus will be equal throughout the specimen types. When recording the strain that the specimen goes through in the mid span the only thing left to calculate the Young Modulus is the stress values. By assuming that equation (2.8) can be used to calculate stress, the Young Modulus can be calculated and if they are shown to be equal then equation (2.8) is validated for this application.

After this stress results from the mid span can be compared. When one specimen records a lower maximum stress at the mid span this means that it reached the maximums stress of the material in the stress concentration zone sooner. This can already tell what specimen type had the lowest overall stress coefficient. By multiplying the maximum stress at the mid span with the stress coefficients from the numerical studies the supposedly maximum stress of the material is calculated. If this calculated stress is equal throughout every specimen type then it means that the stress concentration values are correct validating the numerical studies of this work.

Chapter 4

Numerical Studies

4.1 Study 1

4.1.1 Selection of fixed parameters

In order to obtain easy results to compare and draw conclusions from, fixed parameters are as important as the target ones. These parameters aim to let a researcher focus on the effects intended to be studied by removing influences caused by other geometric variables or external influences. In the case of finite element studies the conditions in which the simulations will take place are identical and the results have little to no external interference between them. If the remaining geometric parameters are fixed the results will only be influenced by the target parameters.

To further facilitate a direct comparison of results, the values of stresses between the various analyzes of the study better be similar. For that to be done all conditions were maintained in the central test zone so that the stress at the mid-span would theoretically have the same value throughout every simulation in this study regardless of the changing target parameters. Therefore, the applied forces and the dimensions of the test region must be fixed to ensure an equal stress field on the central area.

Normally four point bending tests are carried out with a distance between the two central cylinders of half or one third of the span between the two outer ones cylinders according to ASTM D6272 [3] for the purpose of calculating Flexural Properties of Unreinforced and Reinforced Plastics and Electrical Insulating Materials. If such a restriction was applied to this study, by changing the parameters R_x and d the distance between the load and support cylinders would be forced to change. By changing the lever length, changes would also come to the momentum applied in the central zone. To prevent the conditions from being altered in this sector a decision was made to set the distance between the support and load cylinders to 50mm. With the same reasoning and goal as before, the total force applied to the test specimen was kept constant in the simulations at 400N for the sake of maintaining the momentum enforced on the central test zone not altering the momentum applied to the mid-span.

The dimensions of the specimen were all fixed with the exception of the parameters planed to study, the values for the fixed settings are described in the table 4.1 and all parameters unique to finite element simulation and analysis were kept fixed and will be discussed in a later subchapter.

Table 4.1: Fixed parameters for study 1.

Fixed parameters	
Specimen's thickness (t)	10 mm
Length of test zone (tz)	50 mm
Width of mid span (w)	40 mm
Roller diameter (r)	10 mm
Overhang length (Oh)	25 mm
Distance between the support and load cylinders (a)	50 mm
Total force (F_0)	400 N

4.1.2 Selection of target parameter levels

When conducting a one-at-a-time study it is supposed to set base values for the parameters and vary just one of them throughout their entire spectrum. The baseline values are fixed within each series, for example when varying R_y the other two parameters R_x and d remain constant as seen in table 4.2. By doing the study in finite element analysis software there were no limits to the dimensions that the geometry could take, so both the base values of the parameters and the selection of the value spectrum were chosen for the sole purpose of showing the evolution of the results. Not every series is completely separate from one another, there are some simulations with the same input in two different series to help bridge the difference between them.

Table 4.2: Parameter levels (Varying R_x on the left column, R_y in the centre column an d on the right column). Units in millimetres

Rx	Ry	d		Rx	Ry	d		Rx	Ry	d
5	10	10		20	5	10		20	25	0.5
10	10	10		20	10	10		20	25	5
15	10	10		20	15	10		20	25	10
20	10	10		20	20	10		20	25	15
25	10	10		20	25	10		20	25	20
15	20	10		30	25	10		20	5	10
20	20	10		30	30	10		20	5	15
25	20	10		30	35	10		20	5	20
30	20	10		30	40	10		20	5	25
15	20	20		30	25	15		30	25	10
20	20	20		30	30	15		30	25	15
25	20	20		30	35	15		30	25	20
30	20	20		30	40	15		30	25	25

The study started by doing three series of 5 simulations, varying a different parameter in each one, to provide us with the essential information about the evolution of the stress field with the variation of these individual parameters. The three series on the first row would have been sufficient, but in order to get a

glimpse of interactions between variables some additional simulations were made by changing the base values, these can be seen in table 4.2. These additional simulations will be tasked with determining if a factorial experiment is needed to study the interaction if they are too dominant. Through the different series on the same column only one baseline value is changed from one to the next. This is to help either understand or confirm that changing baseline parameter's effect in a part of the study not meant for it as can be seen further in the result discussion.

4.1.3 Construction of the finite element model

The program used to perform all finite element analysis in this work was the Siemens NX 2019. For the initial modelling of the specimen and support and load cylinders the SolidWorks 2018 program was used due to a greater familiarity with the program.

The following construction description is divided into three parts: The creation of the 3D model of the specimen and rollers in computer-aided design (CAD). The elaboration of the finite element model where the 3D model is discretized and transformed into elements and nodes for future analysis (FEM - Finite Element Model). Lastly the generation of the simulation model where the boundary conditions and forces are applied and is where the finite element analysis (FEA) is performed.

The creation of the CAD starts by outlining the specimen profile, in this step two of the target parameters are defined, R_x and R_y, both components that describe the ellipse in the transition of specimen widths. Dimension Z is then added along with the cylinders with the parameter d in mind to simulate the loading and supporting rollers. Since the specimen plus roller assembly is symmetrical, it was decided to model only a quarter of the total specimen in order to save computational resources and simulation time. The files were saved in .STEP format to be imported into Siemens NX. Once the NX file was opened, a preparation step was made to facilitate the process of creating the FEM using the Split Body tool to split the sample into two in the region where the loading cylinder made contact with the specimen.

Moving to FEM, it is initiated by creating 3D Collectors used to define the physical properties of each component. All parts of the model have received PSOLID properties with CTETRA(10) elements. Ideally the element type that should be used is CHEXA(8) elements with 3D Swept Mesh as they help control shear locking effects that appear when solid elements are bent [65] furthermore it is faster to obtain simulation results. Unfortunately a mesh using CHEXA(8) could not be generated due to the curved geometry of the specimen. The use of CTETRA(10) instead of the simpler CTETRA(4) is due to the extreme stiffness of these elements in regards to bending. This stems from the fact that the edges of the tetrahedral elements are perfectly straight while the CTETRA(10) elements have an additional knot in the middle of each edge that defines the curvature of each edge allowing them to deform more freely [66] resulting in more accurate simulations. The dimensions of the elements of the test piece and rollers are 2 mm. After generating the mesh, it was used the Mesh Mating tool to join back the specimen and leave an edge that will be needed for the next step. Elements of two millimetres are overly large compared to the length of the zone directly affected by the cylinders for convincing results. As the available computational resources could not handle a full FEA with all the elements of adequate dimensions it was necessary to

establish a dimension of general elements and a refined dimension to apply to areas prone to premature failure. The edge on the cylinder contact line with the specimen was set to 0.2 mm and the elliptical transition edge 0.5 mm with the Mesh Control - Size on Edge function, the meshed FEM file can be seen in Figure 4.1. Since its just to see how stress fields change with the parameters inputted no kind of absolute precision was required so no convergence of the mesh was studied. Finally, materials were defined to complement the meshes created, the specimen was awarded the ABS and the rollers the AISI 1005 steel, both materials drawn from the Siemens NX included material table. The results from this first study do not need to be absolutely accurate as they will be compared only between each other and not with real life results, so a convergence study was not performed as of now.

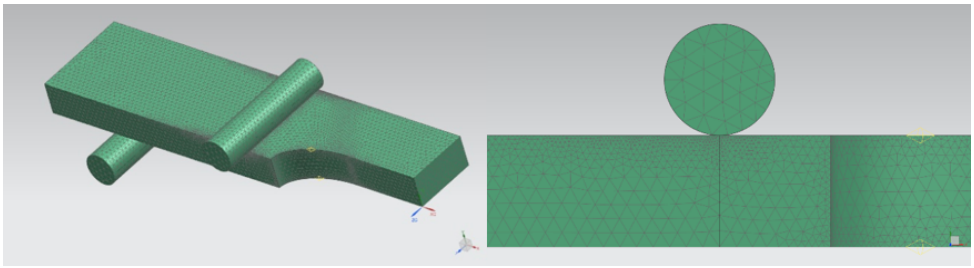

Figure 4.1: FEM of the quarter specimen for study 1

The final step is the FEA, this is where forces and constraints are applied. It starts by choosing the SOL101 Linear Statics as the solution type to analyse the linear region of the specimen. The boundary conditions of symmetry were applied to the faces of the specimen and rollers that were coincident with the symmetry planes. The support cylinder was fixed at all degrees of freedom. The different configurations of the specimen will probably have different values of vertical displacement on the loading rollers which in turn means that each simulation will have distinct final contact zones after the specimen bends if the loading rollers is forced to travel only along the Y axis and fixed in every other degree of freedom. This makes it very hard to do a fair comparison if, in every simulation the loading rollers end up in all sorts of distances relative to the edge used to refine the mesh. A decision was made to only apply a downwards force to the load cylinder this did not restrict the movement of the cylinder but only subjected it to a force of 100N in the $-Y$ direction. Thus the roller always rests at the same point of contact travelling with the specimen along X axis. The advantage of this approach is knowing exactly where the roller will be in contact with the specimen at the end of the simulation, this allows for more accurate and equal placement of the refined mesh areas in all analysis, though not completely realistic. The contact between the specimen and the support and loading rollers was modelled with the Surface-to-Surface Contact tool using a coefficient of friction of 0.3 [67]. When doing this operation one should select the most refined surface of the two as the source surface to get the most contacts, the meshed quarter specimen with full constraints and loads is portrayed in Figure 4.2.

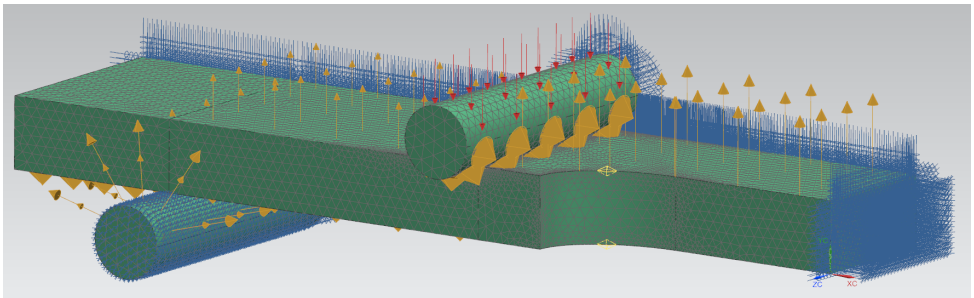

Figure 4.2: FEM with the applied boundary conditions of the quarter specimen for study 1

4.2 Study 2

4.2.1 Selection of fixed parameters

For the geometry to not be completely disassociated from the conventional specimen configuration and to be more easily accepted by researchers the geometry is based on the existing ASTM D6272-10 [3] standard and the dimensions are described in table 4.3. The main difference from the last study is that the overall length of the specimen will be fixed and set at sixteen times the value of the thickness. The span between the inner loading rollers will be one half of the span between outer support cylinders as in the ASTM standard. This configuration was chosen over the one third of the outer span as the interval between the support and loading cylinder is shorter requiring a greater amount of force from the roller to produce the same bending momentum. This will bring forth higher compressive stresses under the loading zone and shear stresses near the the roller resulting in a worse scenario than the one third configuration if the researcher wants to test bending strength that calls for a failure in the uniform stress zone. So, if the specimen fails through compression/tension at the constant cross-section zone the other configuration should be able to do the same. The one half configuration is also advantageous for allowing the four point bending specimen to retain its main feature, the large amount of material being put under the same condition even while its being partially used to make a transition between two different widths.

The diameter of the support and loading cylinder will be 10 millimetres and is equal to the ones found in the testing fixture located at the laboratory and in the standard. As said before one objective of this study is reaching a conclusion on what is the best way to lower the stress coefficient under the loading roller, to do this the space given to the transition has to be a fixed value. The length of the test zone that holds a constant cross-section is fixed along with the fixed inner span to limit the transition's total length. As the large amount of material being put under the uniform stress, which four point bending tests are designed to provide, is one of its main feature the length of the test zone must not be reduced to a point where this advantage is gone. The length of the test zone will be half of the inner span with the other half being dedicated to the transition. The width at the mid-span and the overhang will be respectively one fourth and 10% of the span between the outer cylinders as it is establish as a maximum in the ASTM standard.

Table 4.3: Fixed parameters for study 2.

Fixed parameters		
h	Specimen's thickness	10 mm
L	Specimen's outer span	160 mm
l	Specimen's inner span	80 mm
tz	Length of test zone	40 mm
$R_x + d$	Length of the transition	20 mm
w	Width of mid span	40 mm
r	Roller radius	5 mm
Oh	Overhang length	16 mm
F	Total force applied	666.8 N

4.2.2 Selection of target parameter levels

For the first part of this study the intention is to find the best combination of $R_x + d$ possible in terms of lowering the stress coefficient at the root of the transition zone. To achieve the desired value of SC_r in the contact area the parameter R_y can be raised indefinitely even when the distance between the constant cross-section region to the loading cylinder is fixed. A finite element analysis will be done to five different configurations of $R_x + d$ with a initial arbitrary value of R_y which will then be adjusted after seeing the results from the first simulation in order to reach the objective of a stress coefficient beneath the loading rollers equal or lower than 1.

The values of both the combinations of $R_x + d$ and the initial R_y are displayed in the table 4.4, keep in mind that the initial values of the parameter R_y for all the combinations following the first were chosen with the results obtained from the first simulation taken into account to try and get closer t the objective from the start.

Table 4.4: Different combinations of $R_x + d$ and initial R_y.

$R_x + d$	R_y	
19+1	30	Adjust R_y until $SC_r = SC_t$
		Adjust R_y until $SC_r < 1$
18+2	30	Adjust R_y until $SC_r = SC_t$
		Adjust R_y until $SC_r < 1$
17+3	30	Adjust R_y until $SC_r = SC_t$
		Adjust R_y until $SC_r < 1$
16+4	10	Adjust R_y until $SC_r = SC_t$
		Adjust R_y until $SC_r < 1$
15+5	20	Adjust R_y until $SC_r = SC_t$
		Adjust R_y until $SC_r < 1$

4.2.3 Construction of the finite element model

The finite element model for this study is very closely related to the previous study's model with some slight improvements. It once again begins with the construction of the CAD in a familiar software with the same method behind the modelling only creating one quarter of the full specimen due to the symmetries it presents. This time the supporting and loading cylinders were trimmed to only feature the half that makes contact with the specimen to reduce the computational power needed. Since irregularities in the results under the loading roller were a noticeable problem an alternative method of refining the mesh in that area was enforced. Rather then splitting the body of the specimen once directly under the contact zone it was split twice, one to each side of the contact area with a distance equivalent to the dimension of the refined mesh elements. This way the elements are forced to assume a fixed pattern from simulation to simulation minimizing errors from the random mesh generation, as shown in Figure 4.3.

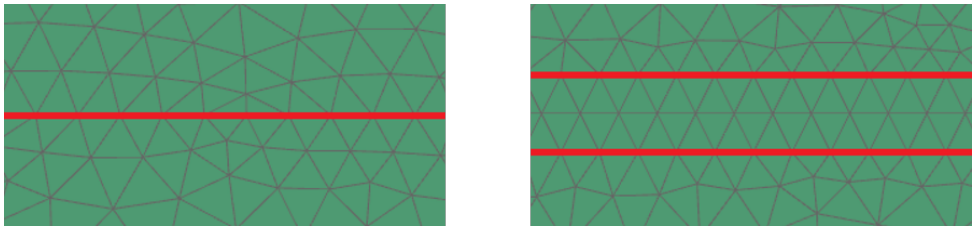

Figure 4.3: Comparison between the mesh from study 1 (on the left) and from this study (on the right) with Split Body edge highlighted in red

Continuing the construction of the FEM, the 3D Collectors generated at the start use the same CTETRA(10) elements created with the 3D Swept Mesh tool. They were assigned the material properties of ABS for the test specimen and AISI 1005 for the rollers, both already existent in the Siemens NX material table. The dimensions given to these elements is 1.5 mm to all parts of the specimen and the supporting roller while the loading cylinders were set to 0.5 mm. The contact zone was refined and has elements of 0.2 mm. The same treatment was also given to the edge of the transition zone on the compressive side and the edge of test zone that is parallel to both rollers and is a part of the symmetry plane. This is to avoid doing comparing von Mises stress of elements and nodes as in the first study.

In terms of a convergence study to see if the dimensions of the elements in the critical areas are refined enough, due to low computational resources a small series of simulations were done to determine to what degree these elements in the critical regions could be refined given a time limit of 5 hours for the simulation of the first specimen constructed in this study $R_x = 15mm \quad d = 5mm$ and $R_y = 20mm$ to finish. With these element dimensions the stress results do not yet converge at the contact zone as if reduced to 0.15mm the stress increases 10%, and when the same is done to the transition zone the stress raises by just 1%. The chosen parameter for the simulation are definitely not the best when it comes to calculating the stress in the contact zone but it is what was possible at the time.

The final step before the simulation can be made is to place all of the boundary conditions on the finite element model. The force applied to the upper flat surface of the trimmed loading cylinder was calculated from equation (2.8) to produce a 20 MPa uniform stress at the mid span. The same approximations were made to the movement of the loading rollers as in chapter 4.1. The contact zone was modelled using

a coefficient of friction of 0.3 and a Max Search Distance of 0.1. The regions of contact were selected manually and the more refined region was designated as the source surface. On the flat bottom of the trimmed supporting cylinder was used a Fix Constraint and both the rollers and the specimen were put under a Symmetry Constraint.

To try and relate this work with existing ones, the wedging stress phenomenon was put under the spotlight on the regular parallelepiped specimen to see if the stress distribution along the central span of the test subject was in any way similar to already established simulations of T. Zhai et al. [6]. To achieve this, after the main set of simulations were finished an alteration to the mesh was made. The edge that runs across the middle of the specimen that due to the symmetry constraints sits along the x direction on the tension plane was refined to the same degree as the other points of interest with elements sporting a dimension of 0.2 mm. The refinement location at the symmetry plane was chosen out of an assumption, because in T. Zhai and his partners' work the location along the width where the measurements were taken is not described. Following the simulation these elements were selected and plotted into a graph using the respective function in Siemens NX.

4.2.4 Mesh comparison

To prove that the changes in the meshing of the specimen improved the precision of the results a small sample of twenty simulations were done using both mesh construction on a specimen from study 1 with $R_x = 15mm \quad R_y = 10mm \quad d = 10mm$. The overall mesh elements were sized to 1,5 mm and the refined edges 0,2 mm, the boundary condition imposed were constant throughout the simulation with the downwards force applied to the roller set to 100N. Every time that the cycle of build, solve and extract results was over the program Siemens NX was restarted to ensure that a random mesh was generated.

Chapter 5

Experimental implementation

This chapter's main objective is to describe every detail of the procedure used to build and test the three types of specimen while providing explanations about the chosen printing parameters, the thickness of the specimen and steps taken immediately prior to the four point bending test.

5.1 Selection of material and equipment

The manufacturing of the test samples for the four point bending test will be done via FDM using a single printer. Using two or more printer would be quite faster if not for the study by Tymrak et al. [62] about the unstandardised parameters within each different printer. So the only printer that will be used for this work will be the Ultimaker S5 depicted in figure 3.4(a) and the slicing software is Ultinaker Cura 4.4 [64] used to produce the G-code that will be inputted in the printer.

Two of the most used filament materials for FDM printing are ABS and PLA. The first mentioned is generally described as having good mechanical properties and being environmental and shock resistant. On the other hand PLA is said to be much more brittle than ABS and when exposed to heat it deforms by itself [68][69]. One advantage that PLA has over ABS is a lower extrusion temperature, this results in a shallower temperature gradient in the printed part, less residual stresses and finally less distortion. A material ideal for knowing where the highest stress concentrations are located would be a brittle material as they will not deform much in a plastic manner and thus not redistribute the concentrated stress to other parts of the specimen's body [32]. With this in mind the material chosen for the test samples is PLA. The PLA originally chosen was the one distributed by Ultimaker, every decision made during this chapter was made with this material in mind. They sell two sizes of filament and the roll that will be used is the largest weighing in at 750 g and a total approximate length of 95 metres with the reported mechanical properties depicted in the annexed table B.1 bellow. Due to someone's mismanagement of this material, when the test specimens had to be reprinted in response to defects found on the first batch there was insufficient material in order to redo everything. The material was later changed to the PLA RepRap PT 2.85 mm with 1 Kg of material rather than 750 g from Ultimaker though the mechanical properties were nowhere to be found.

The four point bending test apparatus in the laboratory does not have an easy way to measure the deflection at the mid point of the specimen. The usual load-deflection curve obtained from these kind of experimental procedures will not be available. This in turn prevents the use of the Elasticity Modulus equation (2.10) from the ASTM standard which relies on the steepest slope of the curve. If the simulation done prior are proven to be valid this fact won't bring any hindrance to the experiment since the equation did not provide the correct results for the geometries proposed during study 1 and 2.

For the new geometries of the four point bending test no current equation listed in the ASTM standard should be trusted as the simulation are not yet valid and any conclusion taken from them should not be viewed as true. Another way to reach the stress values is to know the strain and the Young Modulus of the material. In order to calculate the von Mises stress at the mid span of the specimen the strain data in that location has to be collected.

After some consulting, the strain gauges available in the laboratory were most likely unsuitable for the use in low elastic materials. The strain gauges chosen for these series of mechanical tests are the KPF-series from Kyowa purposely made for the application in plastics. The thermal expansion coefficient of the strain gauge is recommended to be close to the specimen's own properties in order to not cause unrelated strain due to the different expansions of the materials in case the temperature changes between the glueing of the strain gauge and testing. The chosen strain gauges sport a thermal expansion coefficient of $65 \times 10^{-6}/°C$ and PLA has a often reported coefficient of $68 \times 10^{-6}/°C$ [70] [71]. The main disadvantage of this equipment is the 3% strain measuring limitation, this won't allow for the whole test to be observed as the elongation at break of PLA is 5,2% though it will be sufficient to draw conclusions in relation to the validity of use of equation (2.8) on the new geometries.

5.2 Specimen geometry

The specimens used for the mechanical test part of the thesis will be the regular specimen constructed with the ASTM D6272-10 standard, a specimen that presents a stress under the loading roller inferior to the nominal stress in the test zone and finally a specimen with identical stress values in both critical areas and both of these variations are based on that same testing standard.

After running the geometries with 10 mm of thickness found in the last study through the slicing software Cura, the three types of specimen used different lengths of filament to print with the desired printing parameters present in table B.2. To comply with the ASTM standard 6 test samples of each type will be produced to fulfil the "At least five specimens".. The total filament length to print the specimens is calculated in table B.2.

According to Ultimaker's website they have two sizes of rolled up PLA and the larger one measures approximately 95 metres in length. With a total of 307 metres needed to create all of the required specimens the number of different rolls of material used would be just above 3.

Using different batches of materials for the printing of the specimens brings in the need for the use of a blocking method as described in the D.O.E. chapter 2.6 due to the introduction of nuisance factors that in this case are controllable and might have a slight effect on the results. To avoid this,

new specimen geometries will be created using the very same method as the previous study with a reduced thickness. To chose this dimension some approximations were made comparing the volumes of the regular parallelepiped specimens throughout the various thicknesses. To shorten the process the volume of the specimen was written in order of its thickness.

$$V = t \times (L + Oh) \times w \begin{cases} V = t \times (16 \times t + 2 \times \frac{16 \times t}{10}) \times \frac{16 \times t}{4} & \text{if } t \geq 8mm \\ V = t \times (16 \times t + 13) \times \frac{16 \times t}{4} & \text{if } t < 8mm \end{cases} \tag{5.1}$$

Where t is the thickness, L the span between outer supports, Oh the overhang and w is the width. By dividing the 307 metres of total filament length with the maximum allowed of 95 the outcome is how many times smaller the specimens must be to only use a single roll of material. This works since the length of the filament is directly proportional to its volume.

$$\frac{\text{Total length}}{\text{Filament length}} = \frac{307.68}{95} = 3.24 \tag{5.2}$$

$$\frac{V_{10mm}}{3.24} = \frac{10 \times 192 \times 40}{3.24} = 23703mm^3V \tag{5.3}$$

Applying the result of equation (5.3) as the maximum volume that the regular specimen must have so that all the specimens are printed from the same batch of material, the maximum thickness can be deduced:

$$V = 23703 = t \times (16 \times t + 13) \times \frac{16 \times t}{4} \rightarrow t \approx 6.9mm \tag{5.4}$$

Knowing that the maximum is 6.9 mm it was calculated the length of filament needed for the 6 mm variant of the specimen by applying the same thought process but in reverse order:

$$V_{6mm} = 22326mm^3 \rightarrow \frac{V_{10mm}}{V_{6mm}} = 3.44 \rightarrow \frac{307.68}{3.44} = 89.44m \tag{5.5}$$

If the printed specimens were built with 6 mm of thickness the total length of PLA required would be close to 90 metres. That does not leave much margin for defective printings and so the same calculations were made for a specimen with 5 mm in thickness and the total length was 42.44 metres. This will give enough room to accommodate for the approximations done and repeat defective prints.

Another smaller study was done much in the same way as study 2 though this time only focussing on configurations with very high values for the R_x parameter as the optimal specimens are located in that range. The size of the elements present on the critical areas and the loading roller remained at 0.2 mm and 0.5 mm respectively. The final dimensions of the specimens for the mechanical four point bending test are described in Figure 5.1 and table 5.1, the specimens built have as a basis the ASTM D6272-10 and assuming Sheet Material.

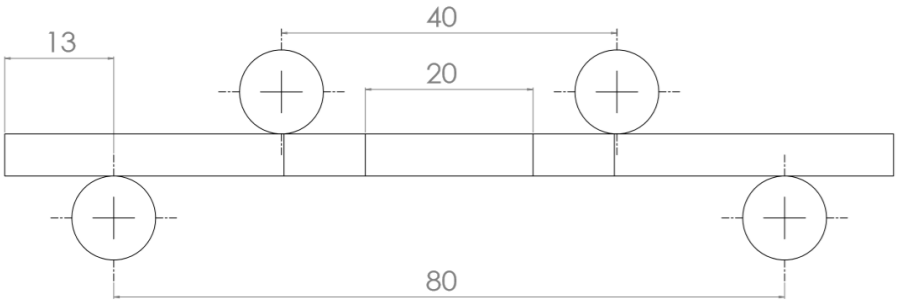

Figure 5.1: Overall dimensions of $t = 5mm$ specimen

Table 5.1: Specimen parameters, dimensions in millimetres

Specimen Type	R_x	R_y	d	w
Regular	-	-	-	20
$SC_r < 1$	9.7	10	0.3	20
$SC_r = SC_t$	9.7	5.2	0.3	20

To print 6 specimens of each configuration for a thickness of 5 mm it would take 41.62 metres of filament according to the Cura slicing software. This result does not deviate much from the approximation done earlier to find a thickness that allowed all of the test samples to be manufactured out of the same batch of material.

The printed specimens were measured with a set of digital callipers and the measurements are displayed in the table B.8. The calipers were tested on the cylindrical loading roller that has a diameter of 10.00 mm and measured always between $\pm$ 0.03 mm with an absolute incertanty of 0.01 mm.

While measuring, the calipers were always closed and reset between every data collection. The top and bottom most layers always protruded a bit more than the rest of the layers and so whenever possible the calipers were positioned to avoid the edges of the printed specimens. This was impossible to do for the groupset B and C for the mid span width. Also the measurement of the distance between the beginnings of the transitions will most certainly have some form of human error as it is very difficult not only to position the calipers at the edge of the transition but also to ensure that it is measuring in a parallel line to the faces of the specimen.

5.3 Selection of printing parameters

In this section printing parameters will be chosen for the manufacturing of the specimen with the insight gained in section 2.7. The objective is to build a specimen that shows where the highest stress concentrations are taking place by fracturing in that area. This is accomplished by reducing the specimen's ductility removing the ability to spread stress to nearby areas.

Tomás Martins [58] using the same parameters for the infill % and Shell wall thickness for different sized specimens witnessed different overall bidimensional densities for the specimens. This resulted

in him having to use a blocking method to account for the difference in the mechanical properties. In this study it is needed to compare the results from specimens with different widths beneath the loading roller and a varying bidimensional density would not allow that to happen so the infill % will be set at 100% so that the mentioned density sits still between the different specimens at 100%.

To reduce the ductility of the test specimen a larger layer thickness will be chosen. In Chancón et al. study [59] they used 0.24 mm and the same is going to be used in this work. The increase distortion when using larger layer thickness values should not be as much of a problem as it was to Y. Zhang [60] as this current work will have specimens built out of PLA rather than ABS. By using a thicker layer thickness the printing time will also be reduced.

Another of Chancón's conclusions is that the vertically printed specimen fractured in a brittle nature while the on-edge reveal a more ductile behaviour with the flat wise specimen being in between the previous two with a slight ductile behaviour, in Figure 2.11. The problem that arises from choosing the vertical orientation is the printing time more than doubles in comparison with the other two options and so the orientation that will be applied to the test specimens in this study will be the flat orientation.

Additionally Chancón noticed a decrease in ductility with the increase of feed rate. Unfortunately when printing with 80mm/s of feed rate the specimen from group B and C developed a small crack beginning at the transition and spanning the entirety of the test zone along the union between the filaments composing the wall and the infill at top side of the specimen as seen in figure 5.2. A crack near a critical area would only serve to develop stress concentrations and provide biased results implying that the transition zone has higher than normal stress coefficients. The printing speed used for this work will be 70 mm/s as it is the recommended feed rate by the maker of the slicing software, the material and the printer.

(a) Defect on a group B specimen

(b) Defect on a group C specimen

Figure 5.2: Photographs of the defects found in group B and C specimens.

According to Sood [61] smaller raster angles lead to lower temperature differences, residual stresses and distortion. For this work it will be used a raster angle of 45 degrees to decrease the chance of distortion. If the raster angle was 0 degrees the regular specimen would be entirely comprised of maximum length rasters. The other two specimens would have same amount of central rasters at their maximum length but overall they would have an average shorter raster that would stop at the curved transition

which may lead to different levels of distortion and could influence the final results. By using the 45° raster angle the difference in length of raster will be lower.

Tomás [58] reveals that significant statistical change in the material properties happen when reducing time between layers from 87 seconds to 38 seconds which resulted in a 5% increase in maximum stress. For this work every single specimen would take more than 120s to print each layer and so according to this study there should be no significant difference between their material properties. Precautions are still going to be applied and the difference in time between deposited layer will be assumed as having a non negligible effect.

All of the 3 types of specimens have the same number of layers and yet all take different times to be completed. This must mean that the time that an individual layer needs to be fully deposited is different for from a specimen type to another. To combat this all three of the sample types will be printed at the same time. This G-code needs to be repeated six times to have a total of six of each type of specimen. This way all test samples will have the same interval of time between layers. Another advantage of using this method is if one print is subjected to some odd uncontrollable conditions every specimen group will have one specimen affected by this peculiar event and help average out this disturbance making it a fair comparison between types. A slight disadvantage is if a print is defective in printing one of the specimen types it will probably affect the other two being printed at the same time rendering them all useless.

The mid-section of all the specimens located between both transitions zones will have the exact same dimensions and printing parameters which should result in equal mechanical properties throughout every specimen type the more important of which being the Young Modulus. This will allow a comparison of the new specimen's von Mises stress in that area with the regular standardized specimen through the strain collected by the gauges.

In short the previously mentioned printing parameters as well as the remaining that comprise the full input introduced in the Ultimaker Cura software are in table 5.2.

Table 5.2: Printing parameters.

Printing parameters	
Print Core	AA 0.4 mm
Layer Height	0.24 mm
Wall Thickness	0.8 mm
Top/Bottom Thickness	0.8 mm
Infill Density	100 %
Infill Pattern	Triangles
Printing temperature	205°
Build Plate Temperature	60°
Print Speed	70 mm/s
Adhesion Type	Brim

5.4 Preparation of four point bending test

The process of mechanical testing the specimens will flow as the ASTM standard implies. There are two ways of performing the tests, Procedure A is designed for samples to fail at relatively low deflection values and is primarily aimed towards calculating the flexural modulus of the material. Procedure B is meant for materials that undergo large deflection before they reach the breaking point and is more suited for uncovering the material's flexural strength. This last procedure is what this work will follow for its tests.

For the test to be done the usual fixtures attached to the Universal Testing Machine have to be replaced for the ones that allow 4PB and are more appropriate for the size of the specimen. The supporting and loading rollers were fixed to their respective positions as demonstrated in Figure 5.1. The following task was to align the specimen with the loading rollers making sure it is centred and with the right distance from the start of the transition to the contact point. This is made possible by lowering manually the loading rollers until they are almost in contact with the specimen for a more accurate placement.

Some consideration was involved when choosing the loading cell used, ideally it has to have a maximum load capacity over the the expected maximum value needed for the test but not to high that it starts to lose sensitivity and resolution. According to Ultimaker their PLA has a yield stress of 49.5 MPA, also looking at Chancón et al.'s work [59] with their printing parameters they registered a little under 70 MPa of maximum stress. Assuming the worst case of 70 MPa the load generated during the test would be 583 N for group A. For groups B and C its better to give a large margin as similar expectations can be wrong. The available loading cell had a 10KN force limit and so it would not incur any risk of damaging itself will in this mechanical tests.

The centre of the of the specimens was marked with a big cross on the tension side. Then the strain gauges were first glued to some clear tape with the numbers on them, in this case 65, readable from the side of the tape. The clear tape along with the strain gauge is then attached to the specimen, the strain gauge as some markings that serve to align the gauges with the centre of the specimen. After the alignment was assured the clear tape was pealed partially separating the strain gauge from the specimen and allowing access to the specimen's surface. This area was then scraped with fine sandpaper to create little anchor points to which the glue can adhere to. The surface was cleaned with rubbing alcohol and the SuperGlue was then applied to the zone. After this the clear tape is quickly put back to its original position with the strain gauge aligned and pressure is applied to ensure a strong bond between specimen and strain gauge. The strain gauges already came with the wires soldered on so the last step in equipping the specimen with a strain gauge is to separate the live wires with insulator tape and guarantee that the wire is not going to touch the rollers during the test. A specimen from group A can be seen with the strain gauge attached in Figure 5.3

The strain gauges were arranged in a half bridge II with an active strain gauge and a passive one, this helps to compensate for any difference in temperatures between tests. Both of these strain gauges were already glued to their respective specimens. The elected specimen with the passive strain gauge

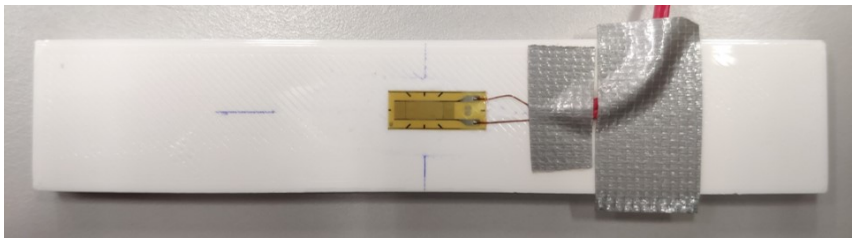

Figure 5.3: Strain gauge glued to Specimen 1A before the four point bending test

was specimen 5A and it was chosen randomly. Since it will be the last to be tested and it will be the only one with a passive strain gauge that is attached to a already deformed specimen it might produce a slightly different result from the rest of its group. This deformed specimen had three days to relax from its test to serving as a passive strain gauge so it should be in its final position and won't be feeding varying values as a reference.

The acquisition of strain gauge data is initiated a few minutes before the test begins, this allows for the gauge's readings to stabilize and provide more reliable information about the test. At this point that the specimen is no longer moved until the end of the 4PB test. However this creates a different problem, the strain gauges and the Universal testing machine will start recording data at distinct times that later have to be adjusted while reviewing the results.

At the beginning of the test the loading rollers are manually lowered until the loading cell registers between 1,5 N to 2 N to ensure there is contact. From then on, the Universal Testing Machine will lower the loading rollers at a steady pace of 2.14 mm/min calculated according to the cross-head rate of the standard ASTM D6272-10 as seen in the formula (5.6) bellow:

$$R = 0.167ZL^2/d \tag{5.6}$$

Where R is the crosshead rate in mm/min, L is the support span in mm, d is the depth of the beam that in the case of this work is equivalent to the measurement t of thickness in mm and finally Z is a constant related to the rate of straining in the outter fibers and has a value of 0.01 mm/mm.

Unfortunately, the temperature and humidity at which the tests will take place can not be controlled as the air conditioning to the laboratory was shut down as a safety measure to prevent the spread of COVID-19, though the temperature readings and relative humidity were taken. The tests were done during the Summer season and the elevated temperatures will make the specimens more ductile which is not the most desirable outcome for this work. The specimens were tested in two separate days, specimen's 1A through 6A excluding the one with the passive strain gauge 5A were tested in the 9th of June where the ambient temperature and humidity were 24° C and 61%. The remaining samples were tested on June 12th with 22° C and 66% of recorded temperature and humidity, in between these two days the test fixture stood unchanged.

Chapter 6

Result Presentation

6.1 Study 1

When the FEA is finished, the process of selecting the intended results begins, our goal is to observe the changes in contact and transition stress fields. The manner in which the results are extracted can affect our perception of the influence of the target parameters; with this in mind the way to obtain the results had to be as careful and as fair as possible throughout the simulations.

Both maximum von Mises stresses of elements in the refined mesh zones, that is, either the transition zone or contact were taken with the help of the Identify Results tool in Figure 6.1. For the contact zone the element selection mode was changed from Single to Box (All) and an area would be delimited that would be analysed. The Box (All) mode was useful for identifying which element had the maximum stress value in a zone not found directly on the surface and therefore they were not visible to another mode of element selection.

The test zone stress values were obtained differently, the Box (Visible) selection mode was used, over the central zone area and pointed the average stress. Instead of looking at the elements it was analysed the element's nodes at the surface of the specimen given the size of the elements in this zone. This decision not only allows us to recognize the influence of the target parameters on the results but also if the values obtained through the equation (2.8) for the outer fibres of the specimen approximates to the values simulated by NX.

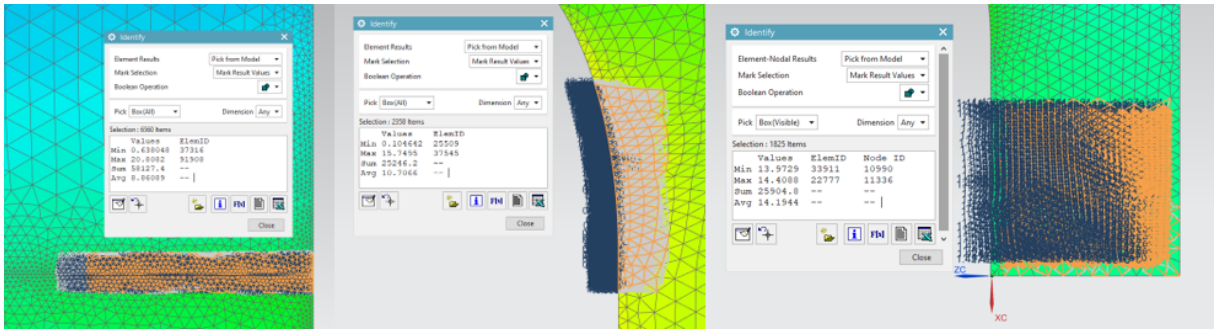

Figure 6.1: Using the tool Identify Results to find intended values

The tables B.3, B.4 and B.5 in Index B show the maximum stress values in the transition zone, contact zone and the average stress on the surface nodes of the test zone. From these results it will be possible to adjust parameters in order to achieve the objectives for the next study. The maximum displacement at the midspan was also taken as an output of the simulations to draw conclusions on the validity of the equation (2.10) provided by the ASTM D6272-10 [3] and if it will still be able to calculate the Young Modulus for this new type of four-point bending test specimen.

6.2 Study 2

The extraction of results from the finished FEA was all in all very similar to the the previous study with the only change coming from the now refined mesh in the midspan of the specimen. This time, with the smaller elements, all their nodes aren't as far from the outer fibres as in the last set of simulations and so there is no need to view only the results of nodes on the surface of the specimen leading to a fairer comparison between elements. The test zone stress values were obtained with the Box (Visible) selection mode. A box was created encompassing the more refined elements of the surface of the test zone, this means the first two or three rows of elements counting from the symmetry plane, and then the average measurement is recorded.

In annex B.6 presents the several iterations needed to reach the desired stress concentration factor as well as the stresses displayed at the critical areas and nominal stress at the midspan.

The $R_x = 19mm + d = 1mm$ was the first combination to undergo the iterative process and so it took the most iterations to find an appropriate result. For following combinations the value of R_y should be slightly lower than the combinations prior leading to less simulation being needed.

6.2.1 Mesh Comparison

The results can be seen in Appendix B.7 and show completely different averages, the single refinement presents a 20,56 MPa average of maximum von Mises stress beneath the loading roller while the double refinement results in an average of 22,59 MPa. This is a considerable difference and prior to the mechanical test it can't be concluded which of these methods more closely resembles reality.

The main reason why another method for constructing the mesh was sought after was due to the large differences in results coming from meshes with the exact same parameters. When comparing the standard deviation from both types of mesh that represents the dispersion of results in a set of values, the single and double refined meshes displays a standard deviation of 0.66 and 0,1 respectively. This shows that the grouping of the results coming from the double refined mesh is much tighter and closer to the average than the previous option. This leads to less confusion due to a random mesh that breaks the trend of the results by distancing far from the average.

In terms of variability of the results in the transition zone, both meshing methods show similar values with near identical averages and little to no change in value in each set of simulations. With this it can be concluded that conclusions taken from study 1 were not affected by abnormal results when it comes

to the analysis of the transition zone.

Table 6.1: Average and standard deviation of the von Mises stress in the Mesh Comparison study.

Mesh type	Under the loading roller		Transition Zone	
	Avg. stress (MPa)	Standard deviation	Avg. stress (MPa)	Standard deviation
Single refinement	20.556	0.659	17.139	0.0022
Double refinement	22.588	0.103	17.154	0.0049

6.3 Experimental testing

In table 6.2, are the results from the small scale study done to find the optimal geometries for a specimen with 5 mm of thickness

Table 6.2: Results the 5 mm thickness specimens, stress in MPa.

Specimen Type	σ_r	σ_t	σ_n	SC_r	SC_t
Specimen A	26.36	—	18.10	1.46	—
Specimen B	18.34	22.6	18.19	1.01	1.24
Specimen C	21.12	20.92	18.16	1.16	1.15

The stress coefficients found on these smaller specimens are lower then the correspondent stress coefficients for the 10 mm thickness versions of the specimen. This may be due to the fact that to achieve the same stress at the mid-span a lower compressive force is required from the loading roller.

To analyse results the information from the Universal testing machine and the strain gauges has to be treated. The data from the strain gauges is comprised of just a series of strain values that are gathered with a rate of 16 Hz while the software from the testing machine records in time increments of 0.1s.

As mentioned before, the strain data recording is started much earlier than the test, to resolve this the start of the test has to be aligned with the strain data. This is achieved by observing the values of the strain, initially they should be very close to zero fluctuating between positive and negative values during the time where we let the strain gauges stabilize. A small increase in strain is then noticed from loading the specimen with a few Newtons of force to ensure contact. After a few seconds the strain values increase at a steady rate. The single point of data right before the steady increase in strain is considered the new zero in time that coincides with the start of the mechanical test and every point of data before is ignored. With this procedure the data collected separately now has a very similar starting time.

The next obvious problem stems from the two contrasting frequencies of data collection. Two options were found, either some linear interpolation was applied to the data that had less frequency to create new points that coincided time wise with the strain data or resort to a common denominator being the frequency of 2Hz. The results recorded always had two points at which the time coincides every second. This would eliminate the need for linear approximations but waste a lot of information as only 1 in every

8 points of data from the strain gauges was useful while in the Universal Testing Machine it was 1 in 5. The latter option was chosen due to its no approximation approach and seeing that the early specimens took around one minute to reach the end of the elastic behaviour, even with the 2Hz frequency it would mean 120 time increments for that region alone. After this both sets of data, from the strain gauge and the testing machine, were synchronized.

6.3.1 Specimen A

The specimens from group A are the only ones that were built according to a testing standard this means that the stress can be directly calculated using the formulas in said standard. In this case equation (2.8) will be applied with $L = 80$mm and both w and h measurements are taken out of the measurements table in Index B.8, and so this will be the only group that presents a typical Stress vs. Strain curve. After synchronizing the data the only thing left was to calculate the stress in order to build the graph stress vs. strain, Figure 6.2. The strain is not calculated from the maximum centre deflection of the specimen as in ASTM D6272-10 but obtained through the strain gauges.

Figure 6.2: Stress-Strain curves for the six specimens in group A

As a first observation, one can see that the test specimen is not as fragile as planned, presenting a fairly large region of plastic deformation. This might be due to the fact that the printers used to manufacture the samples were different from the one used by Chancón et al. [59]. As mentioned this does have more effect on the printed material properties than the printing parameters [62] coupled with the high temperatures during the tests. Another thing to note is that the four point bending tests were stopped before the specimens managed to completely fracture leading to a lack of indication to where the higher stress coefficient is located.

In almost all of the 4 point bending tests the strain gauge, despite measuring above the 3% strain announced, failed first and so there is more load and vertical deflection data related to each test. However if it were to be displayed there would be either time or the deflection of the loading rollers on the X

axis. During the course of the test, with the increase in deflection, the point of contact with the specimen changes as seen in Figure 2.2. Also the direction of the pair of action-reaction force nearing the end of the test, where the roller deflection values were around 12 mm, has substantial amount of the force applied on a horizontal direction. The loading rollers are fixed by magnets, this coupled with their fixture geometry forced the rollers to move inwards towards the centre of the specimen and in the first instance even fully detach itself from the testing fixture. Every following test was stopped as soon as a gap in between the roller and the fixture was noticed as can be seen below in figure 6.3 to prevent damage to the equipment. Just keep in mind that the test ran for longer than is depicted in the Graph 6.2 as the strain gauges failed first.

Figure 6.3: Gap between the loading roller and the test fixture at high values of deflection

The yield strength corresponds to the stress at which the material transitions from a elastic regime usually identifiable for its linear stress-strain curve to the non-linear plastic regime with a mellower slope. For the flexural yield strength the standard suggests looking for a point Y at which the load does not increase with the increase in deflection. This once again involves the use of centre deflection of the specimen which was not recorded. The ASTM standard also recommends the calculation of flexural offset yield strength. This is the stress at at which the stress-strain curve breaks from the linear trendline of the elastic zone by a predetermined strain known as the offset. To further elaborate, a straight line parallel to the initial linear portion of the stress-strain curve will be drawn passing through the point with the coordinates (offset ; 0) and the intersection of this line with the stress-strain curve will give the value of the flexural offset yield strength.

The stress-strain curves from specimen group A present a linear elastic regime with no perceptible Hookean region and thus no need for toe correction. The slope of the initial elastic region was obtained from adapting a linear formula ($y = mx + b$) to every point bellow the 1% strain mark to make sure every point belongs to the linear region. After getting the slope, a new straight line is formed with the offset equal to 0,2% or 0,002 mm/mm following instructions from Note 16 of ASTM D6272-10. The only thing left is to find the intersection of the two curves. The maximum stress can only be calculated through equation (2.8) when the maximum force is applied as an input, so finding the point of data with the highest value of force will lead to the maximum stress at the outer fibres.

While selecting every point bellow 1% strain it was noticed that specimen 1A took 71 s to reach the mark while the rest of the test sample from this group took between 63,5 s to 65 s. This difference

occurs even though they were all tested with the same crosshead rate, leading to the assumption that something went a bit differently in the first this test.

In the table 6.3 bellow can be found the slope for the initial linear section of the stress-strain curve along with the the parallel straight that passes through the offset at the point (0,002 ; 0), the result from their intersection, the maximum force and the deflection of the loading rollers at that point ($D_{F_{max}}$).

Table 6.3: Results from the data analysis of specimen group A.

Specimen	Initial Slope $y = mx + b$		Straight Formula at 0,2% strain				
A	m	b	$y = mx + b$	σ_y (MPa)	ϵ_y	F_{max} (N)	$D_{F_{max}}$ (mm)
1	3533,2	0,0865	$y = 3533,2x - 7,0664$	67,88	0,02124	762,53	-8,09
2	3419,2	-0,039	$y = 3419,2x - 6,8384$	71,09	0,02280	796,92	-9,97
3	3413,2	0,1378	$y = 3413,2x - 6,8264$	72,73	0,02330	818,62	-9,27
4	3265,7	-0,1036	$y = 3265,7x - 6,5314$	69,46	0,02329	803,90	-9,56
5	3353,9	-0,1533	$y = 3353,9x - 6,7078$	69,64	0,02275	795,45	-9,91
6	3255,6	0,0174	$y = 3255,6x - 6,5112$	69,64	0,02275	778,42	-10,06
Average	3341,5	-0,0281	—	70.51	0,02298	798.66	-9.75

The maximum stress was not calculated from the maximum force applied to the specimen due to the specimen's ductility. The tests far surpassed the 5% limit of the ASTM standard. By allowing large deformations the specimen strays further from the original flat position for which equation (2.8) was created. The contact points have changed along with the contact angle that at nearly 10 mm of roller deflection produces a considerable amount of horizontal force. Coupled with the fact that one can no longer assume that the neutral line, where the stress should be zero, passes through the centroid of the cross section [72]. The culmination of all these factors means that there will probably be a large error form the calculated stress to the actual experimental stress .

6.3.2 Specimen B

Group B and C do not have any standard associated with them so it would be biased and incorrect to approach the results the same way as the specimen A which has plenty of more study and validation in its history. Since only in the next chapter will the results be analysed and turned in to something comparable to the data from group A. In Figure 6.4 you will find the data given directly from the Universal Testing Machine and the strain gauges starting at the beginning of the test.

Note that a graph comparing the evolution of Force vs. Strain would be misleading as materials can not be characterized by the force imposed upon them as force is not a material property. The only result that can be shown as of now is only the raw data from the experiment before it is analysed.

First thing to notice is that, once again, the strain gauges fail before the end of the test as they last at most nearly 200 s while the test runs for more than 250 s. The strain gauges would either stagnate the readings reaching a certain value and keep recording that value or they would abruptly spike in value and record negative strains after. This latter can be observed in specimens 2B and 6B only the negative

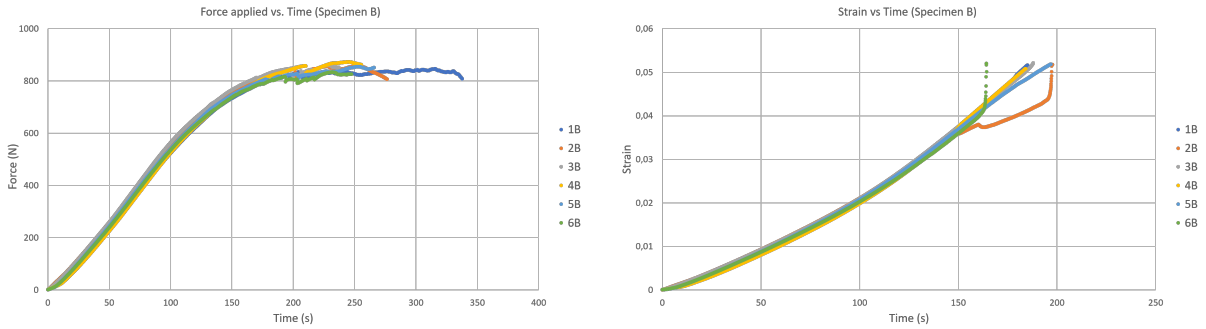

(a) Force vs. Time

(b) Strain vs. Time

Figure 6.4: Raw data from the 4PB tests of Specimen group B with the strain adjusted to start at the 0s mark of the experiments

reading were cut from the graph. Specimen 2B (orange) also has a slight decrease in the strain vs time curve this may be due to poor application of glue on the strain gauge and it breaking mid test partially separating itself from the specimen.

Another observable fact is that the test for specimen 1B ran for a lot longer than any other. This was the product of trying to completely break the test sample as a crack at the root of the transition was spotted giving the impression that it would fail soon in Figure 6.5. The test continued and the crack slowly expanded. Eventually the test was stopped to prevent the loading rollers from being expelled from the test fixture.

The second specimen to be tested developed a crack in the exact same transition zone as the previous one. In order to rule out the possibility of this being caused by the test set-up the specimen position was changed with the end goal of having 50% of them tested in each direction. Every single specimen from groups A, B and C had a small manufacturing defect, they all were thicker on one end by around 0,05 mm probably due to poor bed levelling in the 3D printer. This meant despite the specimen being symmetrical both different ends were distinguishable from each other and a purposeful change in test direction was possible.

Figure 6.5: Crack at the root of the transition of specimen 1B

Throughout every test from group B the location of the crack initiation was noted down, the crack appeared in two different placements. When the thicker side of the specimen was orientated to the right side of the test fixture the crack developed on the right side in the transition closer to the viewer. When the thicker end of the specimen was placed on the left side of the fixture the crack originated on the left side in the transition further away from the viewer. These locations are represented in Figure 6.6. After the tests the specimens were all aligned with the thick end to the same side the crack was shown to

always develop in the same transition despite of the orientation of it during the test. This leads us to believe that the combination of high stress coefficients and an unknown printing defect were responsible for the crack location and that the fixture set-up was not at fault.

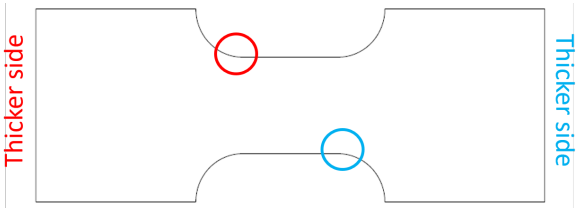

Figure 6.6: Crack position at the root of the transition for specimen group B

Nearing the maximum load of the tests there is always a force drop-off that may be a result of slight separation between printed layers and a release of energy most visible in specimen 4B with the sudden break in the yellow line in figure 6.4 (a). This effect also appeared in the results of specimens 5A and 6A with sudden stress decreases but no visible crack is present in those test samples.

6.3.3 Specimen C

Almost every thing above said about the Group B specimens can be applied to Group C as their geometry is very similar and novel in this kind of mechanical test. The result in figure 6.7 displayed bellow are the raw data from the experiment with the strain graph adjusted so the zero in time coincides with the beginning of the test.

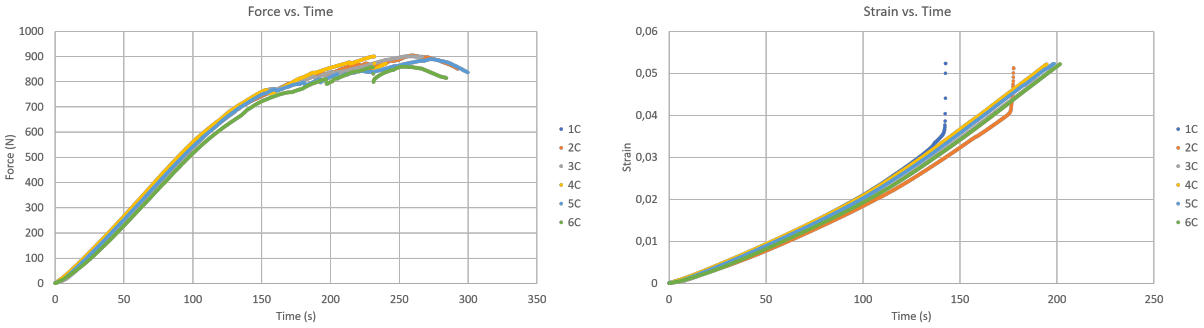

(a) Force vs. Time

(b) Strain vs. Time

Figure 6.7: Raw data from the 4PB tests of Specimen Group C with the strain adjusted to start at the 0s mark of the experiments.

Again, a lot of similarities can be noticed between the curves from specimens B and C, namely the shape of the curves, the force drop-off nearing the maximum load and the type of failure of the strain gauges. Despite showing a sudden decrease in force at the fixture meaning a sudden release in energy akin to the specimen B none of the test samples present any visible damage or cracks post experiment. At the end of the tests specimens 1, 2 and 4 from group C had a partially unglued strain gauges, if any result seems strange not following close to the others this might be the reason.

Chapter 7

Result Discussion

7.1 Study 1

7.1.1 Parameter Rx

Beginning with the parameter responsible for dictating the length that the curved transition will occupy in the specimen. In order to draw conclusions graphs were made to visually see the effects of R_x, Figures 7.1 and 7.2 relates the changes done to R_x with the stress results.

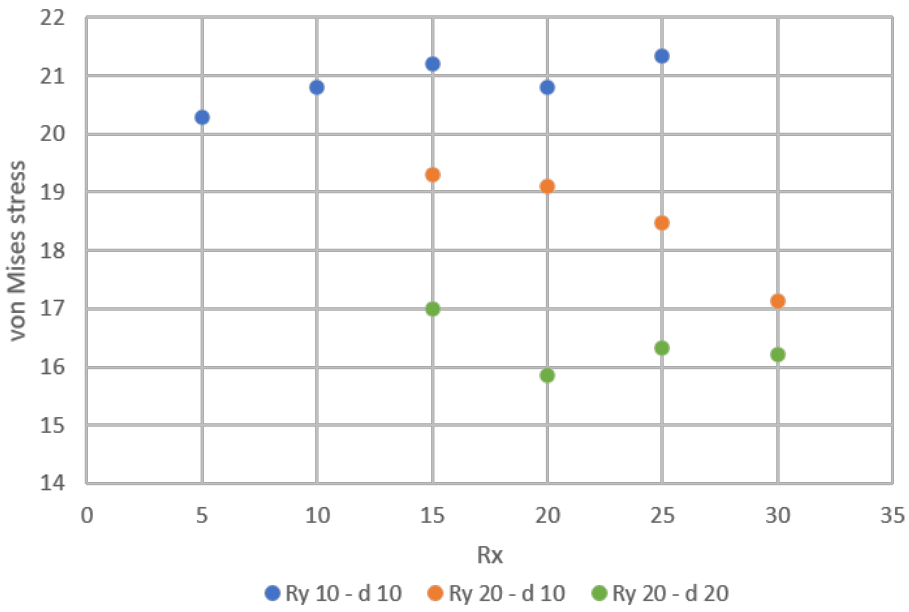

Figure 7.1: R_x vs Maximum von Mises stress (MPa) beneath the loading roller (size in mm)

During the simulations, the results from the stress in the vicinity of the rollers were pretty inconsistent. This might be the outcome of using a single refinement and a fairly large element size on the roller that when meshed was not very close to cylindrical. For example, sometimes when analysing the stress field in that area one or two elements of the 3D mesh would have much higher values then elements

immediately surrounding them. Being unusual to see such a discrepancy of values appearing with no apparent transition between elements the mesh was reformed with the exact same values and a different maximum von Mises stress would be the outcome. For this study since its just to see how stress fields change with the parameters inputted no kind of absolute accuracy was required so, an attempt was made to re-mesh the simulations with these obviously strange maximum values under the roller until a smoother stress distribution was found. Taking into account the inconsistencies of the stress results beneath the loading roller no pattern can be found from this graph alone when it comes to the influence of R_x. The values do not seem to follow any kind of similar path comparing them to each other, the blue and green series of points look like they are not affected by the parameter while the stress for the orange series is clearly diminishing inverse to R_x. This could either be the result of the other parameters influencing the evolution of the stress filed or simply random factors coming from the creation of the mesh.

However, preliminary conclusion for the R_y and d parameters can be drawn when observing the overall differences between series. Comparing blue series to the orange one the change made was an increase of R_y which lead to lower results overall perhaps indicating a pattern to look for in the analysis of that parameter. The d parameter was changed between the orange and green series and a decrease in stress was noticed with its increase for exactly the same values of R_x.

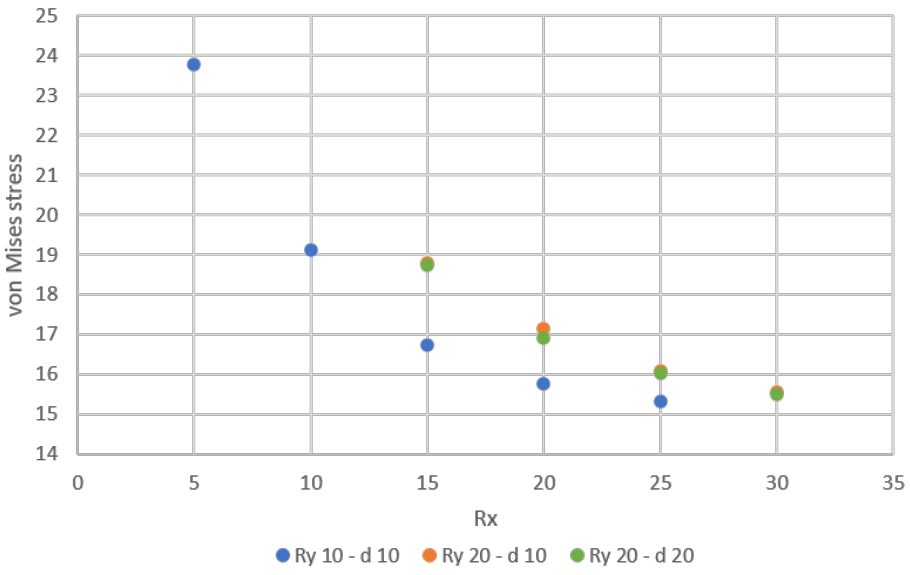

Figure 7.2: R_x vs Maximum von Mises stress (MPa) at the root of the transition (size in mm)

The transition stress did not undergo the same problems as the area under the loading cylinders. Even when some elements under the roller had spikes in value the transition stress remained almost the same throughout the re-meshings of the specimen as long as the geometric and mesh parameters were the same.

By looking at the graph it can be seen that by raising the value of R_x the von Mises stress decreases rapidly for the lower ranges of the parameter. When the stress approaches the stress at the mid span this effect is less noticeable for all of the series of simulations. Comparing the blue and orange series, there

was an increase in the parameter R_y which seemed to lead to a gain in stress. Changing the remaining parameter resulted in almost absolutely no difference in the stress values between the orange and green series with their dots on the graph being almost completely overlapped.

According to equation (3.1) if the parameters of the elliptical fillet were to be introduced in that expression then it would lead to:

$$r_{V_a} = \frac{R_x^2}{R_y} \tag{7.1}$$

Where r_{V_a} is the radius at the root of the transition. This means that the R_x parameter is the main influencer when it comes to the apparent radius of the curve at the point where the stresses are highest in the transition. Being on the numerator side of the equation when R_x is increased r_{V_a} will follow and as seen in several stress concentration factor tables [31] for shapes that resemble the specimen in tension (because there isn't any for bending in the direction of this study) this increase in radius leads the transition stress concentration factor closer and closer to 1 without ever reaching that value. Comparing the results from this study to those previously mentioned stress concentration factor tables, the stress evolves in a similar manner. It decreases as R_x and consequently r_{V_a} increases until the limit of $SC = 1$ is reached or in this case a stress of nearly 15 MPa.

Applying equation (7.1) to calculate the radius of the curved transition at its root for all the simulations the results displayed in Figure 7.3 are similar to typical stress concentration factor graphs found in Peterson's stress concentration factors [31]. Only the series in which R_x was varied were useful. When varying only R_y grouping results that way would leave groups with only one or two points in the graph. When shifting the parameter d the radius to width ratio did not change that forced points to be in the same value of abscissa not forming a curve and overlapping each other.

Where w is the width of the specimen in the constant cross-section zone at the mid-span and W is the width of the specimen taking into account the parameter R_y so it's $W = w + 2 * R_y$ and r is r_{V_a}.

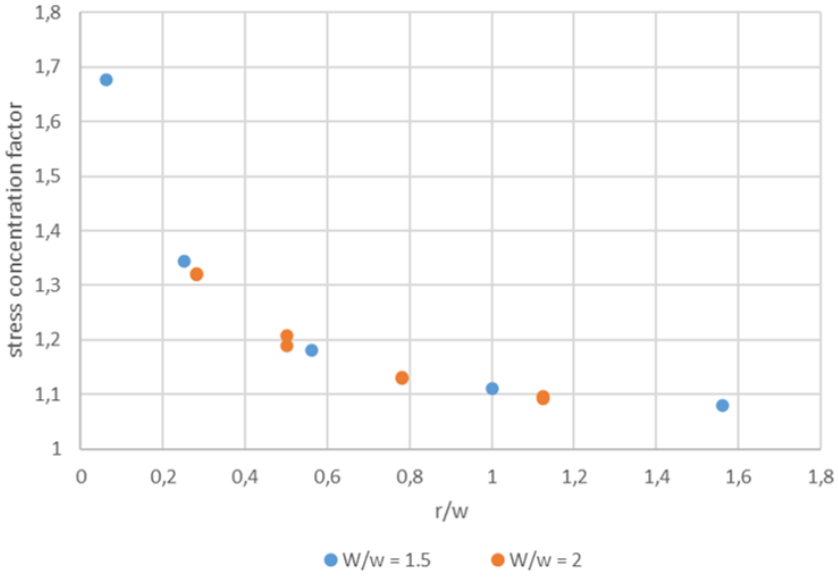

Figure 7.3: Stress concentration table in the transition zone

7.1.2 Parameter Ry

Moving on to the parameter that provides a larger area for the loading rollers to make contact with the test sample, R_y. Once again a visual representation of the results was plotted in Figures 7.4 and 7.5 for easy analysis. Starting with the effect on the stress field under the roller, these series of simulations where also the victim of some the inconsistencies that plagued the first set of simulations.

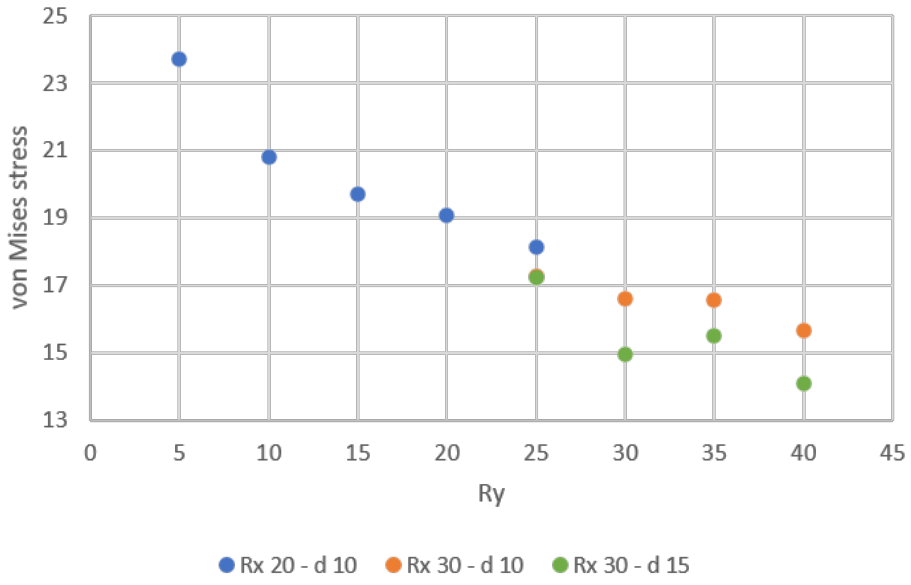

Figure 7.4: R_y vs. Maximum von Mises stress (MPa) beneath the loading roller (size in mm)

Every series of simulations with their different base values for the variations of R_y can be seen lowering the stress under the loading roller most likely due to same reason as the for the specimen that this geometry was based out of, the tensile test specimen. They have wider heads to allow more surface area to be in contact with the loading apparatus so that to the same overall applied force is distributed throughout a larger contact area and the stress is reduced [30].

Here it can also be seen that the changes done to the parameter R_x seem to have little effect on the stress values. As the orange series suggests a curve that follows an identical path to the blue dotted sequence. Trailing the preliminary analysis of the parameter d, the results again assume lower values when this parameter is increased except the for the lowest value of R_y used in both orange and green arrays. These are completely overlapped though it seems to be an exception as the rest of the series shows primarily distinct von Mises stress. This either suggests that maybe parameter d is not effective at lowering the stress values under the rollers for specimens with a reduced R_y or it was affected by the stress inconsistencies noticed in the contact zone.

From figure 7.5 the stress at the transition clearly increases at a linear pace with steady increments of R_y and from equation (7.1) one can come to an understanding as to why it occurs. Being R_y the denominator of that equation as it increases the equivalent radius of the ellipse diminishes at its most stress concentrated area, the root. Looking at this parameter in the same light as R_x, according to those tables by decreasing de radius of a transition while keeping the width of the specimen unaltered

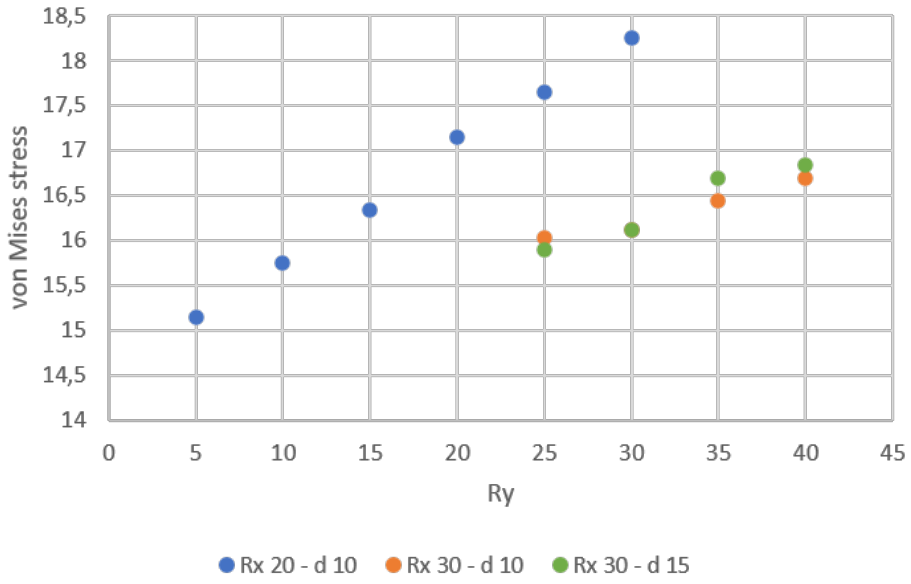

Figure 7.5: R_y vs. Maximum von Mises stress (MPa) at the root of the transition (size in mm)

the stress concentration factor will raise and so the stress value will also increase if the nominal stress remains the same which is the case of these simulations.

The effect of R_x on the transition zone stress is also unmistakably visible in figure 7.5 when changing its value from 20mm to 30mm there is an immediate decrease in stress and also a decrease in the slope of the graph. Altering the value of R_y while R_x occupies a larger length the stress will vary less than with smaller values of R_x. When it comes to the effect of parameter d every point of the green and orange series are almost coincident hinting that perhaps it does not influence the stress in that region.

7.1.3 Parameter d

Finishing of this study's parameter discussion with the parameter d. It dictates the distance between the contact zone and the start of the curved elliptical transition. Again some disparities in results were noticed when measuring the stress on the loading zone.

Observing figure 7.6 the effect that d has on the stress beneath the loading rollers is similar through the various series. Increasing d leads to a general decline in stress, for higher values of R_y this decrease seems to be accentuated indicated by the different slopes of the blue and orange dotted series when compared to the green array of dots. The reason why this parameter lowers the stress in this region is easily visible when comparing the stress distribution in that area using Siemens NX.

Comparing the two extremes of the blue dotted series, the specimen $d = 0.5mm$ in Figure 7.7 shows a lot more of dark blues near the edge. This part of material is not serving much purpose in taking the load from the loading roller, on top of that fact it is noticeable the difference in the stress distribution of the elliptical contact zone. The specimen with $d = 20mm$ shows a much more elongated and well distributed contact area. This difference must be due to the proximity of the contact zone to the two free edges, the side of the specimen and the curved transition. Being so near of both free edges the contact

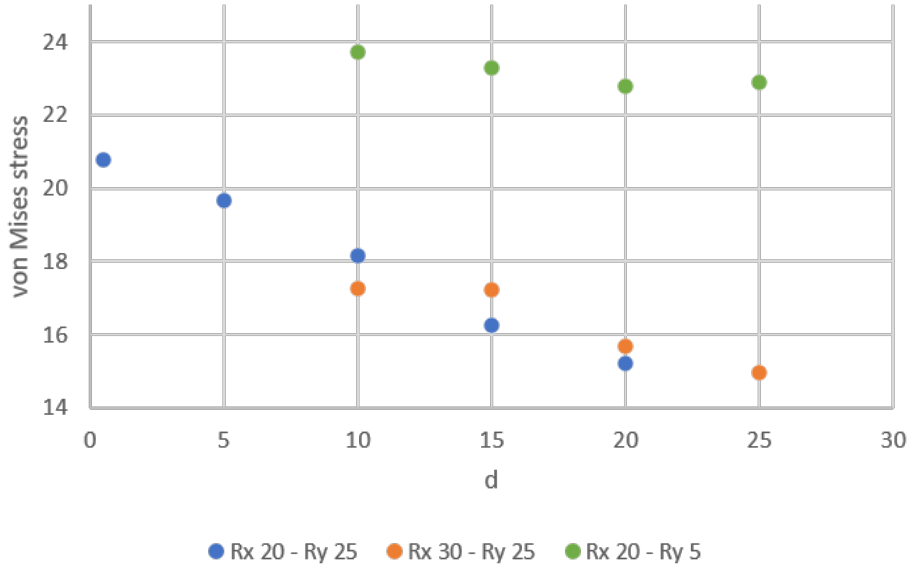

Figure 7.6: d vs. Maximum von Mises stress (MPa) beneath the loading roller (size in mm)

in specimen $d = 0.5mm$ must be unable to provide any resistance to the loading force and thus does not help in supporting the contact force. The specimen with $d = 20mm$ only approaches one of the free edges, the side of the specimen, resulting in that part of the contact zone being more capable to offer resistance against the downwards movement of the of the loading cylinder.

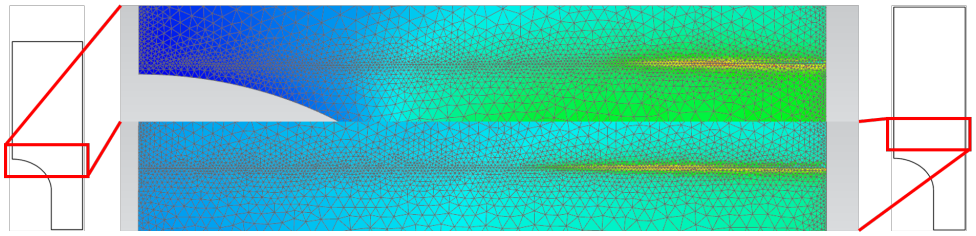

Figure 7.7: Von Mises stress beneath the loading roller with $d = 0,5mm$ (upper image) and $d = 20mm$ (lower image)

It's hard to conclude but, its only logical that this decreasing effect that the parameter has on the stress in this region has to have a limit. If d is extended to huge lengths the specimen would resemble a regular constant rectangular cross-section specimen. This means that the limit must be equal to the stress that a regular specimen with the same width under the roller would reach. For example, the minimum stress that a specimen could reach just by enlarging the d parameter with an original width of 40mm and a R_y of 10 would be equal to a regular parallelepiped specimen with the width of 60mm for an equal stress at the mid-span.

Reinforcing the suspicion that changing the parameter R_x does little to no difference to the stress values under the roller, in the figure 7.8, the orange and blue array of dots show signs of following the same path when the only occurring change between series was done to R_x.

A straightforward conclusion can be taken when it comes to the influence of the parameter d on the von Mises stress at the root of the transition. While changing its length the stress fields in this

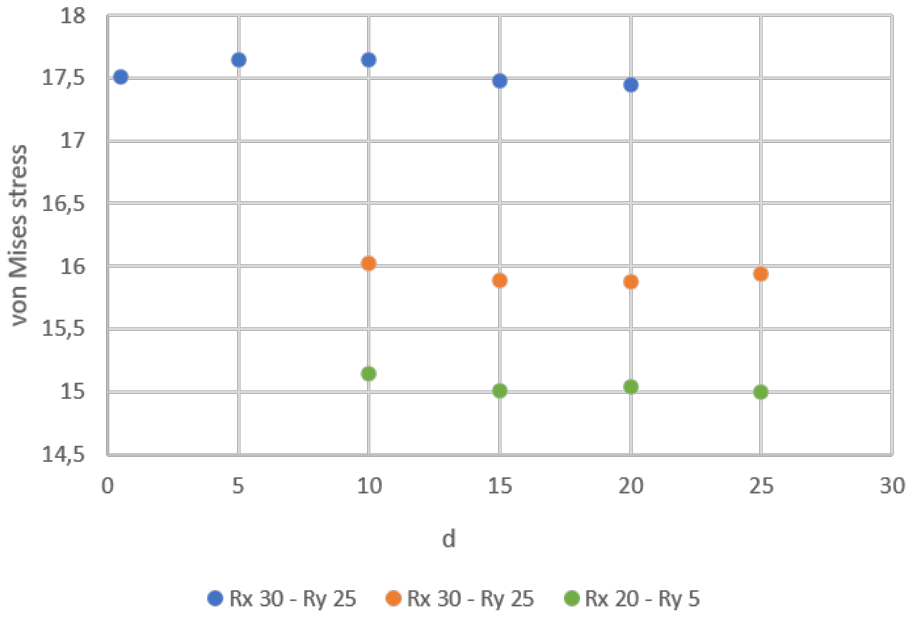

Figure 7.8: d vs. Maximum von Mises stress (MPa) at the root of the transition (size in mm)

area appear to remain undisturbed, only when changes are made to the other two parameters the field evolves in the previously discussed manner.

To sum up this study's results, the maximum stress under the loading roller is decreased by increasing either of the parameters R_y or d. The stress at the root of the elliptical transition can be lowered by increasing the R_x parameter or decrease the value of R_y. The effect of the distance between the loading area and the start of the fillet is enhanced by higher values of R_y and also the other way around, increasing R_y lowers the stress more effectively with a larger d.

7.1.4 Other observations

Due to the way the restrictions on the load cylinders were imposed, some movement in the X direction was foreseeable. Figure 7.9 demonstrates the magnitude of this displacement and also the advantage associated with not fixing the cylinder along that same direction. As can be seen the maximum variation in the lever length of the four point bending test were not of great significance. It ended up increasing a 50 mm length between approximately 0.3 and 0.4 mm which represents less than 1% of the lever. As seen in the equation (2.7) used for the calculation of the maximum stress in the pure bending zone. the distance between load and support rollers is directly proportional to the mid-span stress which shall result in an equivalent increase of less than 1% in the central zone stress of the sample. The advantage referenced earlier can be easily observable just by looking at the Figure 7.9 below, the refined mesh is located directly at the contact zone at the end of rollers movement providing elements of equal size to all simulations.

Using the equation (2.7) to obtain the nominal stress perceived by the test specimen at the test zone and apply the parameters used in the finite element analysis: $F_0 = 400N$, $a = 50mm$, $w = 40mm$ and

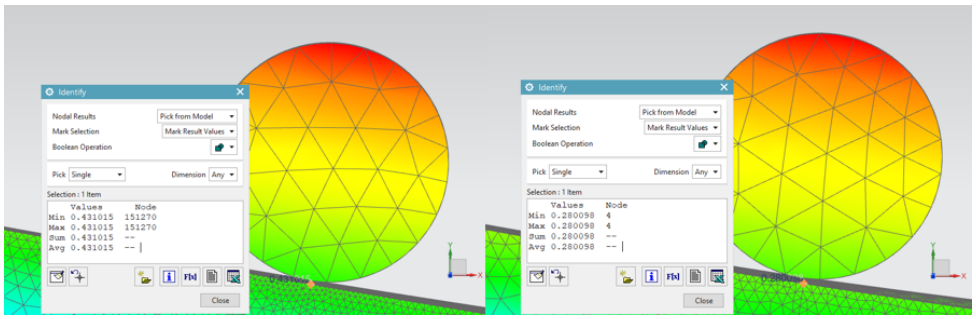

Figure 7.9: Maximum and minimum values of horizontal loading roller displacement found on study 1. Units in mm.

$t = 10mm$, the central zone with the inputted width should be under $\sigma_n = 15MPa$ of von Mises stress. Taking into account the increase in the momentum arm length due to the dislocation of the contact zone and the reduction effect caused by the movement of the other contact zone at the supporting cylinder a different stress is attained.

The loading contact displacement was already determined through the Identify Results tool and the support contact displacement was calculated as follows. First a lateral print screen of the contact area was taken, then the cylinder's diameter is measured in pixels. Since it is known that they are 10 mm in diameter a conversion rate from pixels to millimetres is established. In the lateral view of the whole set, the specimen usually intersects the roller. To find the contact point the average between the start and end of this intersection is made and assumed as the contact point as illustrated in the figure 7.10. In case the graphical display of the deformed specimen does not overlap and thus no intersection is created the process is a bit different. First the centre of the cylinder is found and then a circle concentric to the cylinder is draw and its radius expanded until it contacts with the test specimen and that point is assumed as the new contact point, every step after is the same.

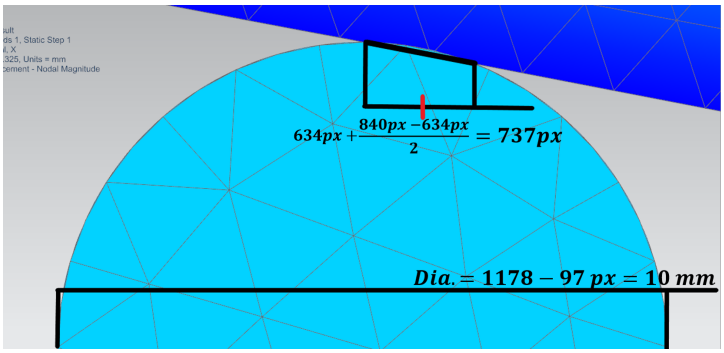

Figure 7.10: Horizontal contact displacement calculation on supporting roller

Finishing the estimation of the true distance between supporting and loading contact areas the centre of the roller in the picture 7.10 is:

$$\frac{1178 - 97}{2} + 97 = 637.5px \tag{7.2}$$

And so the displacement of the contact area is:

$$737 - 637.5 = 99.5px \rightarrow \frac{99.5 * 10}{1178 - 97} = 1.081mm \tag{7.3}$$

Which is more than double of the value obtained from the displacement of the loading roller meaning that the lever arm length is reduced a bit in the finite element analysis. This result was taken from the simulation that presented the highest vertical displacement which should mean a higher contact displacement at the supporting roller since the specimen must be at a higher angle against the roller. The distance between the centres of both rollers is 50 mm, the contact area on the supporting side moves in the positive X direction by approximately 1.08 mm and the loading side moves in the same direction 0.4 mm, so the true distance is $50 - 1.080 + 0.4 = 49,32mm$ and applying this value to equation (2.7)

$$\sigma_n = \frac{12 * 400 * 49.32}{4 * 40 * 10^2} = 14.796 \quad MPa \tag{7.4}$$

This is the resultant stress for the specimen with the highest central vertical displacement. Applying the same method to the simulation which outputted the lowest value of vertical displacement the result should give the other end of the spectrum in terms of change of distance between contact patches. The positive horizontal displacement of both the supporting and loading contact areas are respectively 1.02 mm and 0,3 mm leading to a final lever length of 49.28 mm not much different from the one calculated prior. This results in a stress through equation (2.7) of 14.78 MPa.

One observation that can be made at first glance of the results is the shape of the contact zone between the cylinder and specimen. By selecting the option to output contact force before the simulation is constructed, the option Contact Pressure - Nodal is available to examine. Instead of the contact force being evenly distributed in similar fashion to the force applied to the cylinder itself, it concentrates in the most inner parts of the test specimen an resembles an elliptical shape. This is similar to observations made by W. Cheng et al. [14] in his study on contact with finite element analysis where rather then simulating a slim distributed force on the specimen. He's simulation was made with the force exerted on rollers and achieved an elliptical contact stress distribution.

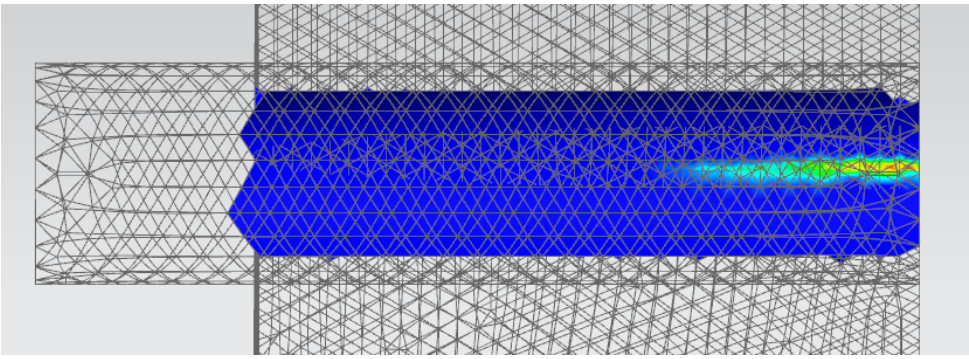

Figure 7.11: Top view of "Contact Pressure - Nodal" of the loading roller

Taking a look at the results one can observe a common trend, no matter what parameter is varying nor the baseline selected the stress at the test zone is more or less unchanged varying between 14.12

MPa and 14.31 MPa indicating that all of the target parameters don't affect the stress at the midspan. If proven simulations are valid, equation (2.8) can be used in future works that involve a similar specimen geometry. The average between the uniform stress calculated from the maximum and minimum vertical displacement simulations using Beam Theory is 14.79 MPa and comparing with the average of the equivalent stress obtained from the finite element model of 14,2 MPa the difference is 3.99%.

Observing now the last row of results for the variation of R_y. This is the only parameter that does not increase the overall span of the specimen, and so when comparing with the equation to calculate de Young Modulus, eq. (2.10), none of the variables there change when only R_y is being varied. The variable m which is the slope of the steepest initial straight line of load-deflection curve is the exception, because the force isn't being altered and the deflection of the beam is. This variable will change the result of the equation suggesting a different Young Modulus when the same material is used throughout all simulations. This therefore leads to the conclusion that this equation is unsuitable for calculating material properties in specimens other than the ones with constant rectangular cross-section.

7.2 Study 2

In this section the focus will be only on the simulations that achieved close to the desired results of $SC_r < 1$ and $SC_r = SC_t$ filtering out the remaining simulations. For the first objective, to build a specimen in which the loading roller does not not affect the test zone stress, meaning that the stress in that area is lower than the nominal stress at the mid-span the important results of each combination are as follows in the table 7.1:

Table 7.1: Results closer to $SC_r = 1$, parameters in mm.

R_x	d	R_y	σ_r (MPa)	σ_t (MPa)	σ_n (MPa)	SC_r	SC_t
19	1	36	19.64	25.38	18.60	1.06	1.36
18	2	25	18.47	24.36	18.55	1.00	1.31
17	3	24	18.61	14.79	18.56	1.00	1.34
16	4	23	18.89	24.98	18.56	1.02	1.35
15	5	22	18.56	25.33	18.56	1.00	1.37

Rounding up the results of the stress coefficient under the rollers to a value of 1, although not completely correct if SC_r was actually equal to 1 the resulting stress coefficient of the transition would not be that much different. The figure 7.12 shows that a minimum stress coefficient at the transition exists near the $R_x = 18mm - d = 2mm$ combination. Looking at the simulated stress field to try and understand why the sudden rise in stress in the combination that breaks the trend a culprit was found. For very small values of d in conjunction with the mandatory increase of the parameter R_y to lower the stress to the intended objective a zone near the border of the specimen begins to reveal an unpredicted and sudden uplift in stress surpassing the region of the contact area near the centre of the specimen as depicted in Figure 7.13. This geometry was simulated many times always ending up with this result.

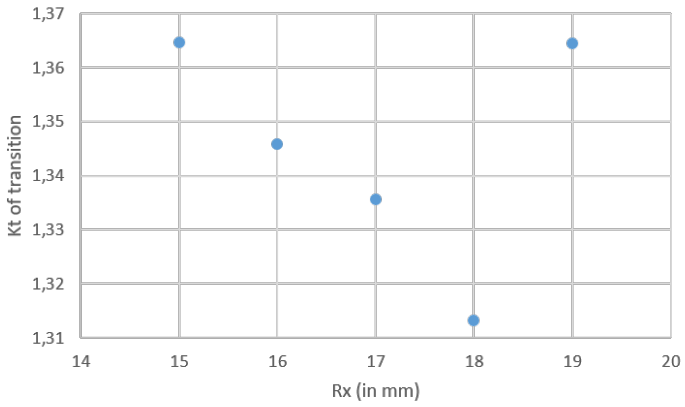

Figure 7.12: SC_t of the results close to the objective

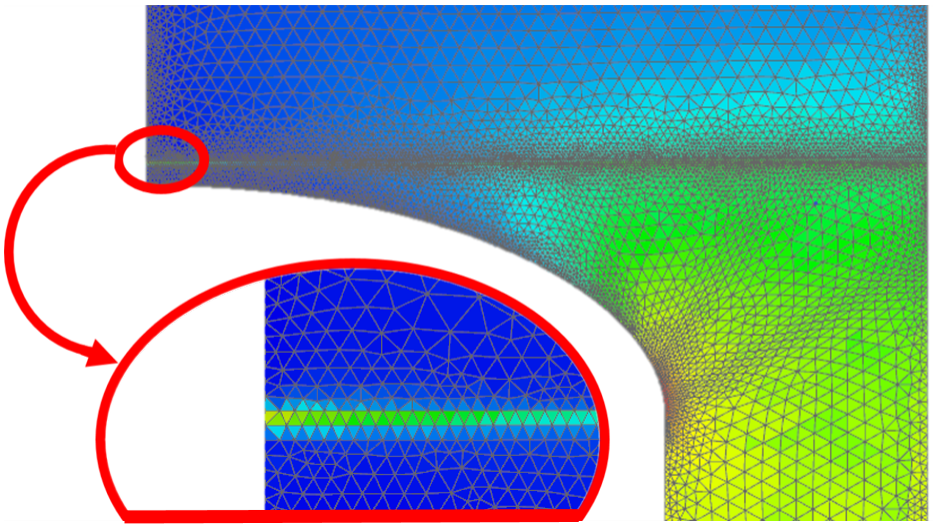

Figure 7.13: The stress field in the contact area near the border of the specimen $R_x = 19mm + R_y = 40mm + d = 1mm$

In the $R_x = 19mm - d = 1mm$ combination this effect was only found for high values of R_y while at lower values the colour of the elements in this area remains a dark blue similar to their surroundings. In the case of the configuration shown above the stress near the centre of the specimen reaches a maximum of 16.71 MPa which is already way below the limit for the objective while the stress in the area highlighted in the figure 7.13 is at 17.83 MPa. This might be in part because the boundary conditions imposed on the loading roller not being completely realistic coupled with exaggerating the geometric parameters to this extent.

For the $R_x = 18mm - d = 2mm$ this effect also made an appearance but, the stress near the border of the specimen was always slightly bellow the stress in the centre. For the configuration with $R_y = 25mm$ the maximum von Mises stress in the contact patch was 18.47 MPa and occurred in the expected zone near the centre while the border underwent a maximum stress of 15.1 MPa.

When it comes to obtaining a specimen where the stress coefficients are identical the table 7.2 portraits the results that were closest to reaching such a goal. It is clear to see that there are no minimums visible in figure 7.14 for the combinations utilized. The configuration that provides both the

best stress coefficients in the contact area and the root of the transition is the $R_x = 19mm - d = 1mm$. The overall stress coefficient is much lower when compared to the previous objective. This difference comes down to the fact that to get to the point where the stress in both critical areas are equal, the parameter R_y did not need to be increased as much as before. The effect witnessed earlier where the stress would rise back up again near the edge of the specimen did not occur. This did not require an extreme increment in R_y to compensate for these abnormally high stress values. By shifting from the combination $R_x = 18mm - d = 2mm$ to $R_x = 19mm - d = 1mm$ in the table 7.1 R_y had to be increased by 11 mm and it still fell short of accomplishing the goal of $SC_r < 1$ while in table 7.2 this increase was only measured at 1 mm.

Table 7.2: Results closer to $SC_r = SC_t$, parameters in mm.

R_x	d	R_y	σ_r (MPa)	σ_t (MPa)	σ_n (MPa)	SC_r	SC_t
19	1	13	21.18	21.94	18.52	1.14	1.19
18	2	12	21.45	22.03	18.52	1.16	1.19
17	3	11	21.71	22.14	18.51	1.17	1.20
16	4	10	21.85	22.22	18.51	1.18	1.20
15	5	9	22.76	22.29	18.50	1.23	1.21

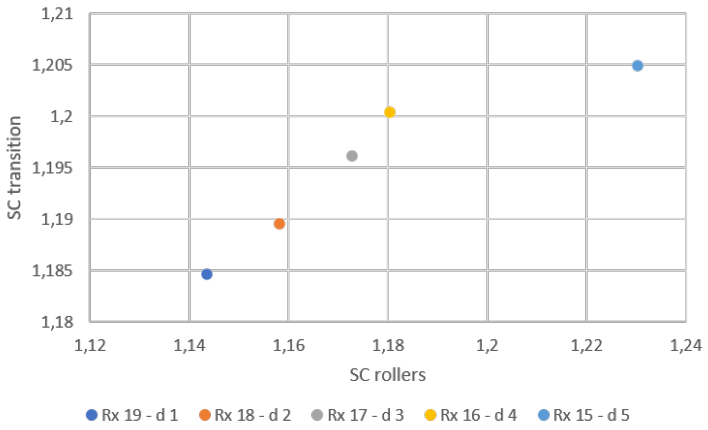

Figure 7.14: SC_r Vs. SC_t of the results closer to the objective

Comparing both specimens, the one optimized for $SC_r < 1$ and the other for $SC_r = SC_t$, to the regular constant rectangular cross-section specimen both options present lower maximum stress concentration factors. When building a sample for equal stress at both critical areas the maximum SC was at its lowest with a value in between 1.14 and 1,18. This allows the measurements done by mechanical four point bending tests results to be more closely related to the real material properties of the specimen according to the simulations. The stress coefficient could be lowered even further if the ASTM D6272-10 [3] wasn't followed by increasing the overall length of the specimen granting the transition the possibility of having larger values of R_x.

In conclusion, to obtain the best parameters for the specimen for the goal of $SC_r < 1$ the results

seemed a bit strange with the highest stress appearing near not one but two free edges, so conclusions will not be taken. For the secondary goal of $SC_r = SC_t$ it is required to use the almost all of the space between the test zone and the contact area as a curved transition to attain the lowest stress coefficients.

To end on a quick comparison between the elliptical curved transition and a more common circular transition, both of the optimal geometries were rebuilt and put through an equal finite element analysis with a circular transition. The way this was done involved using circular arc tangent to the test zone that had to have a starting and finishing point with the same coordinates as their elliptical counterparts. R_x and R_y did not define any kind of radius but rather the position of the end of the transition and the results were as follows:

For the configuration $R_x = 18mm \quad R_y = 25mm \quad d = 2mm$ the circular transition was not possible, the length of the transition was shorter its width resulting in more than a quarter circle. For the configuration $R_x = 19mm \quad R_y = 13mm \quad d = 1mm$ the results appear in the table bellow:

Table 7.3: Comparing elliptical to circular transition.

Transition type	σ_r (MPa)	σ_t (MPa)	σ_n (MPa)	SC_r	SC_t
Elliptical	21.18	21.94	18.52	1.14	1.19
Circular	20.72	22.78	18.53	1.12	1.23
Circular (R_y adjusted)	21.23	22.12	18.52	1.15	1.19

From this one result, using a circular transition lowers the stress underneath the loading rollers while rising the stress at the root of the transition. The contact zone's decrease in stress may be due to the fact that the circular transition moves away from this zone in a faster manner than the elliptical curve leaving a greater average distance from the contact zone to the edge of the transition. Similarly to parameter d increasing this distance reduces stress at beneath the loading cylinder. As for the inflation in the stress at the root of the transition this can be explained by a radii comparison. The elliptical transition has a radius equivalent to 27,77 mm using equation (7.1) while the circular transition presented a radii 20.38 mm taken from the modelling software. Smaller radii produce a more abrupt transition and result in higher values of stress coefficient. When adjusting the parameter R_y on the circular curve to achieved the same goal as the elliptical transition both of the stress coefficients ended up with similar values to the elliptical transition.

7.2.1 Other observations

The same peculiarities in the results of the first study are present here as well. The lever arm that generates the bending momentum is again reduced. Applying the same method as in the previous study for the regular specimen built entirely according to the ASTM D6272-10 [3] standard the dislocation of the contact patch along the X direction on the supporting cylinder is 0.971 mm and at the loading roller is 0,371 mm. This results in a reduction of 0,6 mm out of the 40 mm arm length which instead of the predicted 20 MPa of stress using equation (2.8) results in 19,7 MPa of von Mises stress. When compared to the simulated stress of the regular specimen there is a 6.3% error maybe due to the use of

CTETRA(10) elements that are not the most adequate for bending purposes. The fact that the specimen further away from the original flat position for which the use of equation (2.8) was intended may also be a factor in this difference.

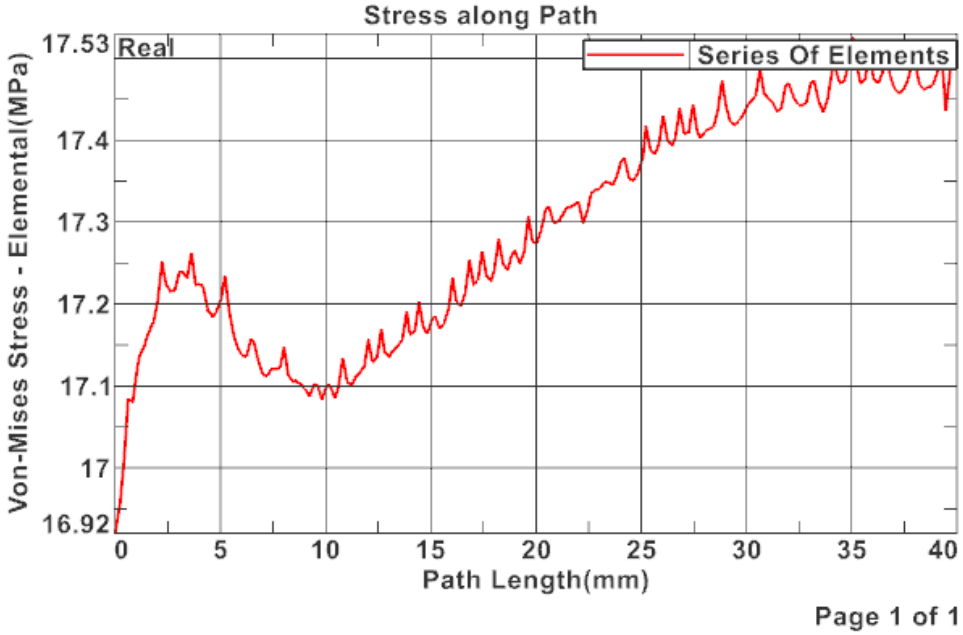

Figure 7.15: Stress distribution along a central line in the tension side of the midspan starting under the loading rollers and ending at the mid point of the regular specimen.

Taking another look to the work done by T. Zhai et al. [6] they studied specimens with loading span/thickness (l/t) ratios between 0.5 and 3 and support span/loading span (L/l) ratios within 2 and 7.5, the specimens built according to the ASTM standard have a l/t of 8 and a L/l of 2 being out of the spectrum mentioned. On high ratios of l/t the maximum stress was located in the near the loading rollers and then it stabilized on lower stress levels near the mid span. As for low values of L/l there is a noticeable peak near the roller and a smooth rise of stress toward the middle of the loading span. Up until this point the simulations only produced a peak near the rollers and unlike the works from T. Zhai and Xiaolong et al. [7] this current work shows the stress rising again towards the mid span. The final difference is the location along the width of the specimen where these measurements were taken. This was not specified probably meaning that the stress along the width of the specimen remains unchanged. In the numerical results from this current work this does not happen.

One oddity that was detected in this simulation was the fact that the stress in the test zone on the tension side of the specimen is slightly lower than the stress on the compressive face. The maximum stress was as seen on Fig. 7.15 is 17.53 MPa, that is 5 % lower when compared to the average stress that was taken from the compressive side and is presented on Table B.6. This fact was later checked on random simulations and persisted throughout all of them.

When applying the same analysis to the tension side of the ”dog bone” geometry it reduces the stress where the width of the test subject is larger than the regular shaped specimen. This includes the area of the graph under the 20mm mark where the transition of widths is in play, the resultant stress distribution

can be seen below in Fig. 7.16. This in turn will help specimen geometries that have high values of wedging stresses, producing a higher stress at the tensile mid-span.

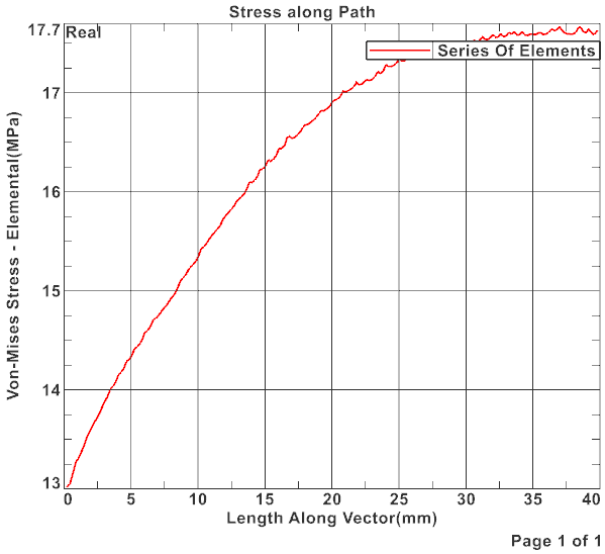

Figure 7.16: Stress distribution along the midspan starting under the loading rollers and ending at the mid point of the ”dog bone” specimen $R_x = 19mm + R_y = 13mm + d = 1mm$.

7.3 Experimental testing

7.3.1 Result analysis

The first step that one should take in order to compare the results from the standard group A specimens to the other two groups is to be able to calculate the stress for the unstandardised specimens. By validating the use of equation (2.8) that was seen to be usable in the numerical part of the work calculating the stress at the mid-span would be possible. This is where the similar printing parameters between groups come into play. Since all specimens were printed out of the same batch of material, with the same proportion of outer walls to filler, same raster angle, along with the rest of the parameters they should theoretically have equal Young Modulus as the material in the test section is identical, this leads to:

$$E_A = E_B = E_C \tag{7.5}$$

Using the first part of equation (2.5):

$$\frac{\sigma_A}{\epsilon_A} = \frac{\sigma_B}{\epsilon_B} = \frac{\sigma_C}{\epsilon_C} \tag{7.6}$$

If equation (2.8) could be used to calculate the stress at the midspan of specimen group B and C then the following would happen:

$$\frac{\frac{3*F_A*L_A}{4*w_A*t_A}}{\epsilon_A} = \frac{\frac{3*F_B*L_B}{4*w_B*t_B}}{\epsilon_B} = \frac{\frac{3*F_C*L_C}{4*w_C*t_C}}{\epsilon_C} \tag{7.7}$$

Obviously the more simplified the equation the more apparent is its physical representation. Variable L may seem to be specific to each specimen much like dimensions w and h however L is the distance between the supporting rollers and thus a dimensions of the test fixture which was never altered during the tests and so L is constant through all tests and will be removed from the equation, leaving us with:

$$\frac{\frac{F_A}{w_A*t_A}}{\epsilon_A} = \frac{\frac{F_B}{w_B*t_B}}{\epsilon_B} = \frac{\frac{F_C}{w_C*t_C}}{\epsilon_C} \tag{7.8}$$

And if the specimens were completely equal to one another:

$$\frac{F_A}{\epsilon_A} = \frac{F_B}{\epsilon_B} = \frac{F_C}{\epsilon_C} \tag{7.9}$$

If equation (7.8) is proven to be true then that must mean that the original assumption of being able to use equation (2.8) is correct validating its application on specimen group B and C. Not only that but also confirming the results of stress at the midspan of the numerical simulations, partially validating them.

Both equation (7.8) and equation (7.9) can be plotted into graphs from the experimental results. Since the specimens have slight variations in dimensions equation (7.8) will be the base to construct the graph with the $\frac{F}{w \times t}$ parcel in the Y axis and the strain on the abscissa to produce a slope equal to the equation. The same process of synchronization between the recorded data from the strain gauges and the Universal Testing Machine was applied to specimens B and C. In Figure 7.17, there can be found the chart with one specimen from each group but from the same print.

From the initial viewing of Figure 7.17 the dots representing each specimen type seem to be nearly identical with almost equal slopes. A mathematical way to compare them would be to associate a formula to the slopes. This is easily done in the elastic zone of the material where the slope seems to be constant. Afterwards that the values of the slopes from group B and C will be statistically proven to be equal to the group A specimens throughout all the tests.

The process starts with the selection of all data points bellow 1% strain as that segment of the curve can be observed to be a straight line. Afterwards a linear regression is applied obtaining the slope and the Y value at the origin. This should be close to zero as the mechanical tests start at nearly zero force and zero strain. This process is practised in every test run and the results can be seen in Figure 7.18 below and individual values are present in Index B.9.

It is worthy to mention that Specimen 2C was recorded to have a slope valued at 62.977 much higher than any specimen from any group. This result was dismissed as the specimen was one that ended the test with a slightly separated strain gauge which in this case must have affected the reading during the elastic region of the material. The rest of the specimens that showed the same separation of the strain gauges had similar results to the specimens in which the test went according to plan.

To prove that the slopes are equal it will be conducted a two-sample t-test as described by Douglas C. Montgomery [57]. First a Hypothesis needs to be placed, in this case is the mean slope of specimen A

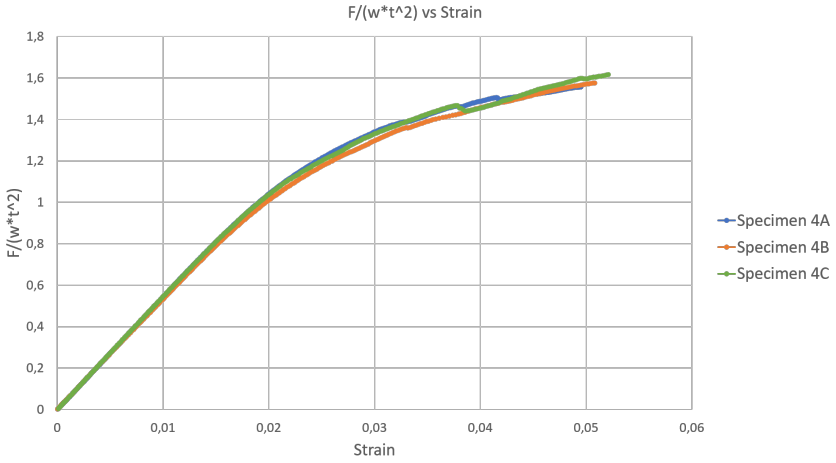

Figure 7.17: Representation of equation (7.8) of print number 4

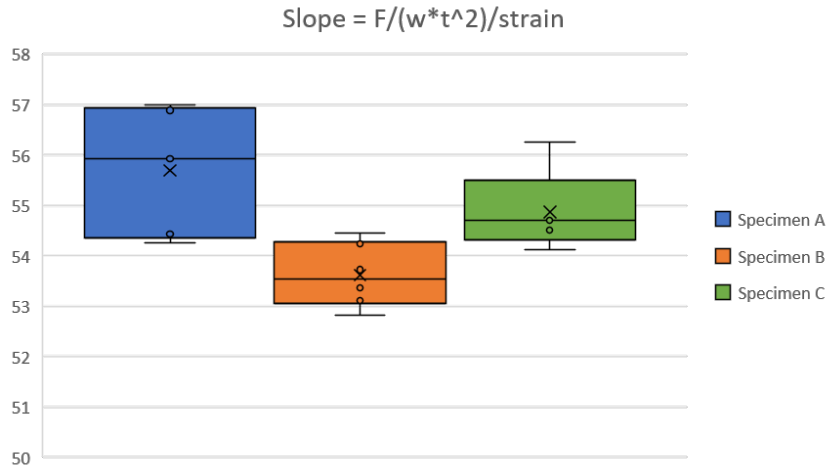

Figure 7.18: Slope value distribution of all specimens separated by group

is equal to the means slope of specimen B. This statement can be formally written as the null hypothesis $H_0 : \mu_A = \mu_B$ were μ_A and μ_B are the respective averages of the group's calculated slope. The procedure is then repeated to compare groups A and C. When testing hypothesis there is the probability of its rejection despite being true (α) and the failure of rejection when false (β).

In order to reject a null hypothesis the value of t_0 must calculated through the following expression:

$$t_0 = \frac{\bar{y_A} - \bar{y_B}}{S_p \sqrt{\frac{1}{n_A} + \frac{1}{n_B}}} \tag{7.10}$$

$$S_p^2 = \frac{(n_a - 1)S_A^2 + (n_B - 1)S_B^2}{n_A + n_B - 2} \tag{7.11}$$

Where $\bar{y_A}$ and $\bar{y_B}$ will be the mean slope values of groups A and B, n_A and n_B are the number of experimental results from each group and S_A and S_B are the sample variance in the respective groups. After t_0 is obtained it must be compared to the t distribution with $n_A + n_B - 2$ degrees of freedom. If t_0 belongs to the upper $\alpha/2$ percentage of the normal distribution with $n_A + n_B - 2$ degrees of freedom,

which can be seen in A.1, then the null hypothesis would be rejected.

$$\text{if} \quad |\, t_0 \,| > t_{\alpha/2;n_A+n_B-2} \quad \text{then } H_0 : \mu_A = \mu_B \text{ rejected} \tag{7.12}$$

In this case study the value of the significance level was set to $\alpha = 5\%$ which corresponds to a confidence level of 95% giving a very low chance of rejecting a true hypothesis. The following tables 7.4 and 7.5 contain all of the variables necessary to conduct the two sample t test and the final results respectively.

Table 7.4: Statistic variables needed for two sample t test.

Group	Mean ($\bar{y_i}$)	Variance (S_i^2)	n_i	Difference from slope A
A	55.69	3.47	5	—
B	53.62	0.40	6	-3,73%
C	54.87	0.65	5	-1.48%

Table 7.5: Testing of the null hypothesis.

Null hypothesis	S_p	t_0	$t_{\alpha/2;n_A+n_B-2}$	Status
$\mu_A = \mu_B$	0.99	3.46	2.26	Rejected
$\mu_A = \mu_C$	0.72	-1.40	2.26	Accepted
$\mu_B = \mu_C$	1.08	-1.90	2.31	Accepted

Assuming that equation (2.8) is valid for usage in specimen groups B and C then the same data processing that specimen A went through in section 6.3.1 can be applied and the results compared. Table contains the average properties, forces and deflections belonging or applied to the specimen.

Table 7.6: Average results from the data analysis all groups.

Specimen	σ_y (MPa)	σ_y difference % from A	ϵ_y	ϵ_y difference % from A	F_{max} (N)	$D_{F_{max}}$ (mm)
A	70.51	—	0.02298	—	798.66	9.75
B	68.36	-3.05	0.02324	1,16	853.56	9.04
C	68.34	-3.07	0.02343	1.99	890.92	9.07

7.3.2 Result discussion

The purpose of this subchapter will be to take a look at the results obtained and developed in the past chapters, figure out what instances lead to those results and compare results from each group. The discussion will approach the problem in a logical path by first determining if the way to calculate stress on the new specimen geometries is valid and only then moving on to stress coefficients and advantages and disadvantages of every group.

Through a two sample t test the average result from equation (7.8) from each group was compared with a 5% significance level. The hypothesis of the average from group B being equal to group A and

thus being able to calculate the stress at the mid-span through was rejected, and the hypothesis for the average slope of group C to be equal to group A was accepted. However the average is close enough to be considered equal to specimen's C average with a 95% confidence. The 3.73% discrepancy in slope may be due to the fact that different geometries flex in different ways producing distinct angles of contact between the loading rollers and the specimen. This would affect how the force applied would translate into momentum to produce the stress in the mid-span, slightly affecting the relation between force and strain. This could be proven if the test was repeated with a stiffer material if the differences in slope would diminish.

Some part of the difference from the slope of equation (7.8) in the mechanical test results may have stemmed from the distinct ways in which the width of the specimen was measured. Specimen groups B and C's mid-span width were measured in a different angle from specimen A due to the existence of a transition zone and probably adding a tenth of a millimetre. Also the results from the slope tended to diverge from the original specimen A with the increase in R_y. This might just be coincidence since only two averages were taken. Because a further increase in the parameter R_y will have no apparent benefit a study to find how the slope changes with the parameter should not necessary since it already provides a good approximation at the maximum R_y needed.

The yield stress of the different groups will not provide any evidence as to the true values of the stress coefficients. Since the specimens turned out very ductile they will yield first at the zone with the highest stress coefficient deforming in plastic regime but spread the excess load to the nearby regions. The yield stress calculated by the four point bending tests was on the central part of the specimen. It will reach its yield point when enough momentum is applied and is far enough away so that any stress concentrations won't influence the readings. The yield stress calculated in the mechanical tests should be the same, as a result of the specimens being built with the same material and printing parameters. However the yield stress of each group of specimens is slightly different perhaps showing the disparity in the calculated slope from table 7.4 as the percentage difference is fairly similar.

What would provide a great insight of the stress coefficients would be the maximum stress at the mid-span. Because specimens with high stress coefficients fail in that region when the maximum stress that a material can hold is reached this in turn will not allow the mid-span section to develop any more stress as the specimen starts to fail. Specimens with higher stress coefficients develop lower mid-span stress as the materials in the stress concentrated region reaches its maximum stress sooner than the other specimens that will also reach that level of stress while letting the mid-span region withstand more load.

Example, the maximum stress of a given material is 100 MPa and one specimen has a SC_1 of 1.5 and the other has a SC_2 of 2. The specimen will fail when the most loaded region reaches 100 MPa. The maximum stress at the mid-span (σ_n) will be calculated with equation (3.2):

$$SC_1 = 1.5 = \frac{100}{\sigma_{n1}} \rightarrow \sigma_{n1} = 66.6\text{MPa} \tag{7.13}$$

$$SC_2 = 2 = \frac{100}{\sigma_{n2}} \rightarrow \sigma_{n2} = 50.0\text{MPa} \tag{7.14}$$

As can be seen the specimen with the highest stress coefficient shows a lower measurement of stress at the mid-span. This is the logic that will be used to figure out the stress coefficients of the four-point bending test.

Another challenge was the fact that the mid span stress for this experimental work cannot be accurately determined due to the ductility of the specimens. The test geometry was far off being approximate to the initial flat position of the specimen, changing the distance between contact points of the supporting and loading rollers and altering the angle of contact between a cylinder and the flat surface of the specimen, as seen in figure 2.2, dividing the initial vertical force into horizontal and vertical components.

Despite not being able to confidently calculate the maximum stress at the mid-span of the specimen there is still ways to compare them as the specimens reached the maximum force of the test at nearly the same loading roller displacement in table 7.6. This gives the set ”text fixture + specimen” approximately the same geometry, making it so the angle of the forces and the distance between contact points are similar between groups B and C though group A presents a significant difference to the other two groups. This means that for equal forces the momentum and thus the stress applied to the mid-span should be almost identical despite their value being unknown to us. Considering the test at the point of maximum force a curved beam undergoing pure bending then the neutral stress line is no longer in the centroid of the specimen and is located nearer to the compression side. Still the stress at both sides, compression and tension, of the specimen are directly proportional to the momentum imposed and so are also directly proportional to the force applied [73]. This means that the maximum force applied during the tests can help to determine if the stress coefficient from table 6.2 are valid.

If the stress from the mid-span could be accurately calculated, then when applying equation (3.2) by multiplying the two parts of the equation that are known, the stress coefficient that we want to confirm and the hypothetical stress at the mid-span, the result would be the maximum stress that the specimen’s material can hold. This value should be very close in all of the groups since the maximum stress is a property of the material from which they were all made. If the maximum stress at the mid-span and the corresponding highest stress coefficients from each group are multiplied then the result should be similar values of maximum stress. In case this does not happen then the simulations were incorrect.

When the maximum force during a test is applied, the stress at the mid span has a certain value bellow the maximum stress that the material can hold. The zone with the highest stress coefficient however as reached its maximum stress and this value can be calculated as said above. For the specimen to break at the mid span where stress can be calculated through the force applied it would have to withstand maximum stress. This is $\times SC$ greater then it is at the moment maximum force applied. Since forces in the case of curved beams under bending are directly proportional to the stress imposed that means that the maximum force would have to be $\times SC$ greater than the maximum force applied during the test to reach that stress for the same ”test fixture + specimen” geometry. So the following can be said:

$$SC_r = \frac{\sigma_r}{\sigma_n} = \frac{F_u}{F_{max}} \tag{7.15}$$

Where F_{max} is the highest recorded force in the mechanical test and F_u is the ultimate theoretical force that would take to provoke failure at the mid-span. Either one of the formulas can be applied as long as the highest stress coefficient found in the specimen is used.

For the regular specimen group A the highest stress coefficient is found under the loading rollers [14] which aligns with its simulated stress coefficient from table 6.2. Specimen B has its highest stress coefficient in the root of the transition. The location of maximum von Mises stress in specimen C should be in both transition and contact zones but it is yet to be confirmed by mechanical tests. Starting of by comparing the specimens in which we know the locations of the most elevated stress values.

$$SC_{rA} = 1.46 = \frac{F_{uA}}{798.66} \rightarrow F_{uA} = 1166.0N \tag{7.16}$$

$$SC_{tB} = 1.24 = \frac{F_u}{853.56} \rightarrow F_{uB} = 1051.3N \tag{7.17}$$

As mentioned before the results should be roughly the same, however the ultimate force for specimen A is 1166.0N while for specimen B is 1051.3N which represents a almost 10% difference. This means that either the stress under the loading rollers was exaggerated in the simulations producing stress coefficients above the real value leading to an overestimation of the ultimate force or that the transition stress coefficient was undervalued. This last option is doubtful because when the mesh was changed from study 1 to study 2 despite the stress beneath the loading cylinders changing the transition von Mises stress stayed unaffected. Another hypothesis is that between specimen A and specimens B and C there is a significant difference in the displacement of the loading rollers that makes comparing forces instead of stresses much less feasible.

$$SC_{rC} = 1.16 = \frac{F_u}{890.92} \rightarrow F_{uC} = 1033.5N \tag{7.18}$$

$$SC_{tC} = 1.15 = \frac{F_u}{890.92} \rightarrow F_{uC} = 1024.6N \tag{7.19}$$

Both results from specimen C are very close to the ultimate force calculated for specimen B, representing a difference of only 1.6% and 2.6%, and this might mean one of two things.

One of the options is that both of the stress coefficient of the rollers and the transition are correct in the simulations and the ”test fixture + specimen A”’s geometry is not comparable to the other two groups due to the difference in deflection. This option validates the second numerical study by confirming that the stresses in at least one of the critical areas are correct. It can not be said for certain whether the two are valid because it is not known if it is just one of the coefficients that is correct while the other is below the simulated value not affecting the maximum stress at the mid-span. If specimen C turned out to be fragile the location of the breaking point could be assumed as the highest stress coefficient.

The second option is admitting that the ”test fixture + specimen A”’s geometry is still close enough for comparison. This implies that there is an exaggeration of the stress under the loading rollers. The ultimate force calculated from the SC_{rC} is higher than normal resulting in the ultimate force from this specimen being close specimen B because group C was built to have the same stress coefficients under the rollers as in the transition zone. This leaves only the transition zone as the one with the highest stress coefficient. The ultimate force calculated from the SC_{tC} is still very similar to the one calculated for specimen B meaning that at least the stress coefficients of the transitions in the numerical study are correct, independently of the option.

Even if ”test fixture + specimen A”’s geometry are not comparable to the other groups there is another phenomena that might be happening. In the simulations the contact point was kept the same independently of how much the travel from the loading rollers was to simplify the refinement of this zone. In the mechanical tests this contact zone moves away from the transition zone effectively increasing the parameter d as the rollers descend further resulting in a reduction of the stress coefficient beneath the loading rollers as seen in Figure 7.19. So most likely the stress coefficient under the rollers is not correct in the simulations and if it is, it was merely by chance as the stress coefficient is varying with the deflection and movement of the contact points.

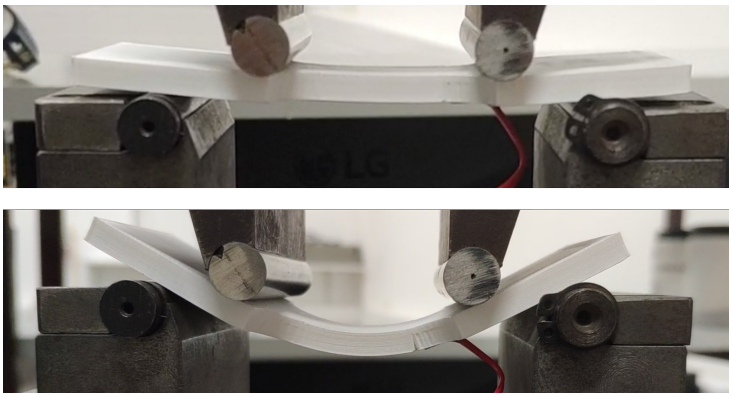

Figure 7.19: Contact zone at the beginning of the four point bending test (above) vs. contact zone at the end of the four point bending test (bellow).

Chapter 8

Conclusions

The four point bending test is a somewhat flawed way of evaluating material properties. The parameters used in test definitely made an impact on the original stress distribution from specimens built with the ASTM standard leading the highest stresses away from the contact zones. At the end of the mechanical tests the stress coefficient values for the transition found in the numerical study 2 were validated. Unfortunately the results were inconclusive when it came to the stress coefficient in the contact zone. If the specimens built turn out with a more brittle behaviour the location of the highest stress coefficient could have been uncovered by the breaking of the specimens. Still, despite the values of stress in this area being unconfirmed conclusions can still be taken out of the numerical studies. Even if there is a slight shift from the real values they are still comparable within each study. Some of the major conclusions are:

- Parameter R_x's direct effect is the increase in the effective radii at the root of the transition, this in turn lowers the stress coefficient in that region. If space is limited then the increase of this parameter means the decrease of the length between the contact zone and the start of the transition which results in a boost to the stress under the rollers. This parameter cannot reduce the stress coefficient in the transition zone below 1.00.

- Parameter R_y decreases the stress under the loading rollers by providing more contact area for the cylinder to spread its load, as a side effect. If the transition length is limited then it also decreases the effective radii at the root of the transition raising the stress in that area.

- Parameter d dictates the separation between the rollers and the start of the transition. This determines the distance at which the contact zone sits in relation to the free edge generated by the transition. The further away the contact zone is from this free edge the lower its stress will be. By increasing d it implies a decrease in the parameter R_x if the space is limited, resulting in a simultaneous decrease in stress beneath the rollers and a increase at the root of the transition. If parameter d is increased infinitely the end result would resemble a specimen with a width of the mid-span plus two times R_y and so the minimum achievable stress is equivalent to a regular specimen of those dimensions. The influence that this parameter has on the stress under the rollers

also depends on the value of R_y.

- The best combination of parameters to obtain the overall lowest stress coefficients in both critical areas is to use a shorter parameter d and maximize the length of the curved transition.

- Equation (2.8) is a good approximation to use when calculating the stress at the mid-span for these novel specimen geometries in four-point bending, and if by any chance the difference in results from equation (7.8) increases with R_y there is no reason to further increase this parameter other then seeing if this truly is the case as the stresses at the contact zone are lower then at the mid-span.

- Parameter d will increase with the loading rollers deflection through the course of the test, lowering the stress coefficient in the contact zone. So, the only way to obtain correct numerical results is performing a more complex simulation.

8.1 Achievements

Definitely the biggest achievement of this work was facilitating future studies on these geometries in four point bending by proving that equation (2.8) from the ASTM standard and based on General Beam Theory is a good approximation for calculating the stress at the mid-span of the specimen.

Next on the list is how the geometric parameters chosen for the specimen affect the stress field in the critical areas through numerical studies. Even though they are not perfect, and in the case of the contact zone might not correspond to the values in real mechanical testing, it serves as a reference and a general guideline to what the parameters are expected to influence in the future.

The final big achievement is realizing that the stress under the loading rollers is probably lower than what the numerical part of the work deduced from the maximum force during the mechanical tests. This only means that the stress coefficient in the contact zone is bellow to what was expected and can be adjusted to the goals set for the specimens to produce lower overall stress coefficients.

8.2 Future Work

The main flaw of this work was the materials available for testing. Yes it was quick and cheap to produce the specimens for the test but made the results a bit harder to analyse and some approximations had to be done leaving some doubts on whether or not the conclusions taken were accurate. The most important follow up to this work would be a similar one done with stiffer materials that wont allow high deflections such that it wouldn't be unreasonable to use equation (2.8) throughout the whole duration of the test.

Another option for material is manufacturing specimens out of beams that are known to fail due to indentation, measure how this new proposed geometry would help in obtaining the material properties with a four point bending test, and see if it results in a new failure mode for that type of material.

Normally for curved transition there are stress concentration factor tables but along the course of this work it was never found one with the bending in this particular direction in relation to the transition. If this geometry starts being used and researchers begin to adapt it with new parameters to fit their needs then a stress concentration factor table would be helpful not only to help validate the numerical studies but also apply to calculate the maximum stress of the material if it is located in the transition. A huge limitation in this work was the computational power available, many decision were made in regards to this factor and so if there is the opportunity to do a more refined numerical study it would certainly be an improvement in the accuracy department over this thesis.

When searching for a suitable size for the specimens intended for mechanical testing a reduction from a thickness $t = 10$mm to $t = 5$mm was necessary. The linear measurements to the later specimen were all one half of the original specimen, so it was only a scaled down version. However the stress coefficients where different from one another, this might imply that these changes are applicable through every size of specimen. A study pertaining this effect would be necessary if this geometry were to be used while applying different thickness values.

In section 2.4 various methods of reducing stress concentration factors were looked at, for example the ESO or Evolutionary Structural Optimization. Perhaps in the future these can be utilized to additionally increase the similarity between the point with the highest stress on the specimen with the stress calculated for the mid-span.

Taking a last look at the ASTM 6272-10 standard there are some formulas that involve the mid-span deflection which was not recorded during the mechanical tests. Further studies could confirm whether or not they are applicable in this new geometry and if not then propose approximations. These formulas are for calculating the mid-span deflection, strain and the Elasticity Modulus.

Lastly this work only encompassed one of the option for four point bending where the loading span is half of the support span. The other option is to use a one third ratio between the loading span and the support span. Of course this diminishes the test zone length but the rollers also have to provide less downwards force to impose the same momentum on the mid-span. This might lead to shorter values of R_y and shorter transitions and can actually provide lower stress coefficients while having equal test zone length.

Bibliography

[1] https://www.iso.org/about us.html. International Standard Organization's website.

[2] https://www.astm.org/ABOUT/history_book.html. American Society for Testing and Materials's website.

[3] *Standard Test Method for Flexural Properties of Unreinforced and Reinforced Plastics and Electrical Insulating Materials by Four-Point Bending*. ASTM International, 100 Barr Harbor Drive, PO Box C700, West Conshohocken, PA 19428-2959. United States, April 2010.

[4] H. Fukuda. A new bending test method of advanced composites. *Experimental Mechanics*, pages 61–80, September 1989.

[5] B. Hammant. The use of 4-point loading tests to determine mechanical properties. *Composites*, pages 246–249, September 1971.

[6] T. Zhai, Y. Xu, J. Martin, A. Wilkinson, and G. Briggs. A self-aligning four-point bend testing rig and sample geometry effect in four-point bend fatigue. *International Journal of Fatigue*, 21:889–894, 1999.

[7] X. Dong, H. Zhao, L. Zhang, H. Cheng, and J. Gao. Geometry effects in four-point bending test for thin sheet studied by finite element simulation. *Materials Transactions*, 57(3):335–343, 2016.

[8] A. Pronk. Theory of the four point dynamic bending test part 1: General theory, December 2006.

[9] F. Mujika. On the difference between flexural moduli obtained by three-point and four-point bending tests. *Polymer Testing*, 25:214–220, 1971.

[10] S. Timoshenko. *Strenghth of Materials Part: II Advanced Theory and Problems*, chapter I.10 Limitations of the Method of Superposition.

[11] T. Lube, M. Manner, and R. Danzer. The miniatturisation of the 4-point-bend test. *Fatigue Fract. Engng Mater. Struct*, 20(11):1605–1616, 1997.

[12] G. D. Quinn. Design data for engineering ceramics: A review of the flexure test. *Journal of the American Ceramic Society*, 74(9):2037–2066, 1997.

[13] D. Theobald, J. McClurg, and J. G. Vaughan. Comparison of three-point and four-point flexural bending tests. In *Convention, International composites*, INTERNATIONAL COMPOSITES EXPO PROCEEDINGS, pages 5–B. SPI, 1997.

[14] W. C. Cui and M. R. Wisnom. Contact finite element analysis of three and four-point short-beam bending of unidirectional composites. *Composites Science and Technology*, 45:323–334, 1992.

[15] W. C. Cui, M. R. Wisnom, and M.Jones. Failure mechanisms in three and four point short beam bending tests of unidirectional glass/epoxy. *The Journal of Strain Analysis for Engineering Design*, 27:235–243, October 1992.

[16] A. E. H. Love. *Mathematical Theory of Elasticity*. Dover Reprints, 1944.

[17] R. G. C. Arridge and M. J. Folkes. Effect of sample geometry on the measurement of mechanical properties of anisotropic materials. *Polymer*, 17:495–500, June 1976.

[18] M. J. Folkes and R. G. C. Arridge. The measurement of shear modulus in highly anisotropic materials: the validity of st venant's principle. *J. Phys. D: Appl. Phys*, 8:1053–1064, 1975.

[19] C. Horgan and J. K. Knowles. Recent developments concerning saint-venant's principle. *Advances in applied mechanics*, 23:179–262, 1983.

[20] R. A. Toupin. Saint-venant's principle. *Arch. Rational Mech. Anal.*, 18:83–96, 1964.

[21] J. K. Knowles. On saint- venant' s principle in the two-dimensional linear theory of elasticity. *Arch. Rational Mech. Anal.*, 21:1–21, 1966.

[22] I. Choi and C. Horgan. Saint-venant's principle and end effects in anisotropic elasticity. *Journal of Applied Mechanics*, pages 424–430, 1977.

[23] C. Horgan. On saint-venant's principle in plane anisotropic elasticity. *Journal of Elasticity*, 2(3): 169–180, 1972.

[24] G. D. Quinn, B. T. Sparenberg, P. Koshy, L. K. Ives, S. Jahanmir, and D. D. Arola. Flexural strength of ceramic and glass rods. *Journal of Testing and Evaluation*, 37(3):1–23, 2009.

[25] C. Berg, J. Tirosh, and M. Israeli. Analysis of short beam bending of fiber reinforced composites. *Composite Materials: Testing and Design*, pages 206–218, 1972.

[26] P. E. Sandorff. Saint-venant effects in an orthotropic beam. *J. Composite Materials*, 14:199–212, 1980.

[27] S. Timoshenko and J. N. Goodier. *Theory of Elasticity*, chapter I.10 Limitations of the Method of Superposition.

[28] J. R. Yates, W. Zhang, and K. J. Miller. The initiation and propagation behaviour of short fatigue cracks in waspaloy subjected to bending. *Fatigue and Fracture of Engineering Materials and Structures Ltd*, 16(3):351–362, 1993.

[29] S. Güngör and L. Edwards. Effect of surface texture on the initiation and propagation of small fatigue cracks in a forged 6082 aluminium alloy. *Materials Science and Engineering*, 12:17–24, 1993.

[30] D. de Albuquerque Simões, J. T. P. de Castro, and M. A. Meggiolaro. Improved fatigue test specimens with minimum stress concentration effects. *67th abm international congress*, pages 1911–1923, 2012.

[31] W. D. Pilkey and D. F. Pilkey. *Peterson's stress concentration factors*. John Wiley and Sons, Inc., third edition edition, 2008.

[32] M. G. Garrell, A. J. Shih, E. Lara-Curzio, and R. O. Scattergood. Finite-element analysis of stress concentration in astm d 638 tension specimens. *Journal of Testing and Evaluation*, Vol.31(No.1): 1–6, 2003.

[33] C. Mattheck and S. Burkhardt. A new method of structural shape optimization based on biological growth. *Int J Fatigue*, 2(No.3):185–190, 1990.

[34] C. Mattheck. Teacher tree: The evolution of notch shape optimization from complex to simple. *Engineering Fracture Mechanics*, 73:1732–1742, 2006.

[35] R. V. Baud. Fillets profiles for constant stress. *Product engineering*, pages 133–134, April 1934.

[36] F. O. Sonmez. *Structural Optimization Using Simulated Annealing*, chapter 14, pages 281–306. I-Tech Education and Publishing, 2008.

[37] R. Das, R. Jones, and Y. Xie. Design of structures for optimal static strength using eso. *Engineering Failure Analysis*, 12:61–80, 2005.

[38] H. Neuber. Zur optimierung der spannungskonzentration. *Sonderdruck 9 aus den Sitzungsberichten*, 1971.

[39] A. Shanyavskiy. Fatigue cracking simulation based on crack closure effects in al-based sheet materials subjected to biaxial cyclic loads. *Engineering Fracture Mechanics*, 78:1516–1528, 2011.

[40] R. Cláudio, M. Freitas, L. Reis, B. Li, and I. Guelho. Multiaxial fatigue behaviour of 1050 h14 aluminium alloy by a biaxial cruciform specimen testing method. *10th Int. Conf. Multiaxial Fatigue Fract*, 2013.

[41] R. Baptista, R. Claudio, L. Reis, J. Madeira, I. Guelho, and M. Freitas. Optimization of cruciform specimens for biaxial fatigue loading with direct multi search. *Theoretical and Applied Fracture Mechanics*, 2015.

[42] Y. Hanabusa, H. Takizawa, and T. Kuwabara. Numerical verification of a biaxial tensile test method using a cruciform specimen. *Journal of Materials Processing Technology*, 213:961–970, 2013.

[43] W. Müller and K. Pöhlandt. New experiments for determining yield loci of sheet metal. *Journal of Materials Processing Technology*, 60:643–648, 1996.

[44] I. Zidane, L. Leotoing, D. Guines, and E. Ragneau. Development of an in-plane biaxial test for forming limit curve (flc) characterization of metallic sheets. *Measurement Science and Technology*, pages 1–23, 2010.

[45] L. Leotoing, D. Guines, I. Zidane, and E. Ragneau. Cruciform shape benefits for experimental and numerical evaluation of sheet metal formability. *Journal of Materials Processing Technology*, 213: 856–863, 2013.

[46] F. Chen, S. Bazhenov, A. Hiltner, and E. Baer. Flexural failure mechanisms in unidirectional glass fibrereinforced thermoplastics. *Composites*, 25(No.1):11–20, 1994.

[47] G. Shih and L. Ebert. Flexural failure mechanisms and global stress plane for unidirectional composites subjected to four-point bending tests. *Composites*, 17(No.4):309–320, 1986.

[48] C. Weaver and D. Williams. Deformation of a carbon-epoxy composite under hydrostatic pressure. *Journal of Material Science*, 10:1323–1333, 1975.

[49] B. W. Rosen and N. F. Dow. *Mechanics of failure of fibrous composites*, chapter Chapter 8, pages 612–672. 1972.

[50] I. Daniel, E. Gdoutos, K. Wang, and J. Abot. Failure modes of composite sandwich beams. *International Journal of DAMAGE MECHANICS*, 11:309–334, October 2002.

[51] D. B. Marshall. Failure mechanisms in ceramic-fiber/ceramic-matrix composites. *Journal of the American Ceramic Society*, 68(No.5):225–231, May 1985.

[52] T. Parry and A. Wronski. Kinking and tensile, compressive and interlaminar shear failure in carbon-fibre- reinforced plastic beams tested in flexure. *Journal of Material Science*, 16:439–450, 1981.

[53] S. Belouettar, A. Abbadi, Z. Azari, R. Belouettar, and P. Freres. Experimental investigation of static and fatigue behaviour ofcomposites honeycomb materials using four point bending tests. *Composite Structures*, 87:265–273, 2009.

[54] A. Petras and M. Sutcliffe. Failure mode maps for honeycomb sandwich panels. *Composite Structures*, 44:237–252, 1999.

[55] E. Gdoutos, I. Daniel, and K. Wang. Indentation failure in composite sandwich structures. *Experimental Mechanics*, 42(No.4):426–431, December 2002.

[56] J. Sha, T. Yip, and S. Wong. In situ surface displacement analysis of fracture and fatigue behaviour under bending conditions of sandwich beam consisting of aluminium foam core and metallic face sheets. *Matrerial Science and Technology*, 22(No.1):51–60, 2006.

[57] D. C. Montgomery. *Design and Analysis of Experiments*. John Wiley and Sons, fifth edition edition, 1997.

[58] T. S. Martins. Influência dos parâmetros de fabrico nas propriedades mecânicas de peças obtidas por impressão 3d com um único material. Master's thesis, Instituto Superior Técnico, October 2017.

[59] J. M. Chacón, M. A. Caminero, E. García-Plaza, and P. J. Núñez. Additive manufacturing of pla structures using fused deposition modelling: Effect of process parameters on mechanical properties and their optimal selection. *Material and Design*, 124:143–157, 2017.

[60] Y. Zhang and K. Chou. A parametric study of part distortions in fused deposition modelling using three-dimensional finite element analysis. *J. Engineering Manufacture*, 222:959–967, 2008.

[61] A. K. Sood, R. Ohdar, and S. Mahapatra. Parametric appraisal of mechanical property of fused deposition modelling processed parts. *Materials and Design*, 31:287–295, 2010.

[62] B. Tymraka, M. Kreigerb, and J. Pearce. Mechanical properties of components fabricated with open-source3-d printers under realistic environmental conditions. *Material and Design*, 58:242–246, 2014.

[63] J. T. (https://math.stackexchange.com/users/48862/john tan). Radius vs radius of curvature of an ellipse. Mathematics Stack Exchange. URL `https://math.stackexchange.com/q/1159928`. URL:https://math.stackexchange.com/q/1159928 (version: 2018-08-04).

[64] Ultimaker cura download link. Online, December 2019. https://ultimaker.com/software/ultimaker-cura.

[65] R. Marat-Mendes, R. Martins, A. Garcia, and L. Reis. Flexural testing and analysis of full-strain-fields in sandwich composites. *Frattura ed Integrità Strutturale*, 49:568–585, 2019.

[66] T. Proulx. *Structural Dynamics*, volume Volume 3, page 815. Springer, 2010.

[67] Coefficient of friction, rolling resistance and aerodynamics. Online, September 2020. https://www.tribology-abc.com/abc/cof.htm.

[68] 3d printer filament comparison guide. Online, December 2019. https://www.matterhackers.com/3d-printer-filament-compare.

[69] Pla vs abs – filaments for 3d printing compared. Online, December 2019. https://all3dp.com/1/pla-vs-abs-filament-3d-printing/.

[70] Cosine materials. Online, January 2020. https://www.cosineadditive.com/en/materials.

[71] Simplify3d filament properties table. Online, January 2020. https://www.simplify3d.com/support/materials-guide/properties-table/.

[72] F. P. Beer, E. R. Johnston, J. T. DeWolf, and D. F. Mazurek. *Mechanics of Materials*. McGraw Hill, sixth edition edition, 2012.

[73] R. G. Budynas and J. K. Nisbett. *SHIGLEY'S MECHANICAL ENGINEERING DESIGN*, chapter Chapter 3-18. McGraw-Hill, ninth edition edition, 2008.

[74] Ultimaker pla technical data sheet. Online, December 2019. https://ultimaker.com/en/resources/49911-pla.

Appendix A

Statistical material

	Percent											
75	*90*	*95*	*97.5*	*99*	*99.5*	*99.75*	*99.9*	*99.95*	*99.975*	*99.99*	*99.995*
	One-sided α											
.25	*.10*	*.05*	*.025*	*.01*	*.005*	*.0025*	*.001*	*.0005*	*.00025*	*.0001*	*.00005*
	Two-sided α											
.50	*.20*	*.10*	*.05*	*.02*	*.01*	*.005*	*.002*	*.001*	*.0005*	*.0002*	*.0001*
df												
1	1.00	3.08	6.31	12.71	31.82	63.66	127.32	318.31	636.62	1273.24	3183.10	6366.20
2	.82	1.89	2.92	4.30	6.96	9.22	14.09	22.33	31.60	44.70	70.70	99.99
3	.76	1.64	2.35	3.18	4.54	5.84	7.45	10.21	12.92	16.33	22.20	28.00
4	.74	1.53	2.13	2.78	3.75	4.60	5.60	7.17	8.61	10.31	13.03	15.54
5	.73	1.48	2.02	2.57	3.37	4.03	4.77	5.89	6.87	7.98	9.68	11.18
6	.72	1.44	1.94	2.45	3.14	3.71	4.32	5.21	5.96	6.79	8.02	9.08
7	.71	1.42	1.90	2.37	3.00	3.50	4.03	4.79	5.41	6.08	7.06	7.88
8	.71	1.40	1.86	2.31	2.90	3.36	3.83	4.50	5.04	5.62	6.44	7.12
9	.70	1.38	1.83	2.26	2.82	3.25	3.69	4.30	4.78	5.29	6.01	6.59
10	.70	1.37	1.81	2.23	2.76	3.17	3.58	4.14	4.59	5.05	5.69	6.21
11	.70	1.36	1.80	2.20	2.72	3.11	3.50	4.03	4.44	4.86	5.45	5.92
12	.70	1.36	1.78	2.18	2.68	3.06	3.43	3.93	4.32	4.72	5.26	5.69
13	.69	1.35	1.77	2.16	2.65	3.01	3.37	3.85	4.22	4.60	5.11	5.51
14	.69	1.35	1.76	2.15	2.63	2.98	3.33	3.79	4.14	4.50	4.99	5.36
15	.69	1.34	1.75	2.13	2.60	2.95	3.29	3.73	4.07	4.42	4.88	5.24
16	.69	1.34	1.75	2.12	2.58	2.92	3.25	3.69	4.02	4.35	4.79	5.13
17	.69	1.33	1.74	2.11	2.57	2.90	3.22	3.65	3.97	4.29	4.71	5.04
18	.69	1.33	1.73	2.10	2.55	2.88	3.20	3.61	3.92	4.23	4.65	4.97
19	.69	1.33	1.73	2.09	2.54	2.86	3.17	3.58	3.88	4.19	4.59	4.90
20	.69	1.33	1.73	2.09	2.53	2.85	3.15	3.55	3.85	4.15	4.54	4.84

Figure A.1: t-distribution table

Appendix B

Numerical and experimental data

Table B.1: Printed Ultimaker's PLA properties [74]

Printed PLA parameters	
Tensile modulus	2,346.5 MPa
Tensile stress at yield	49.5 MPa
Tensile stress at break	45.6 MPa
Elongation at yield	3.3%
Elongation at break	5.2 %
Flexural strength	103 MPa
Flexural modulus	3,150 MPa

Table B.2: Length of filament usage per optimal specimen with 10 mm of thickness

Specimen Type	Metres used		Nº of Specimens		Total
Regular	12.18	$\times$	6	=	73.08
				+	
$SC_r < 1$	21.92	$\times$	6	=	131.52
				+	
$SC_r = SC_t$	17.18	$\times$	6	=	103.08
				=	
Total					307.68

Table B.3: Results from the variation of R_x, parameters in mm.

R_x	R_y	d	$\sigma_{r_{max}}$ (MPa)	$\sigma_{t_{max}}$ (MPa)	σ_n (MPa)	Max Deflection (mm)
5	10	10	18.70	24.63	14.18	4.504
10	10	10	20.81	19.11	14.21	5.074
15	10	10	21.20	16.64	14.18	5.670
20	10	10	20.81	15.75	14.19	6.305
25	10	10	21.35	15.32	14.18	6.977
15	20	10	19.31	18.79	14.22	5.414
20	20	10	19.09	17.14	14.20	6.013
25	20	10	18.47	16.09	14.21	6.648
30	20	10	17.12	15.55	14.19	7.232
15	20	20	16.99	17.64	14.21	6.337
20	20	20	15.85	16.90	14.21	6.986
25	20	20	16.32	16.03	14.20	7.669
30	20	20	16.22	15.49	14.18	8.384

Table B.4: Results from the variation of R_y, parameters in mm.

R_x	R_y	d	$\sigma_{r_{max}}$ (MPa)	$\sigma_{t_{max}}$ (MPa)	σ_n (MPa)	Max Deflection (mm)
20	5	10	23.71	15.14	14.18	5.366
20	10	10	20.81	15.75	14.19	6.305
20	15	10	19.72	16.34	14.18	6.130
20	20	10	19.09	17.14	14.20	6.013
20	25	10	18.15	17.64	14.21	5.921
30	25	10	17.27	16.02	14.31	7.202
30	30	10	16.59	16.11	14.23	7.107
30	35	10	16.55	16.44	14.21	7.031
30	40	10	15.67	16.69	14.21	6.968
30	25	15	17.22	15.89	14.22	7.756
30	30	15	14.97	16.11	14.23	7.644
30	35	15	15.51	16.69	14.23	7.554
30	40	15	14.07	16.83	14.22	6.484

Table B.5: Results from the variation of R_y, parameters in mm.

R_x	R_y	d	$\sigma_{r_{max}}$ (MPa)	$\sigma_{t_{max}}$ (MPa)	σ_n (MPa)	Max Deflection (mm)
20	25	0.5	20.78	17.51	14.17	5.003
20	25	5	19.66	17.64	14.21	5.434
20	25	10	18.15	17.64	14.21	5.921
20	20	15	16.25	17.48	14.22	6.423
20	25	20	15.20	17.45	14.22	6.941
30	25	10	17.27	16.02	14.31	7.202
30	25	15	17.22	15.89	14.22	7.756
30	25	20	15.66	15.88	14.22	8.322
30	25	25	14.96	15.94	14.22	8.901
20	5	10	23.71	15.14	14.18	5.366
20	5	15	23.30	15.01	14.17	7.193
30	5	20	22.79	15.04	14.14	7.849
20	5	25	22.88	15.00	14.12	8.529

Table B.6: Results of all combinations of study 2, parameters in mm.

R_x	d	R_y	σ_r (MPa)	σ_t (MPa)	σ_n (MPa)	SC_r	SC_t
Regular specimen			28.24	—	18.45	1.54	—
19	1	10	22.56	21.35	18.51	1.22	1.15
		13	21.18	21.94	18.52	1.14	1.19
		17	20.25	22.79	18.53	1.09	1.23
		30	20.00	24.65	18.56	1.08	1.33
		33	19.78	25.00	18.58	1.07	1.35
		36	19.64	25.38	18.60	1.06	1.36
		40	17.83	26.08	18.59	0.96	1.40
18	2	12	21.45	22.03	18.52	1.16	1.19
		25	18.47	24.36	18.55	1.00	1.31
		30	17.90	25.01	18.56	0.96	1.35
17	3	11	21.71	22.14	18.51	1.17	1.20
		24	18.61	14.79	18.56	1.00	1.34
		30	18.03	25.56	18.57	0.97	1.38
16	4	10	21.85	22.22	18.51	1.18	1.20
		23	18.89	24.98	18.56	1.02	1.35
15	5	9	22.76	22.29	18.50	1.23	1.21
		20	19.32	24.92	18.56	1.04	1.34
		22	18.56	25.33	18.56	1.00	1.37

Table B.7: Results comparing simple and double refined meshes.

Simple Refined mesh		Double refined mesh	
Loading roller (MPa)	Transition (MPa)	Loading roller (MPa)	Transition (MPa)
19,13	17,14	22,95	17,15
20,96	17,14	22,62	17,15
18,77	17,14	22,53	17,16
20,58	17,14	22,58	17,15
20,05	17,14	22,63	17,16
21,10	17,14	22,71	17,15
21,10	17,14	22,49	17,16
21,39	17,14	22,54	17,16
20,92	17,14	22,59	17,16
20,47	17,14	22,55	17,16
20,47	17,14	22,47	17,15
20,40	17,14	22,60	17,15
21,48	17,14	22,58	17,15
20,47	17,14	22,58	17,15
20,40	17,14	22,55	17,15
20,87	17,13	22,46	17,15
20,47	17,14	22,57	17,15
20,70	17,14	22,58	17,15
20,92	17,14	22,63	17,15
20,47	17,14	22,54	17,16

Table B.8: Measurements of the printed specimens. Units in mm

Name	$L + (2 \times Oh)$	w	W	t	tr
Group A - Regular specimen					
1A	106.05	20.11	—	4.99	—
2A	106.01	20.07	—	5.00	—
3A	106.02	20.09	—	5.02	—
4A	106.02	20.09	—	5.05	—
5A	106.05	20.04	—	5.04	—
6A	106.04	20.11	—	5.00	—
Group B - $SC_r < 1$					
1B	105.98	20.23	40.13	5.01	39.08
2B	105.96	20.24	40.11	5.02	39.08
3B	105.91	20.26	40.10	5.05	39.00
4B	105.94	20.25	40.08	5.08	39.09
5B	105.92	20.23	40.09	5.06	39.07
6B	105.96	20.23	40.12	5.06	39.05
Group C - $SC_r = SC_t$					
1C	106.07	20.19	30.52	5.02	39.09
2C	106.00	20.18	30.48	5.05	39.04
3C	105.98	20.19	30.49	5.06	39.07
4C	106.01	20.19	30.47	5.09	39.05
5C	105.99	20.20	30.47	5.08	39.10
6C	106.01	20.18	30.48	5.03	39.09

Table B.9: Slope and offset from first 1% strain of the graph $\frac{F_A}{w_A * t_A}$ vs ϵ_A.

Specimen	$\frac{\frac{F}{w*t}}{\epsilon}$	offset (+b)
Group A - Regular specimen		
1A	58.88	0.00
2A	59.99	0.00
3A	56.88	0.00
4A	54.43	0.00
5A	55.92	0.00
6A	54.26	0.00
Average	55.69	
Group B - $SC_r < 1$		
1B	52.83	0.00
2B	54.45	0.00
3B	54.23	0.00
4B	53.36	0.00
5B	53.72	0.00
6B	53.12	0.00
Average	53.62	
Difference %	-3.73	
Group c - $SC_r = SC_t$		
1C	54.13	0.00
2C	62.98	0.00
3C	56.25	0.00
4C	54.70	0.00
5C	54.51	0.00
6C	54.76	0.00
Average	54.87	
Difference %	-1.48	

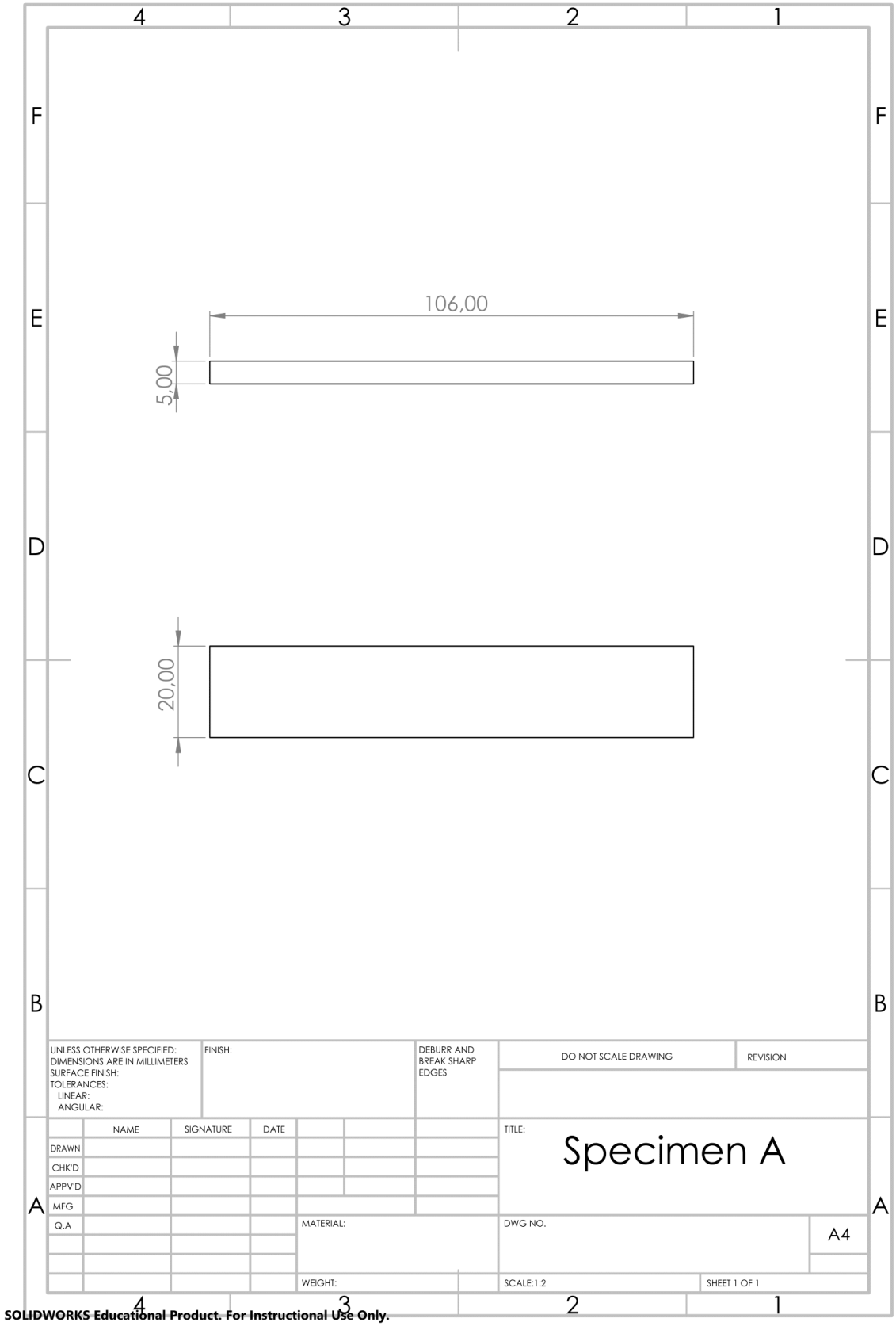

Figure B.1: Technical Drawing of Specimen A

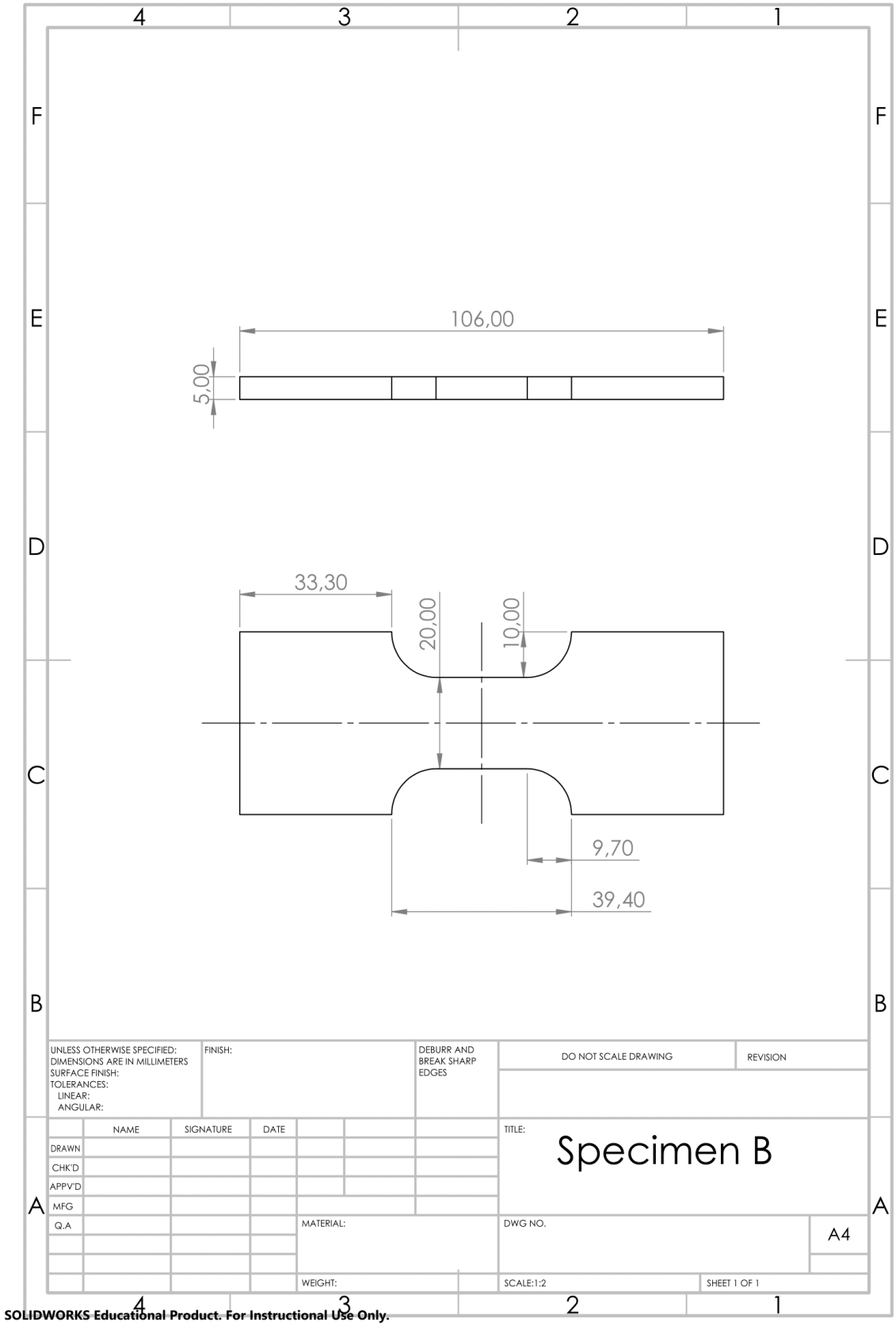

Figure B.2: Technical Drawing of Specimen B

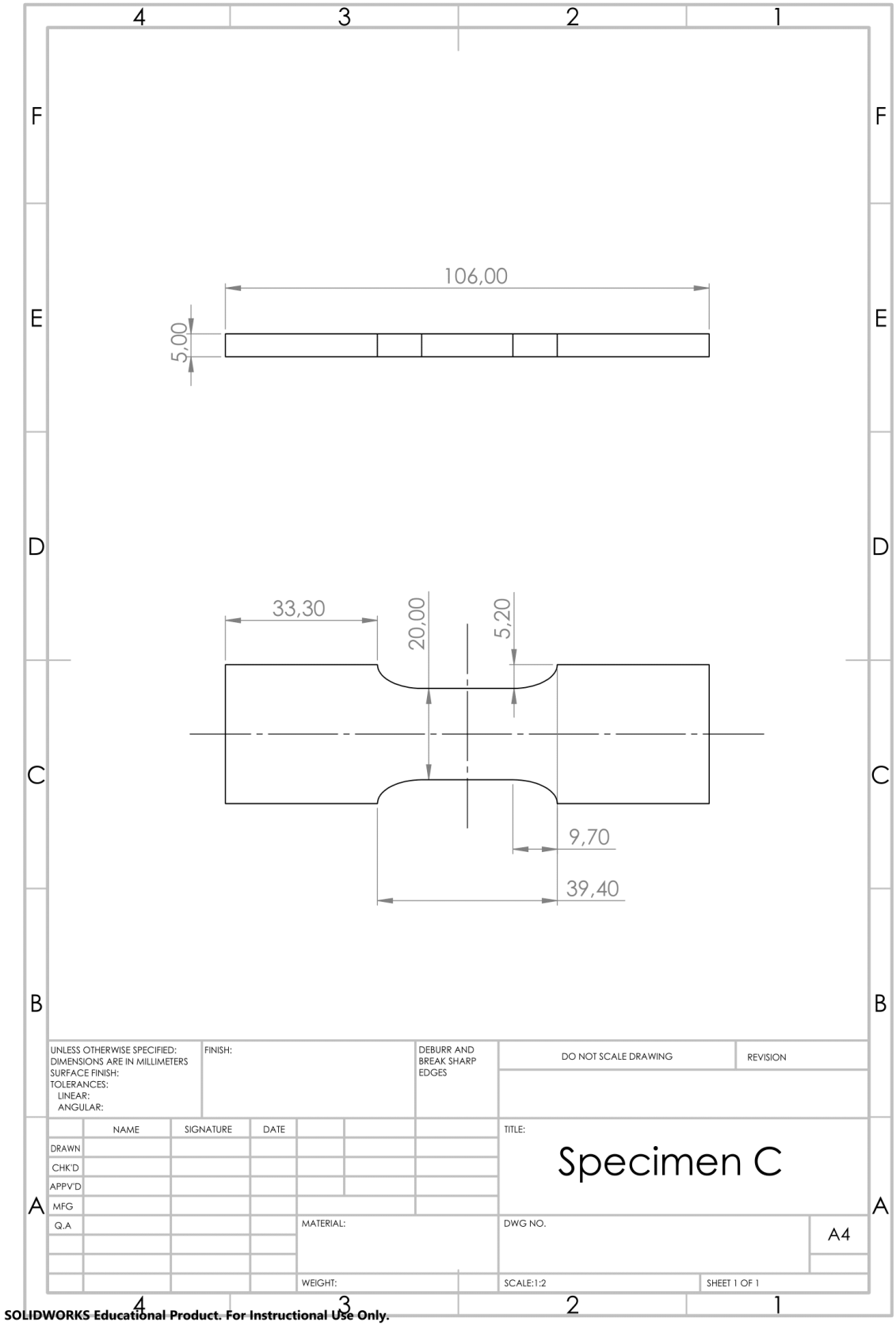

Figure B.3: Technical Drawing of Specimen C